Astroparticle Physics 2023/24

1. Historical introduction - basic properties of cosmic rays
2. Hadronic interactions and accelerator data
3. Cascade equations
4. Electromagnetic cascades
5. Extensive air showers
6. Detectors for extensive air showers
7. High-energy cosmic rays and the knee in the energy spectrum of cosmic rays
8. Radio detection of extensive air showers
9. Acceleration, Astrophysical accelerators and beam dumps
10. Extragalactic propagation of cosmic rays
11. Ultra-high-energy energy cosmic rays
12. Astrophysical gamma rays and neutrinos
13. Neutrino astronomy
14. Gamma-ray astronomy

lecture 8
Radio detection of extensive air showers
Gaisser chapter 16

16 Extensive air showers

First radio detection of air showers 1965

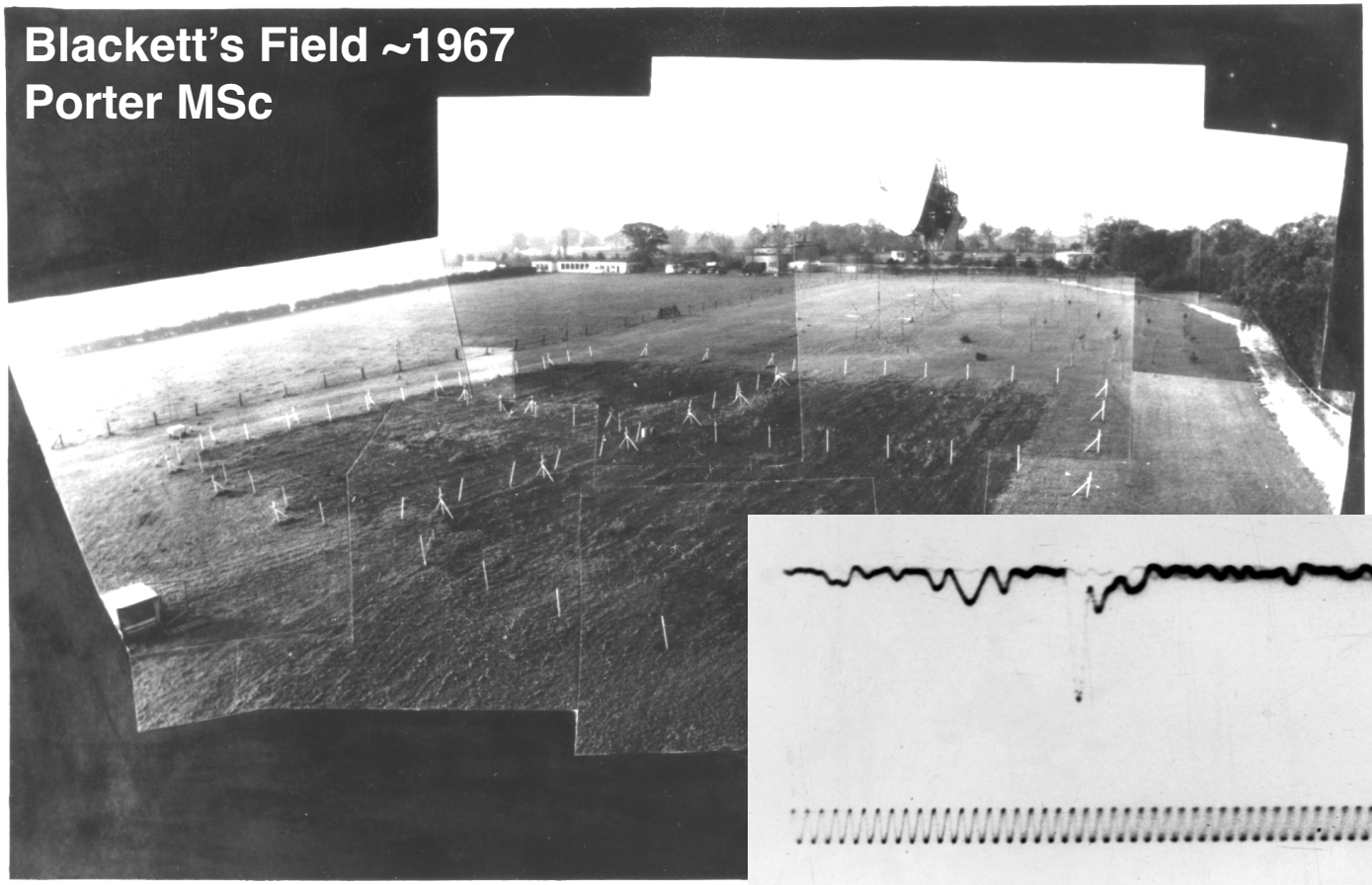

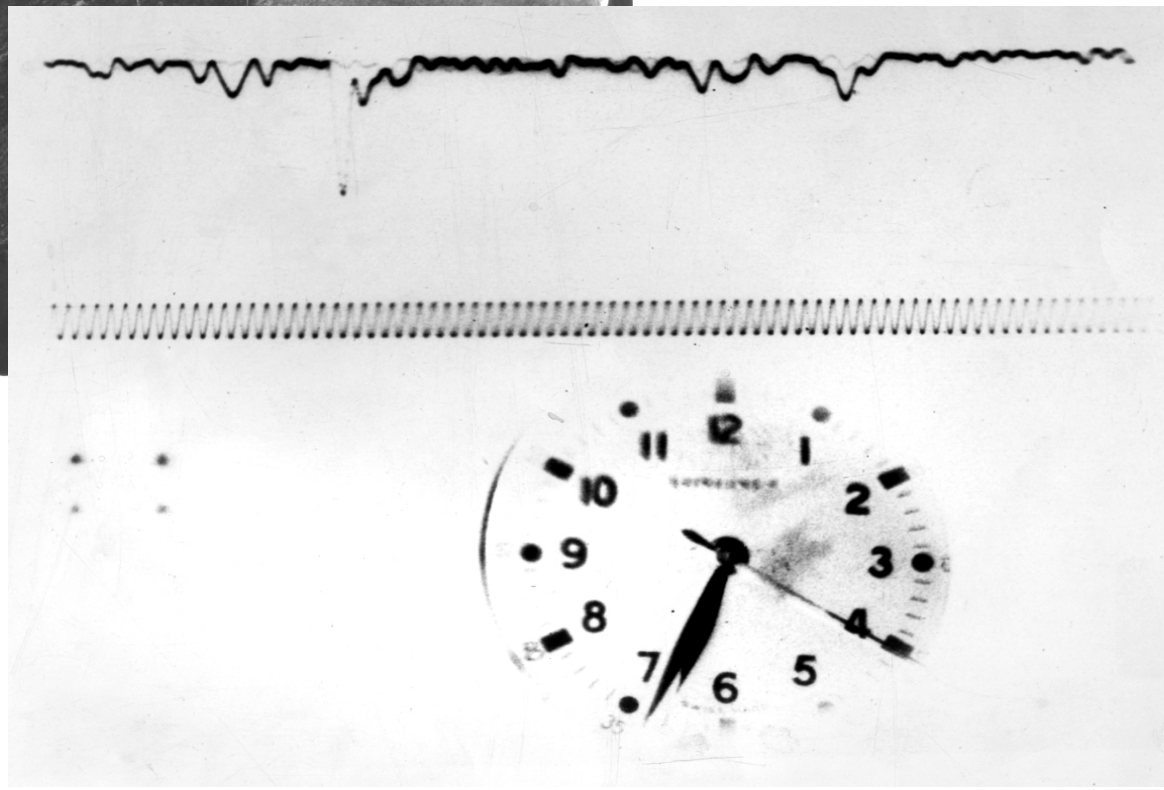

Jelley et al Nature 1965
R. A. Porter MSc Thesis 1967

33RD INTERNATIONAL COSMIC RAY CONFERENCE, RIO DE JANEIRO 2013
THE ASTROPARTICLE PHYSICS CONFERENCE

ICRC 2013

The renaissance of radio detection of cosmic rays

TIM HUEGE[1]

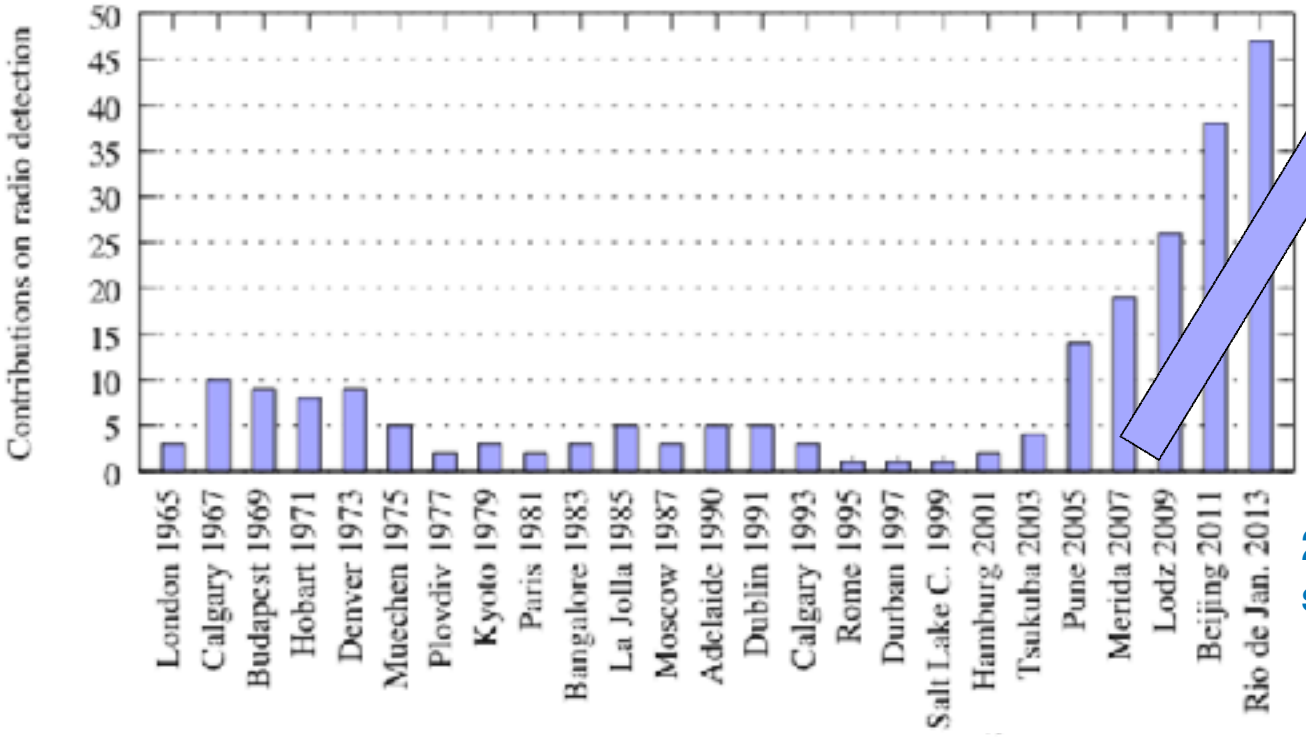

2018: beyond capabilities of standard installations

2016: radio technique mature: properties of cosmic rays

2014: understanding the emission processes

2005: understanding the signal

Figure 1: Number of contributions related to radio detection of cosmic rays or neutrinos to the ICRCs since 1965. The field has grown very impressively since the modern activities started around 2003. Data up to 2007 were taken from [11].

Radio Detectors

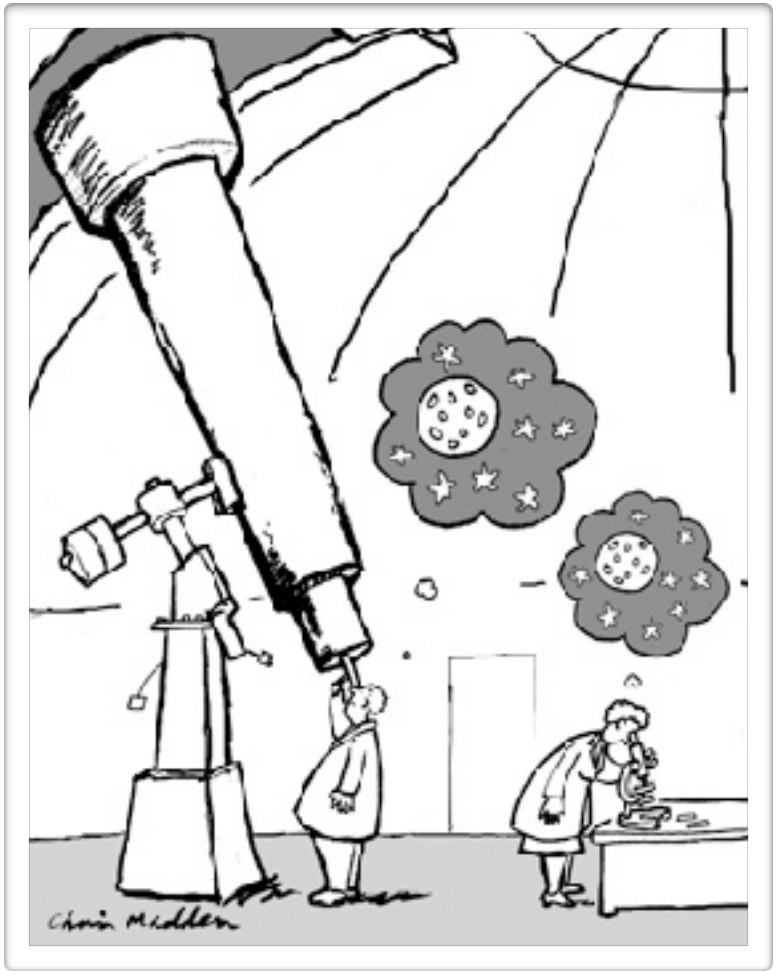

Radio detection of extensive air showers around the world

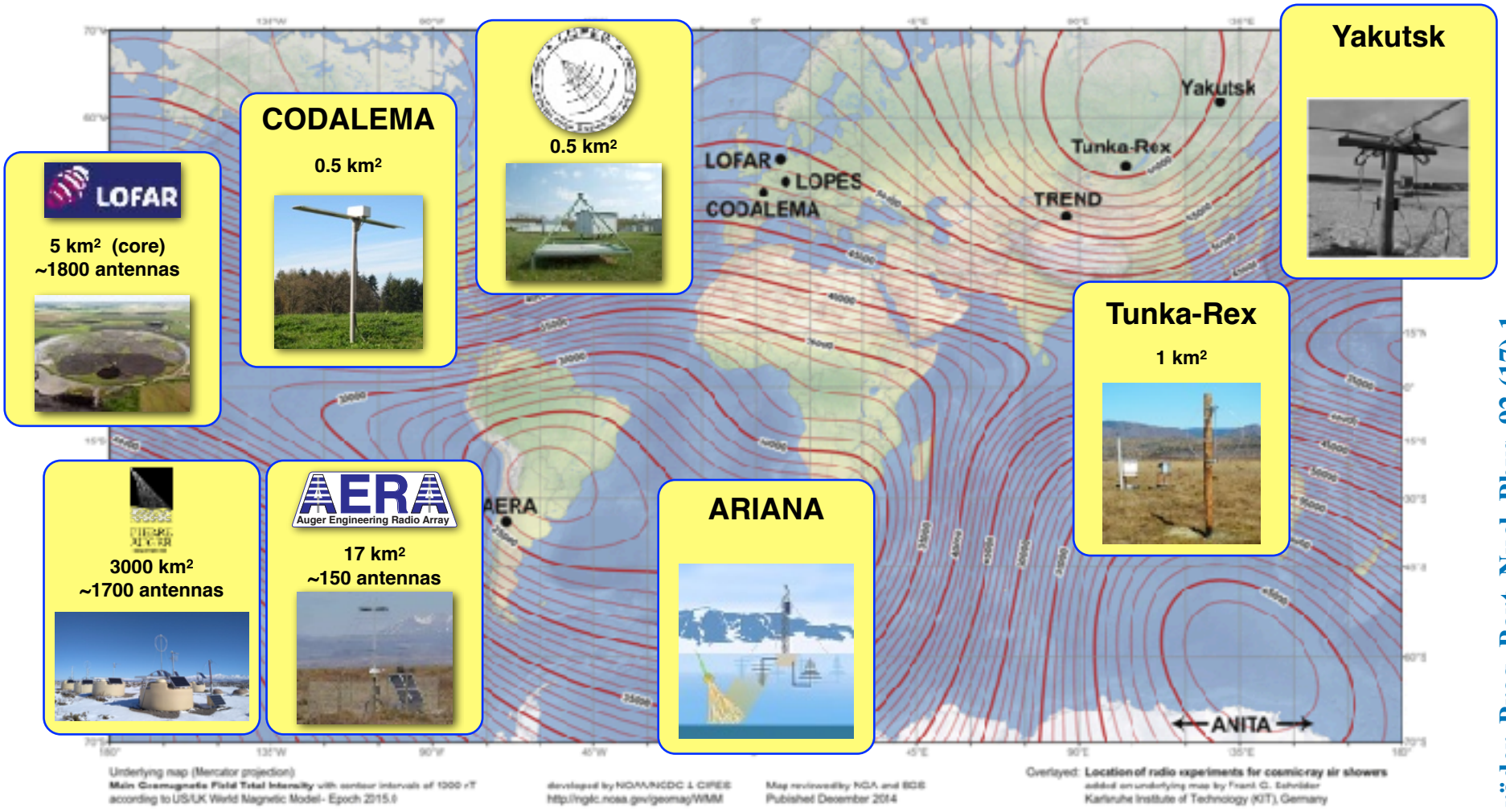

Fig. 21. Map of the total geomagnetic field strengths (world magnetic model [207]) and the location of various radio experiments detecting cosmic-ray air showers.

F.G. Schröder, Prog. Part. Nucl. Phys. 92 (17) 1

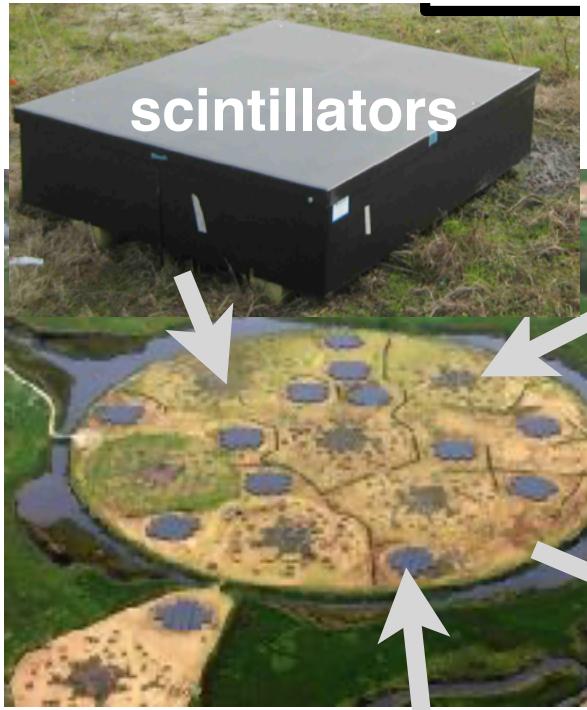

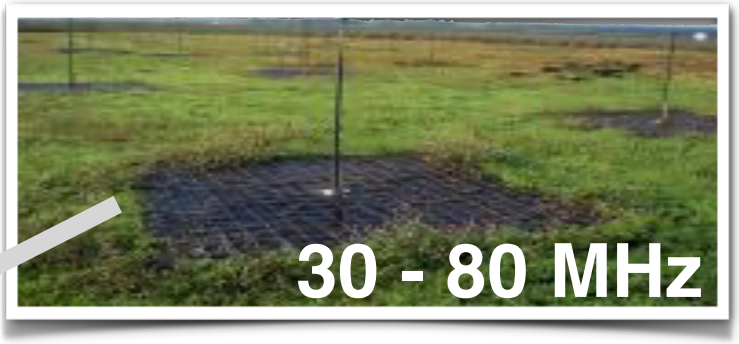

LOFAR

core
23 stations ~5 km²

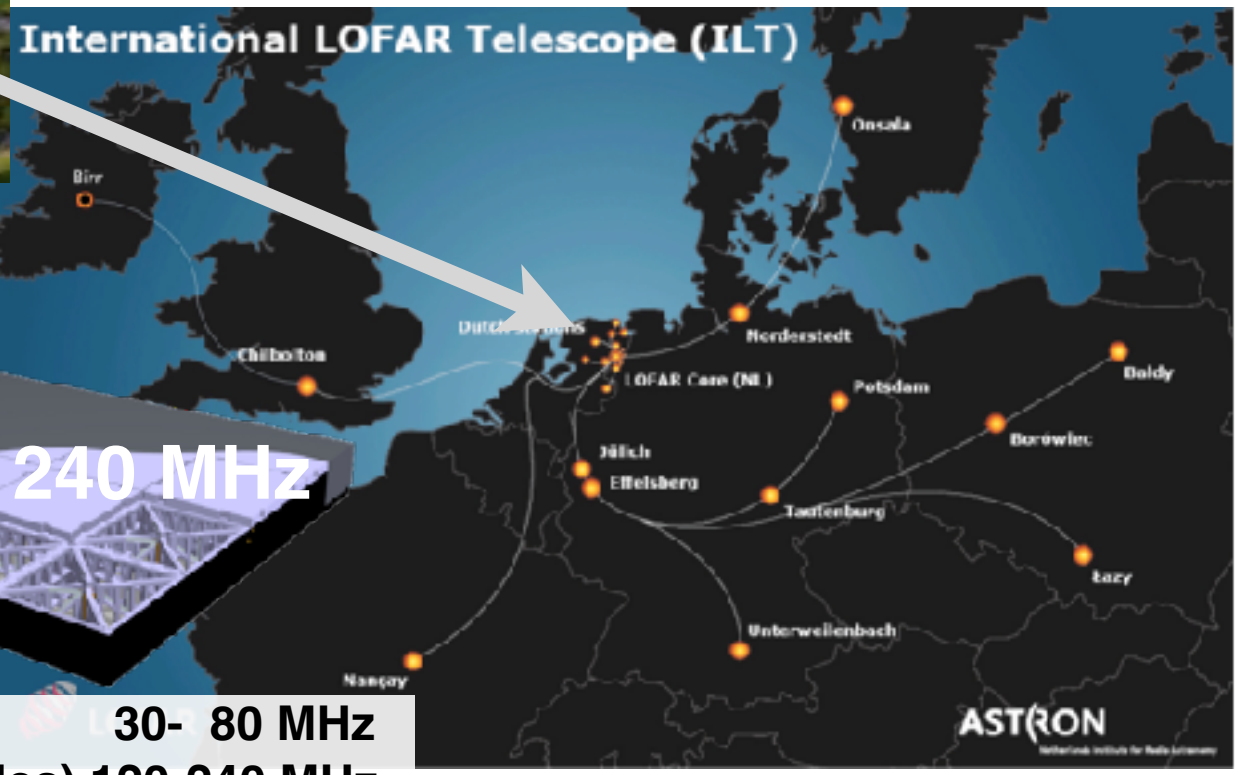

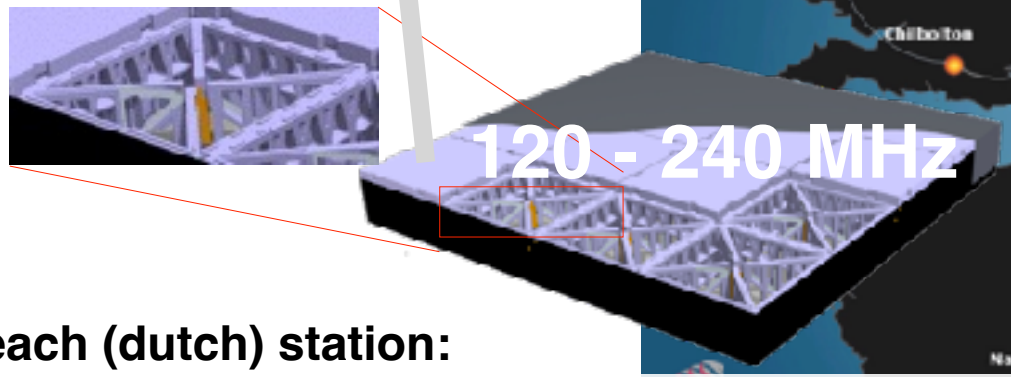

each (dutch) station:
96 low-band antennas 30- 80 MHz
high-band antennas (2x24 tiles) 120-240 MHz

M. van Haarlem et al., A&A 556 (2013) A2

S. Thoudam et al., Nucl. Instr. Meth. A 767 (2014) 339

LORA
LOFAR Radboud Array
scintillator detectors

Superterp:
* diameter ~ 300 m
* 20 LORA detectors
* 6 LBA stations
  (= 6 x 48 antennas)

* more LBA stations around superterp

trigger: 13 of 20 detectors

offline analysis
P. Schellart et al., A&A 560, 98 (2013)

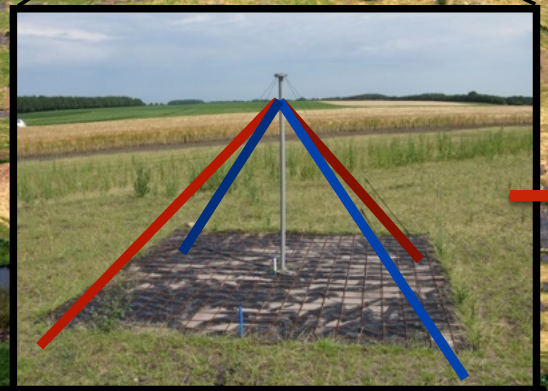

Low Band Antennas (LBA)
30 - 80 MHz

buffer
2 ms read-out

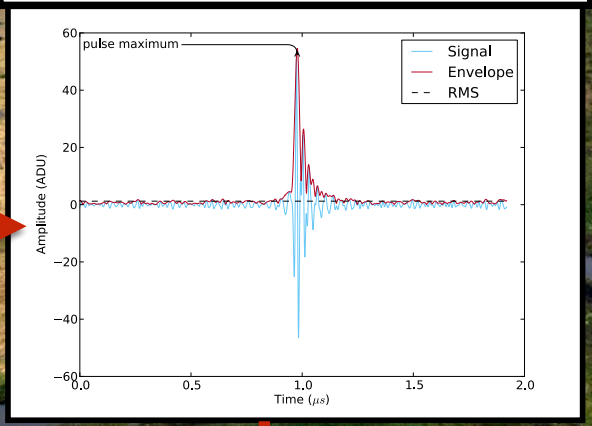

Selection this analysis:
4+ LBA stations

PIERRE AUGER

AERA
Auger Engineering Radio Array

~150 antennas
~17 km²
30-80 MHz

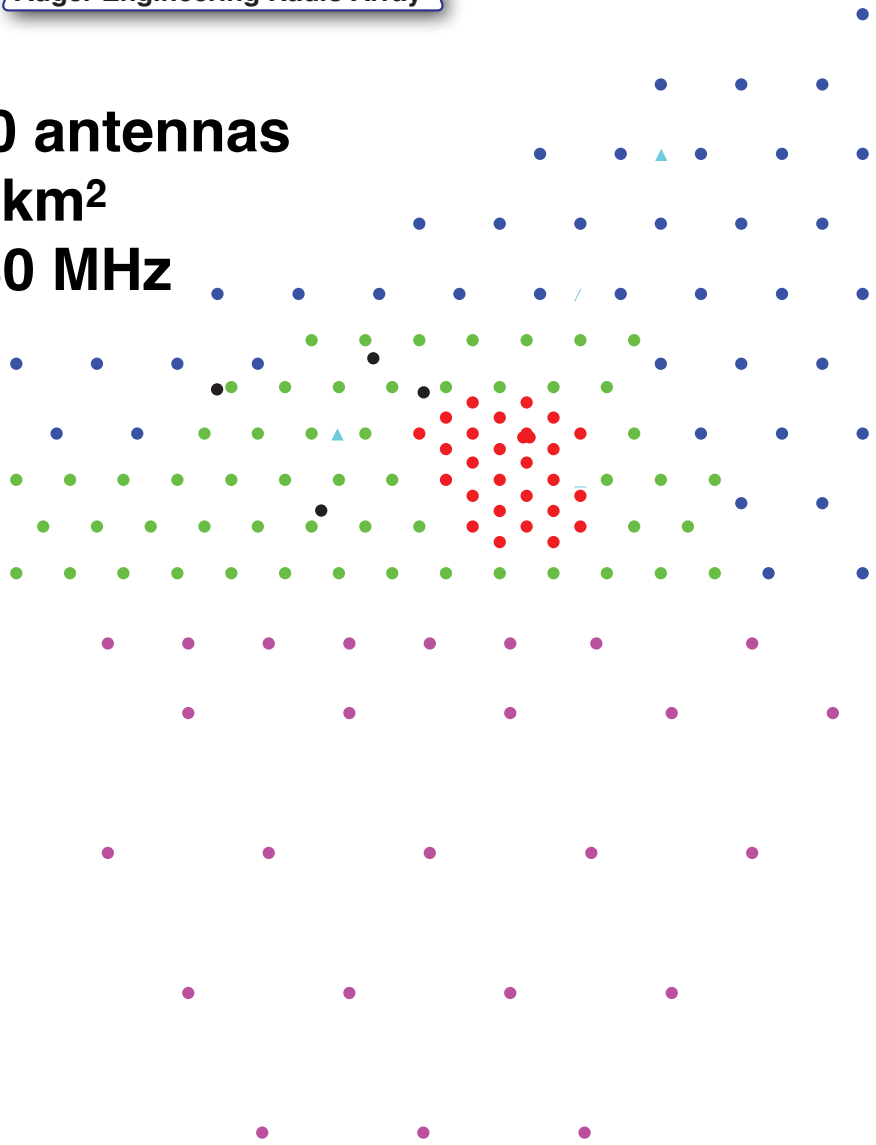

LOFAR core
23 stations ~5 km²

>2000 antennas

1 km

AERA
Auger Engineering Radio Array

PIERRE AUGER

~150 antennas
~17 km²
30-80 MHz

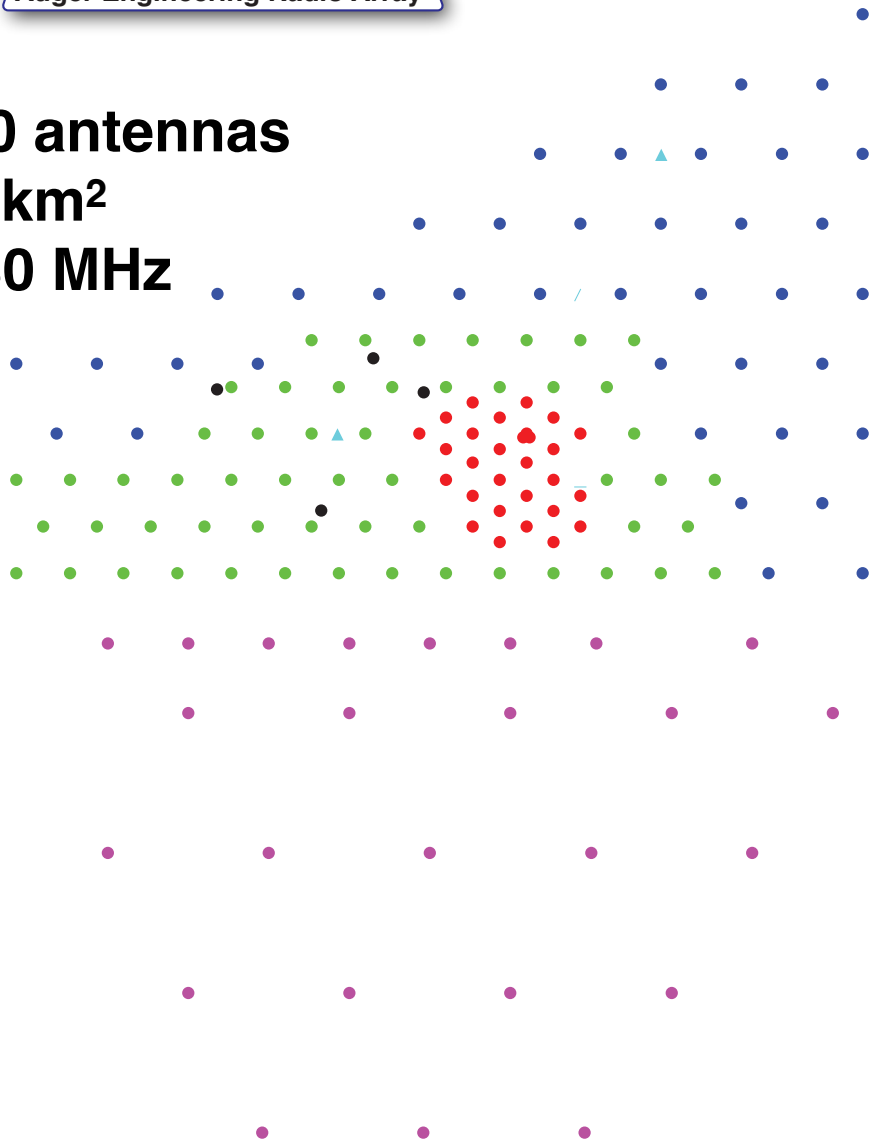

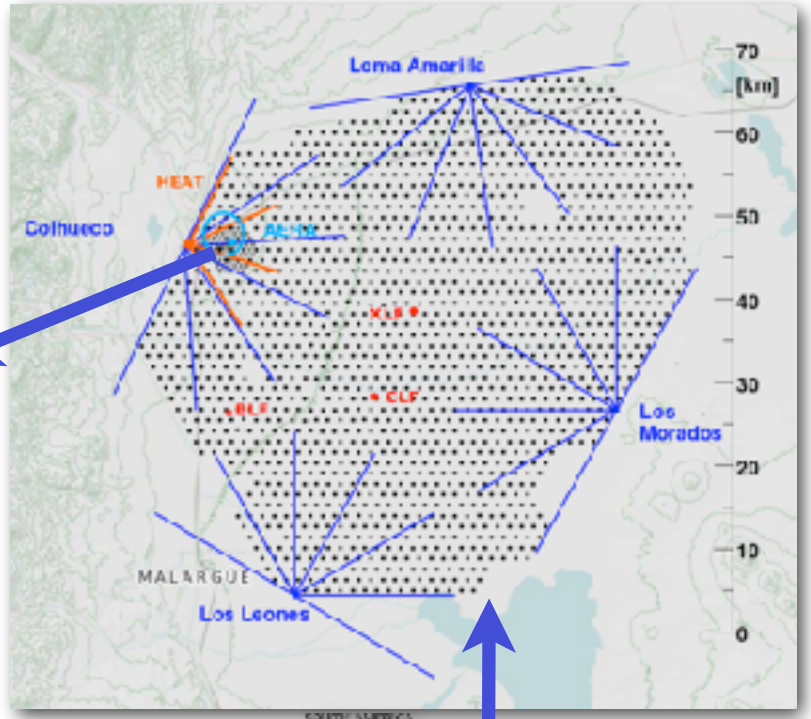

PIERRE AUGER

AERA
Auger Engineering Radio Array

~150 antennas
~17 km²
30-80 MHz

A measured air shower

angular difference particles - radio

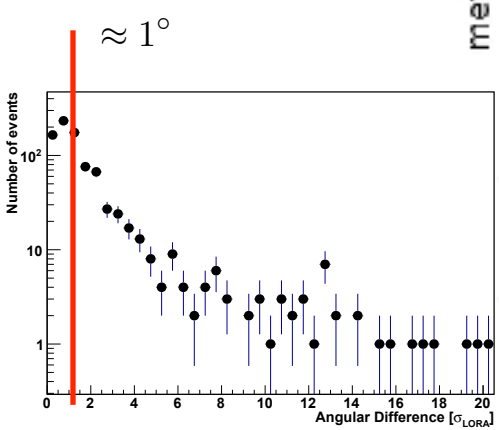

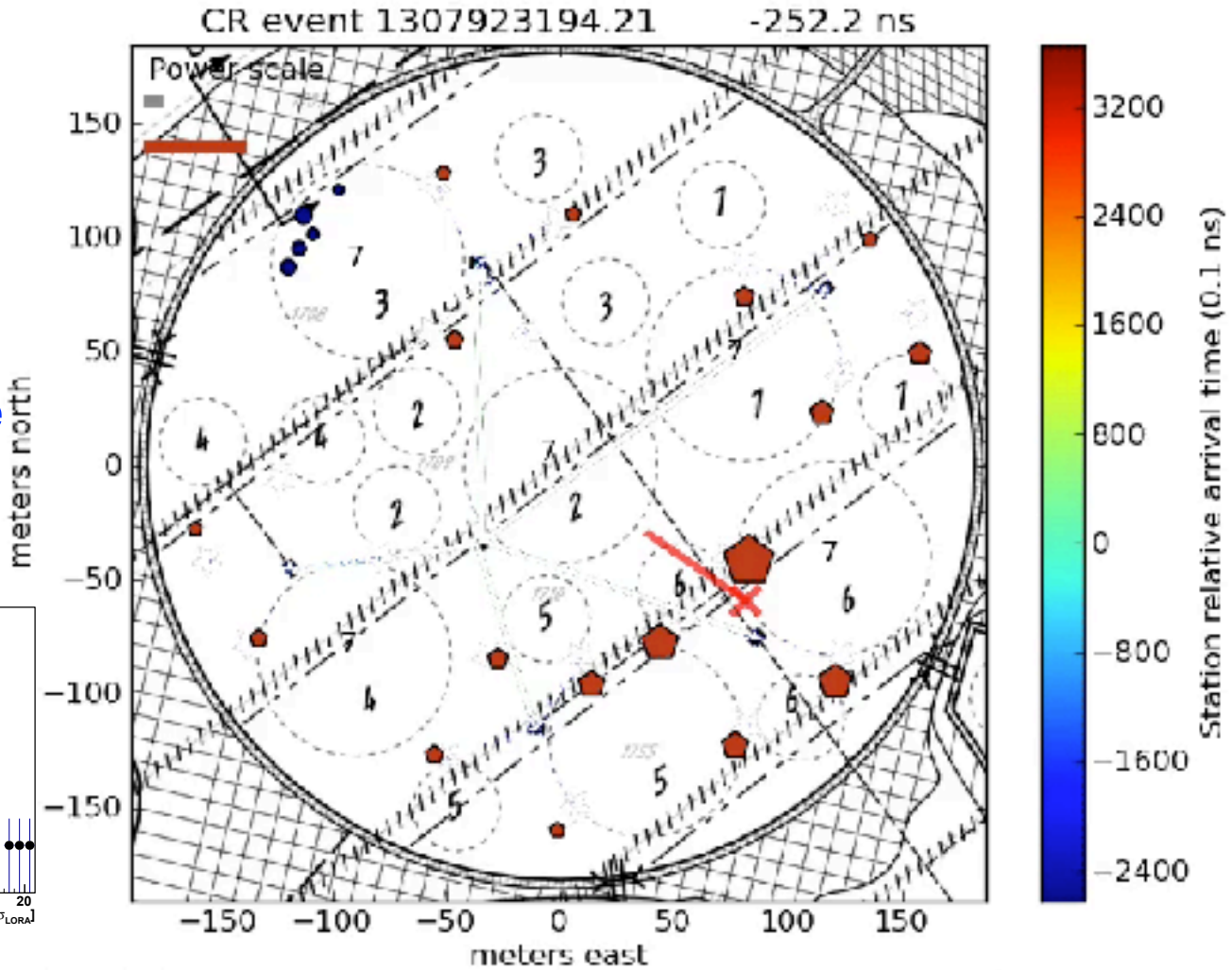

Radiation Processes

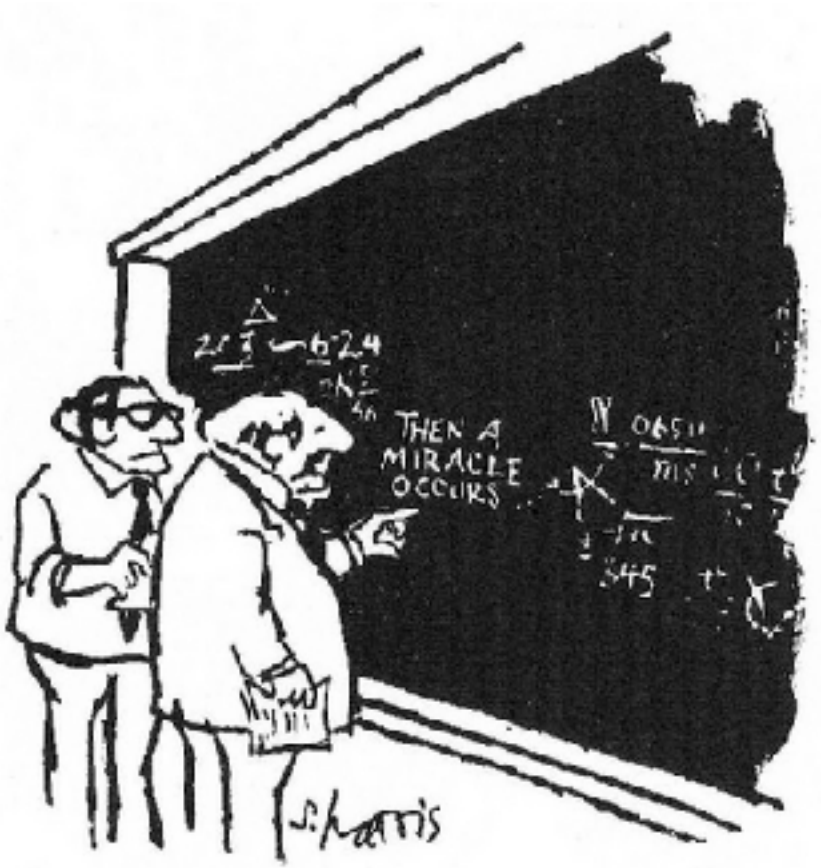

"I think you should be more explicit here in step two."

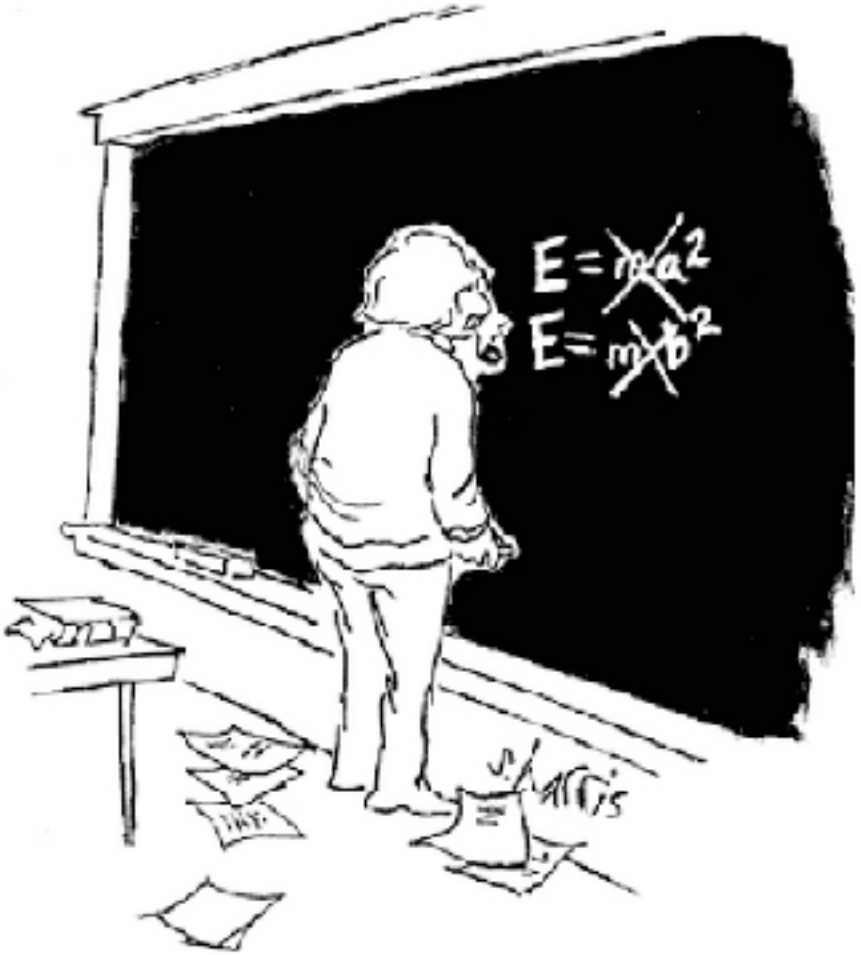

Radio Emission in Air Showers

Mainly: Charge separation in geomagnetic field

$$\vec{E} \propto \vec{v} \times \vec{B}$$

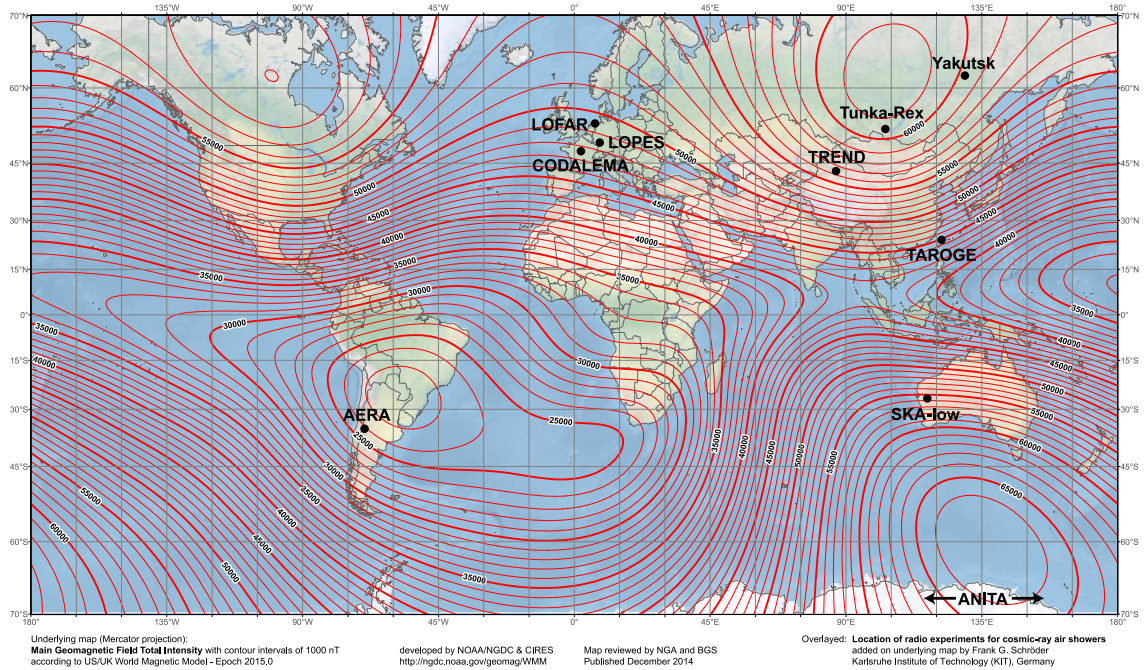

F. Schröder, Prog. Part. Nucl. Phys. 93 (2017) 1

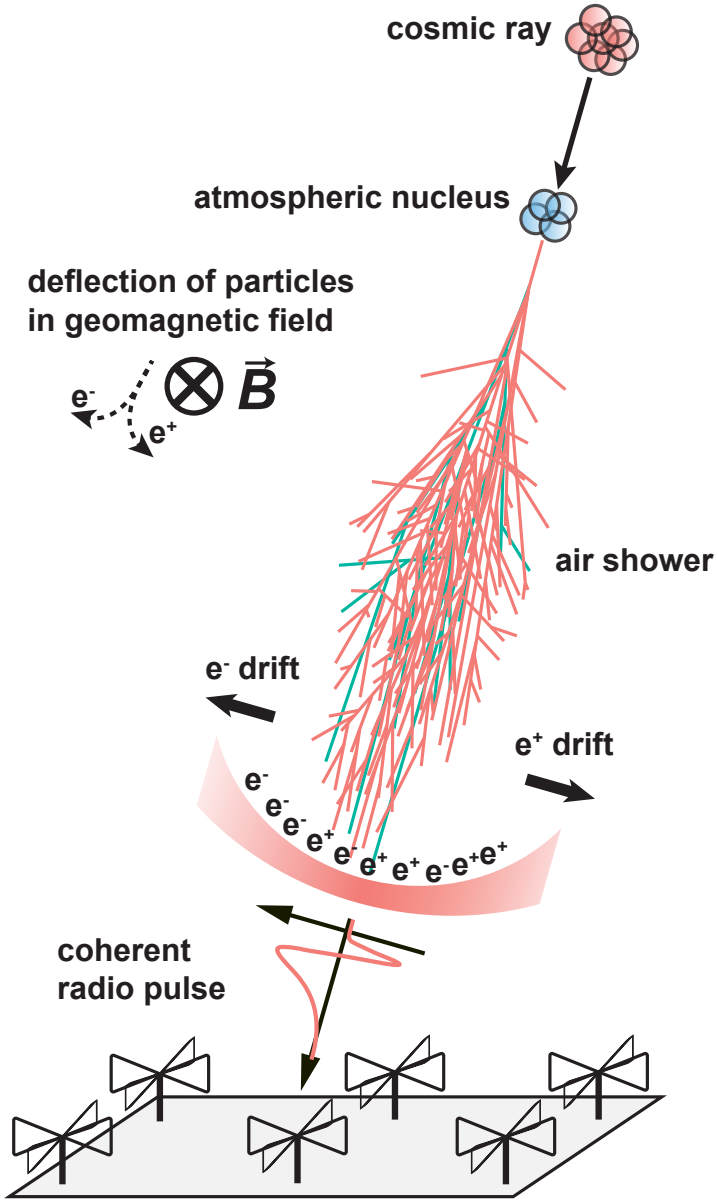

Arrival direction of showers with strong radio signals

north-south asymmetry
v x B effect

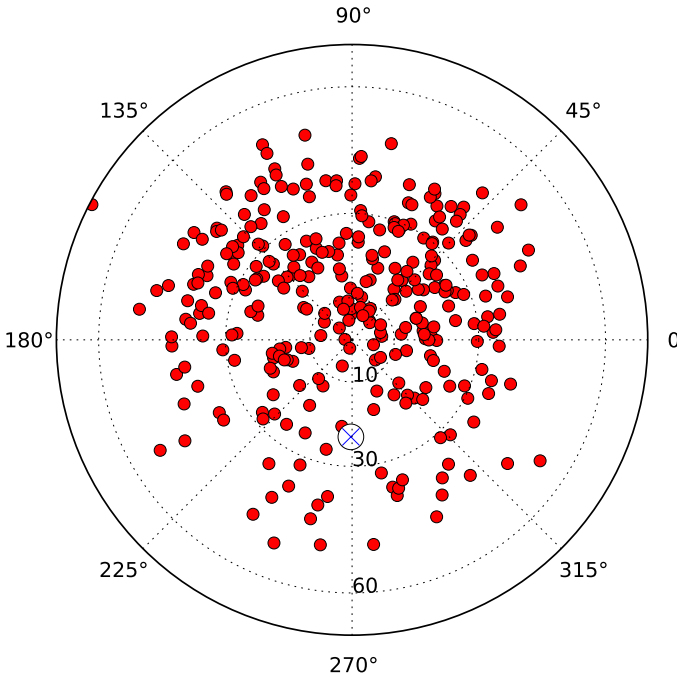

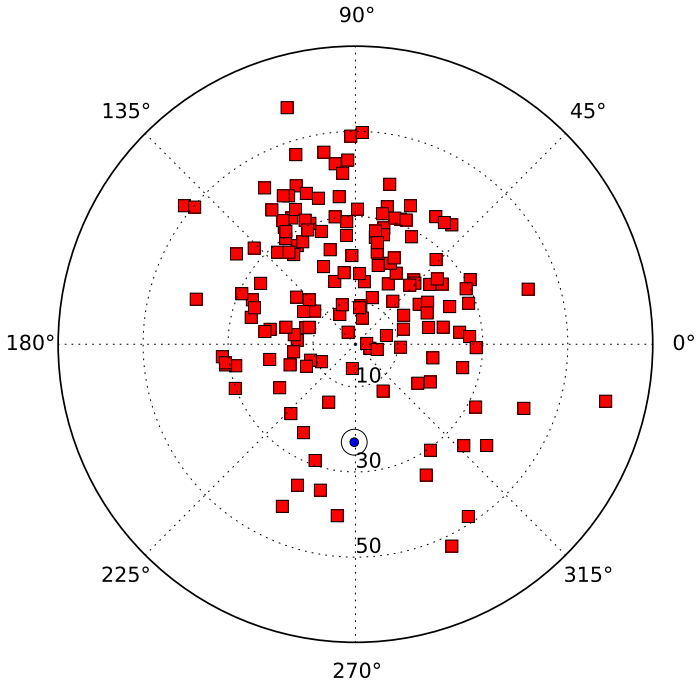

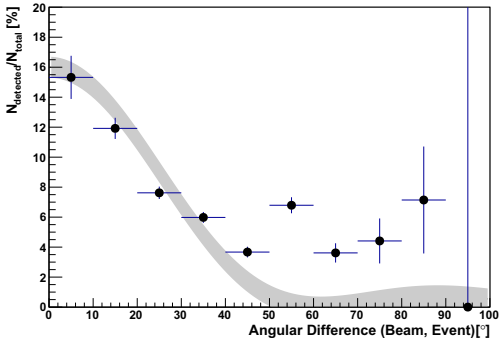

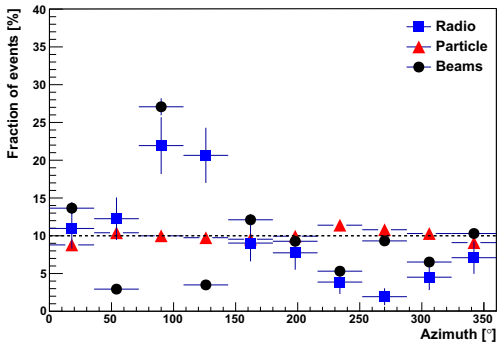

LOFAR

30 - 80 MHz **110 - 190 MHz**

P. Schellart et al., A&A 560 (2013) A98

A. Nelles et al., Astroparticle Physics 65 (2015) 11

Arrival direction of showers with strong radio signals

north-south asymmetry
v x B effect

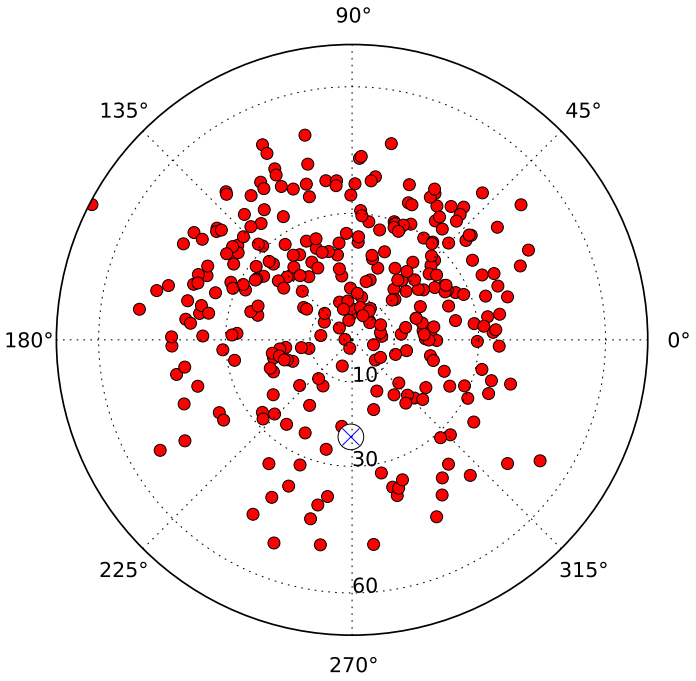

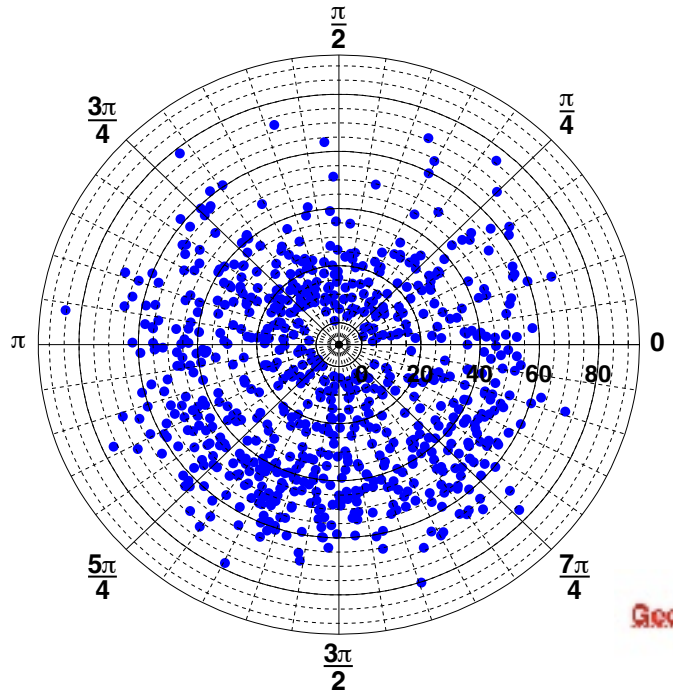

LOFAR

AERA
Auger Engineering Radio Array

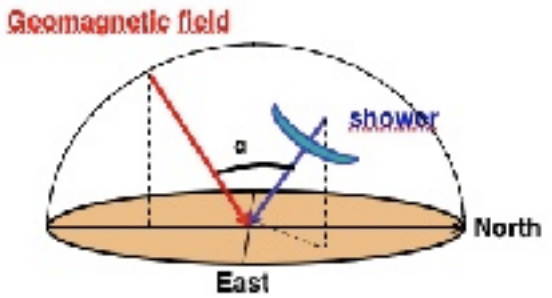

30 - 80 MHz

P. Schellart et al., A&A 560 (2013) A98

Geomagnetic effect

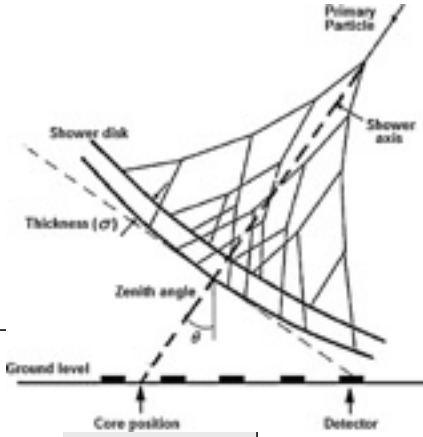

T. Huege / Physics Reports 620 (2016) 1–52

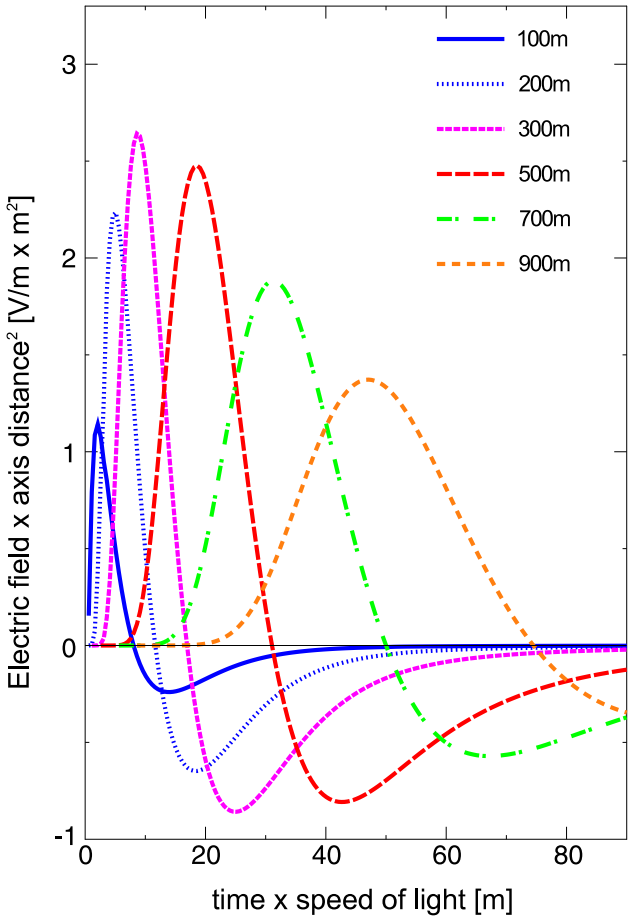

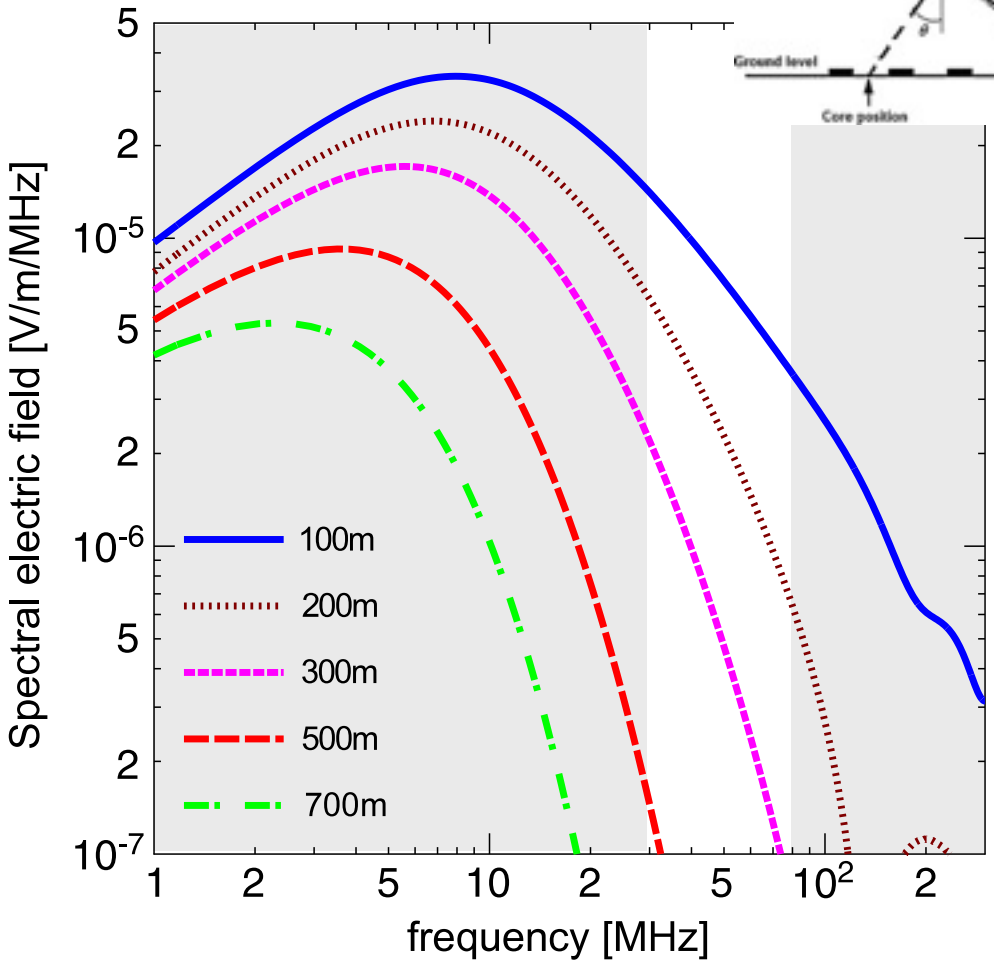

Fig. 4. Radio pulses (top) arising from the time-variation of the geomagnetically induced transverse currents in a 10^{17} eV air shower as observed at various observer distances from the shower axis and their corresponding frequency spectra (bottom). Refractive index effects are not included.
Source: Adapted from [18].

Radio Emission in Air Showers

- **Mainly: Charge separation in geomagnetic field**

$$\vec{E} \propto \vec{v} \times \vec{B}$$

Theory predicts additional mechanisms:

- **excess of electrons in shower: charge excess**
- **superposition of emission due to Cherenkov effects in atmosphere**

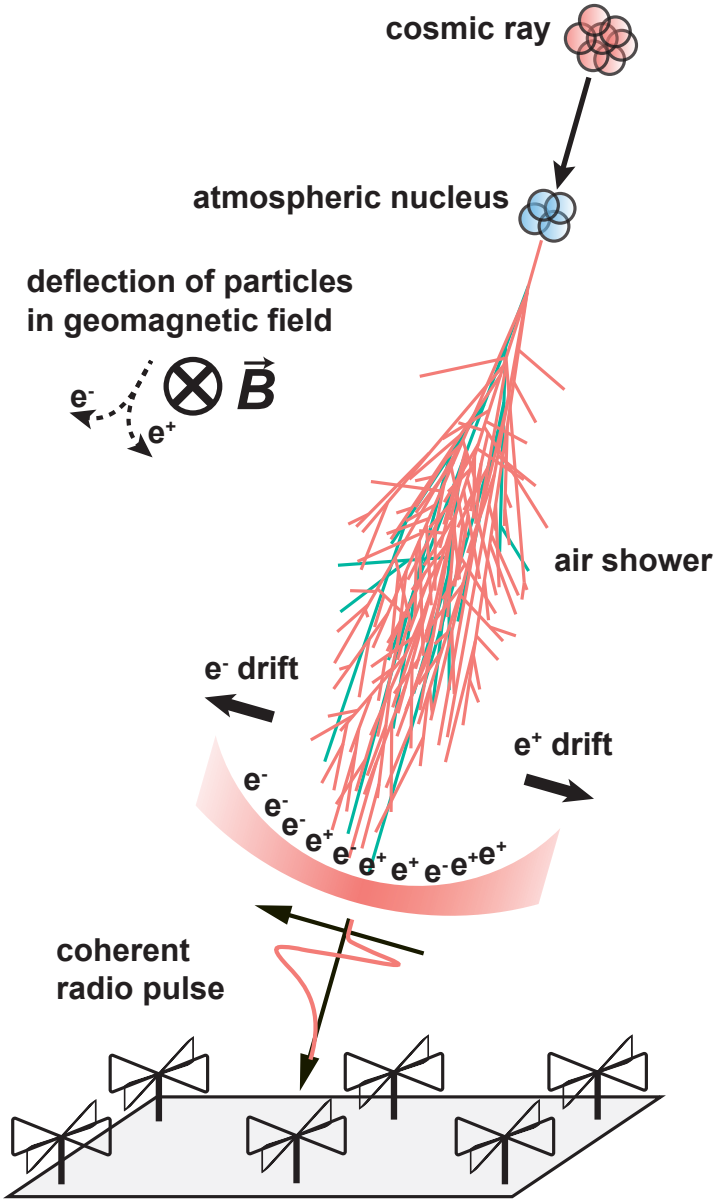

polarization of radio signal

geomagnetic **Askaryan**

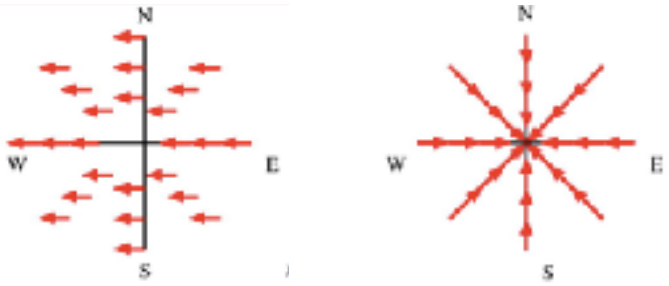

Polarization footprint

of an individual air shower

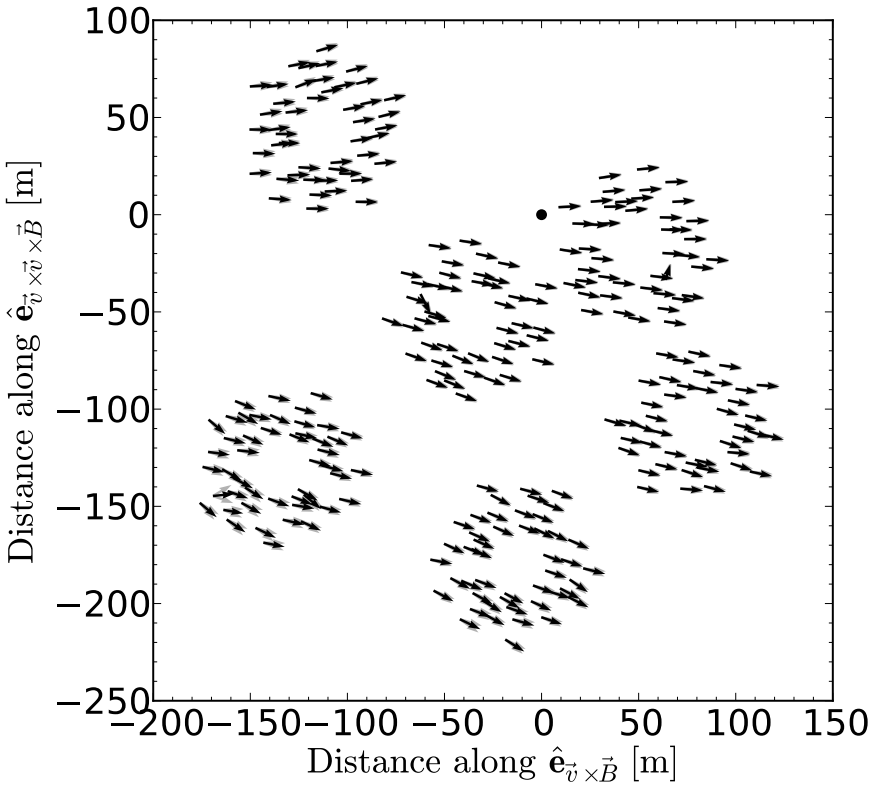

geomagnetic

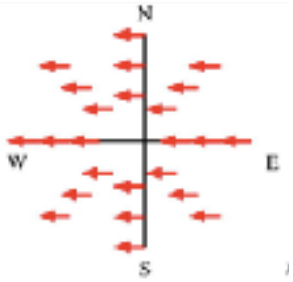

Askaryan

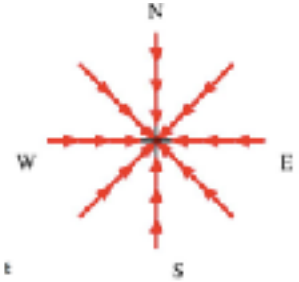

LOFAR

P. Schellart et al., JCAP 10 (2014) 014

Charge excess fraction

Askaryan
geomagnetic

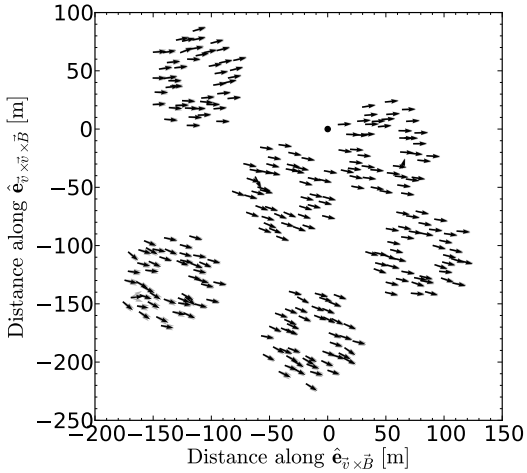

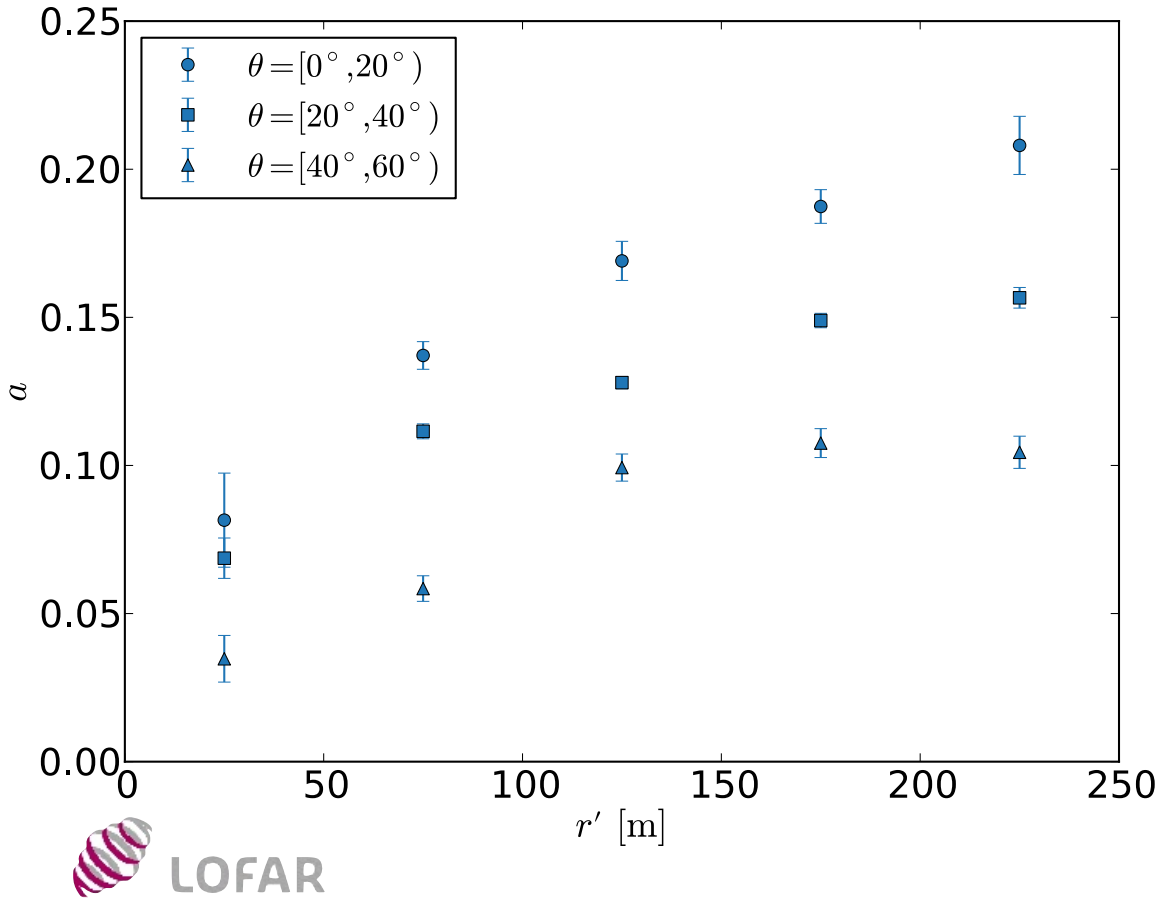

geomagnetic **Askaryan**

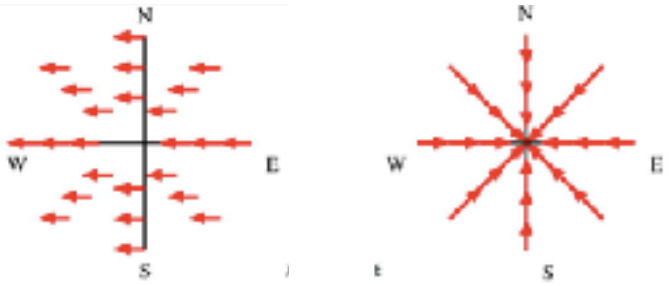

P. Schellart et al., JCAP 10 (2014) 014

Charge excess fraction

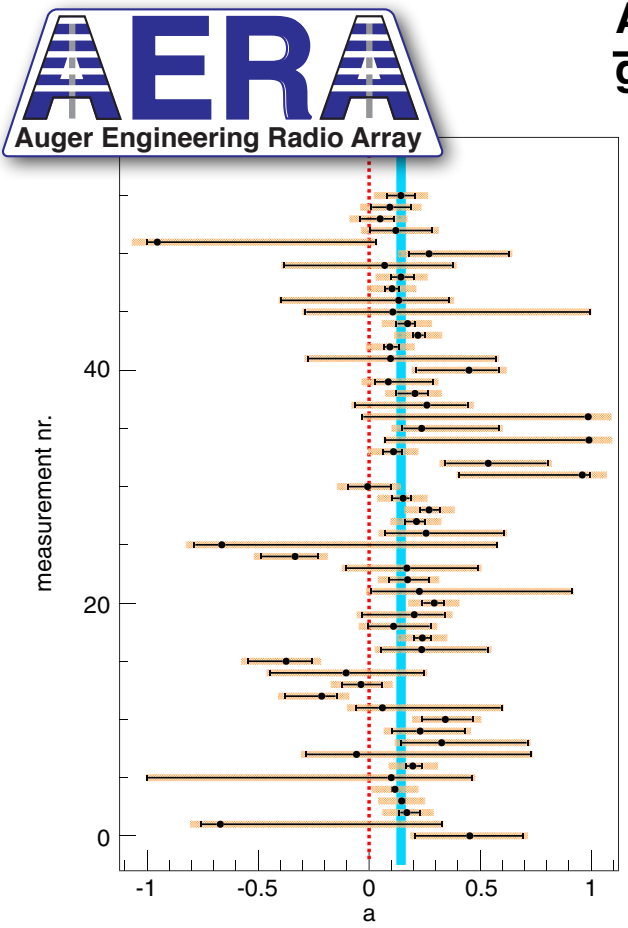

Askaryan
geomagnetic

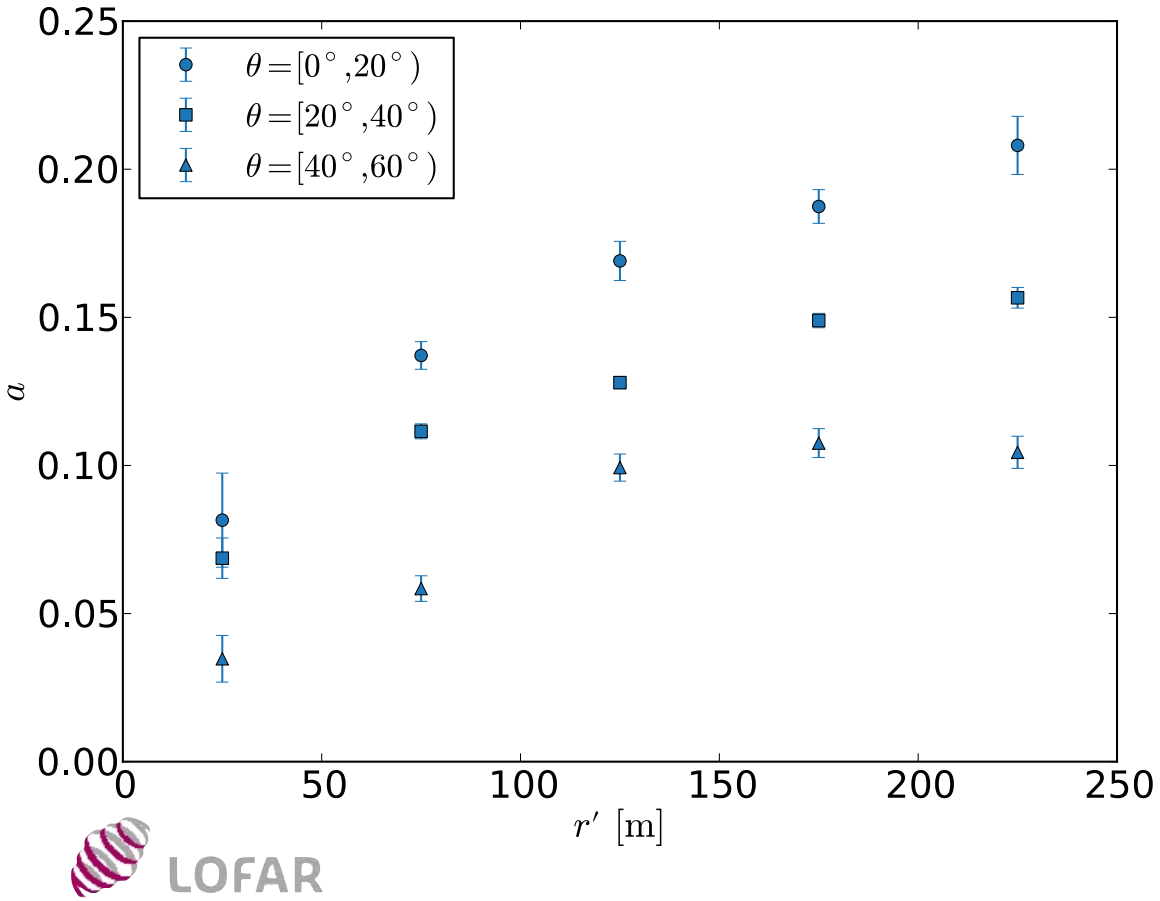

LOFAR

A. Aab, PRD 89 (2014) 052002

P. Schellart et al., JCAP 10 (2014) 014

Footprint of radio emission on the ground

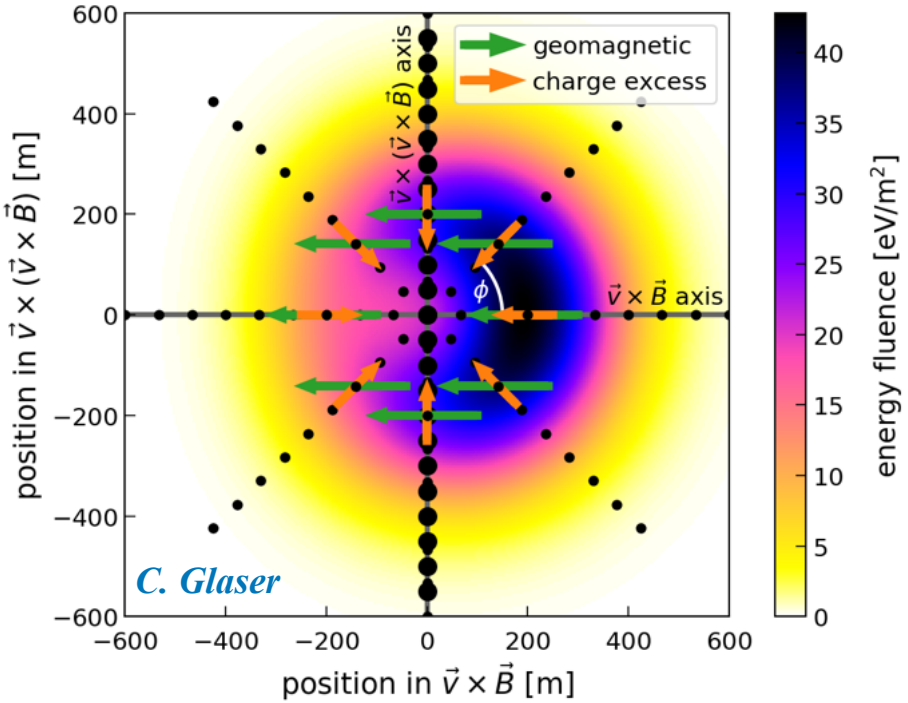

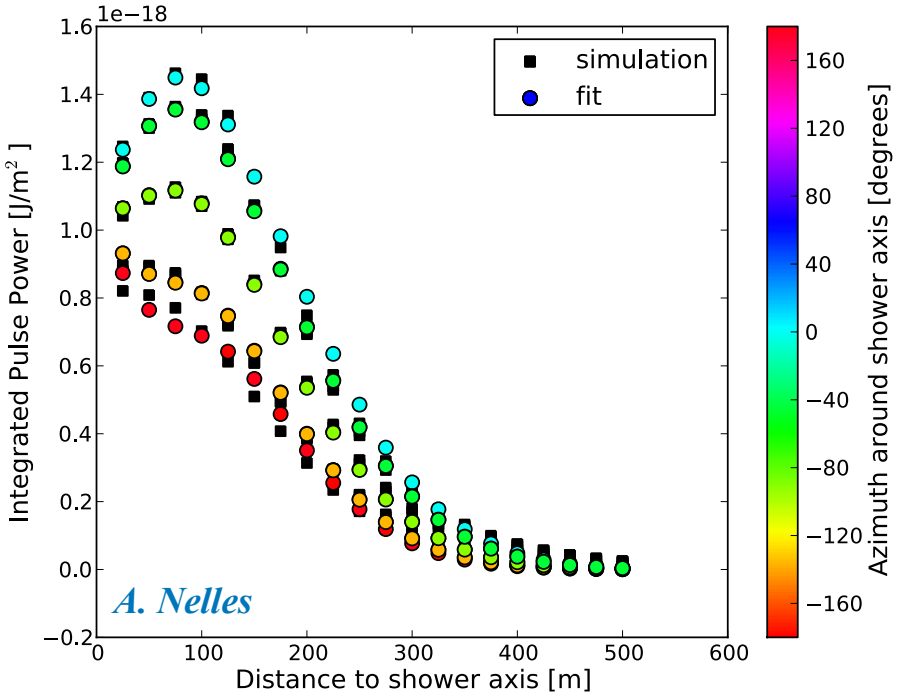

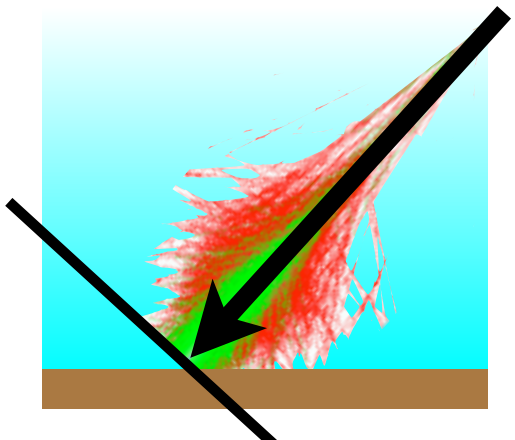

Lateral distribution of radio signals

not rotationally symmetric —> fit two Gaussian functions

v x (v x B)

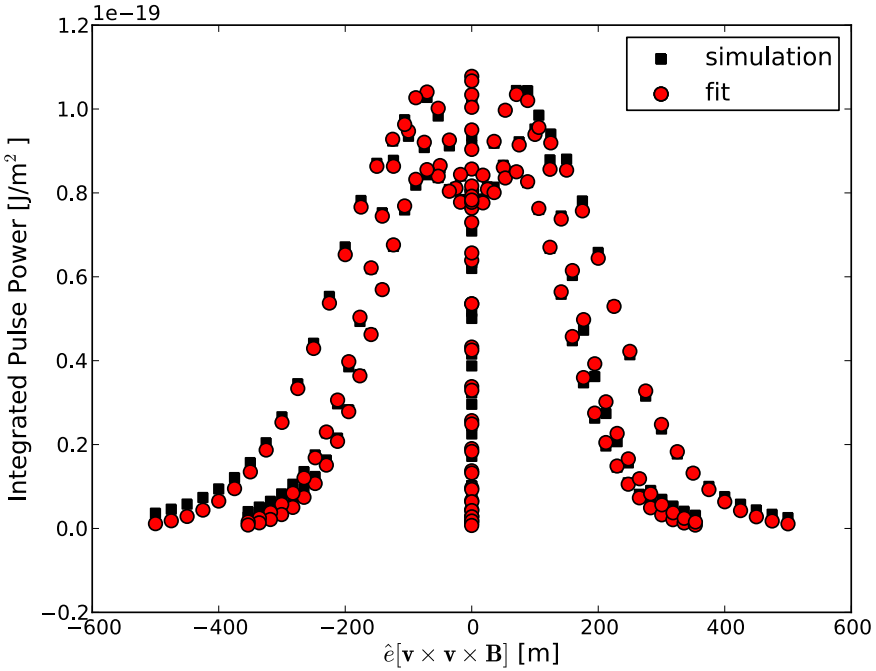

v x B

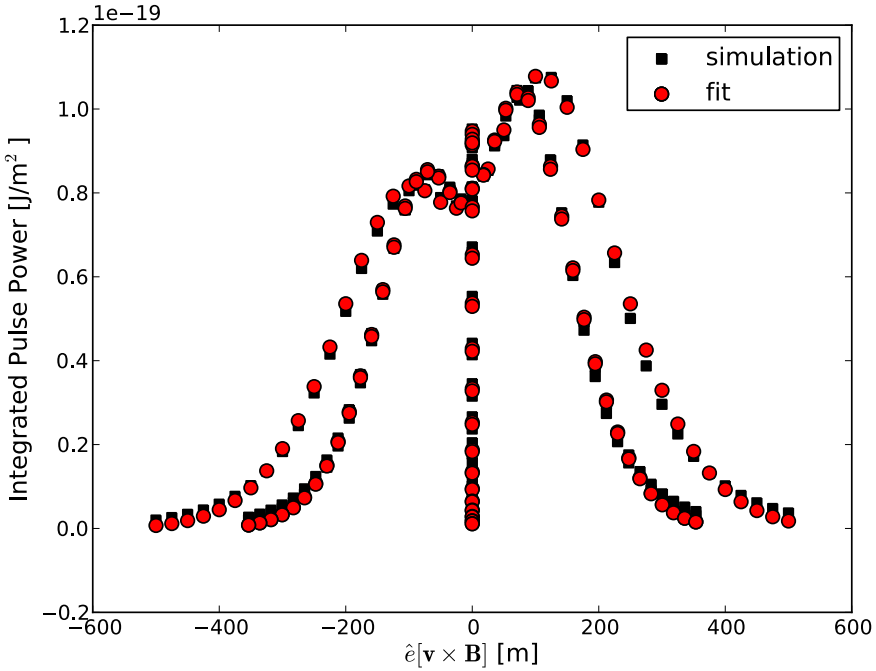

$$P(x',y') = A_+ \cdot \exp\left(\frac{-[(x'-X_+)^2+(y'-Y_+)^2]}{\sigma_+^2}\right) - A_- \cdot \exp\left(\frac{-[(x'-X_-)^2+(y'-Y_-)^2]}{\sigma_-^2}\right) + O$$

A. Nelles et al., Astropart. Phys. 60 (2015) 13

Properties of incoming cosmic ray

- direction
- energy
- type

Direction

Shape of Shower Front

fit quality

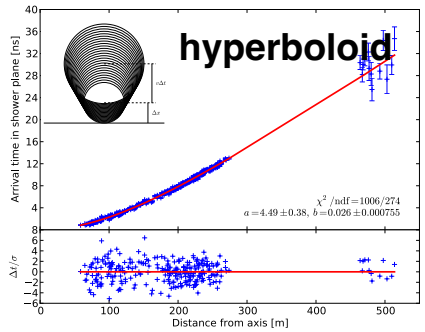

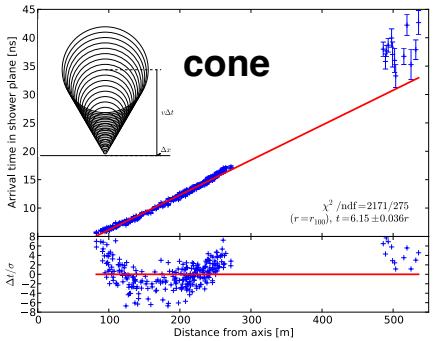

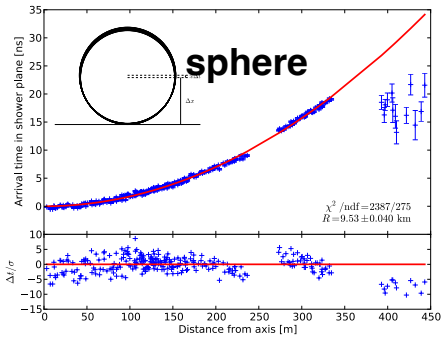

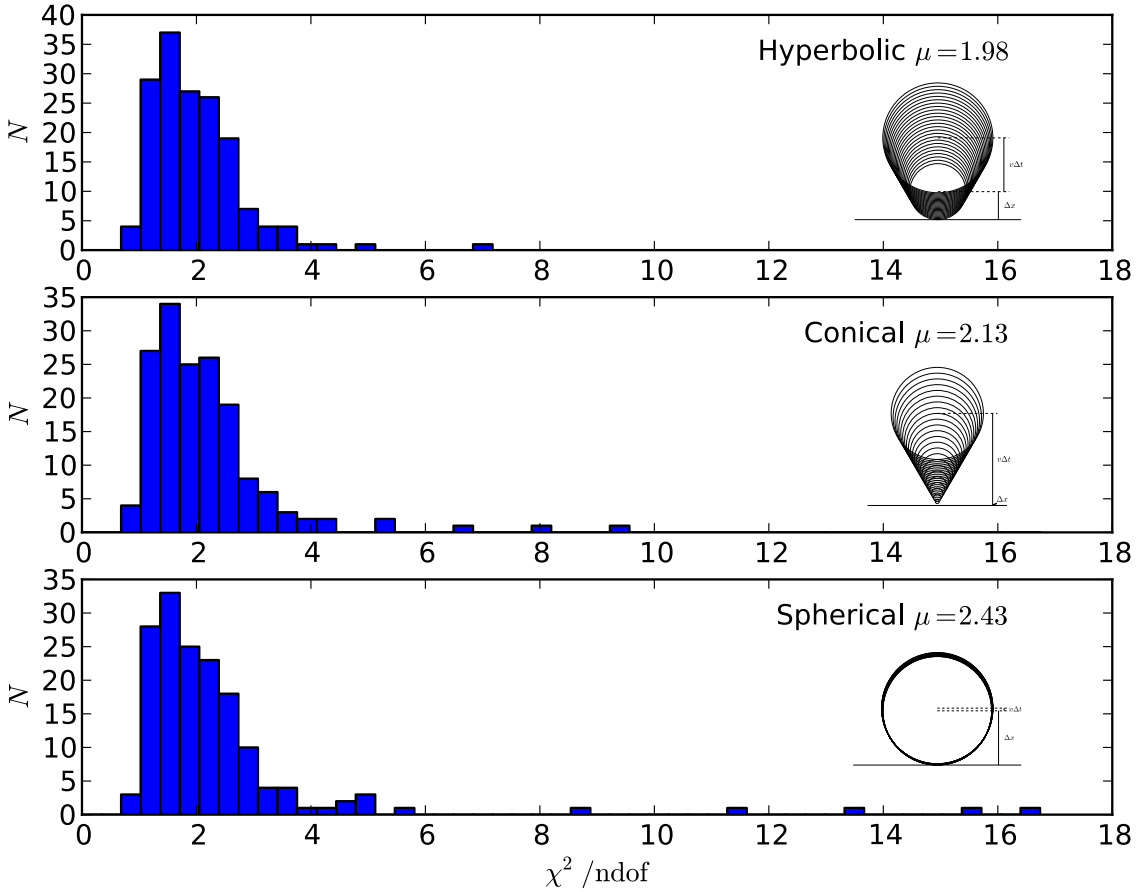

A. Corstanje et al., Astropart. Phys. 61 (2015) 22

Shape of Shower Front

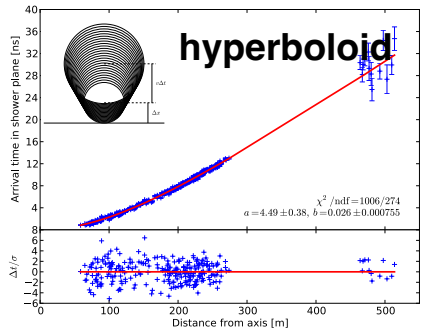

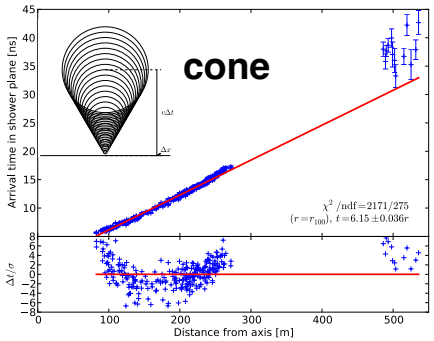

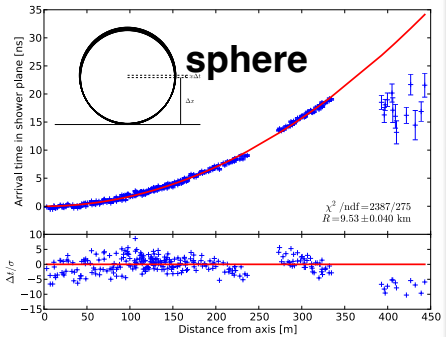

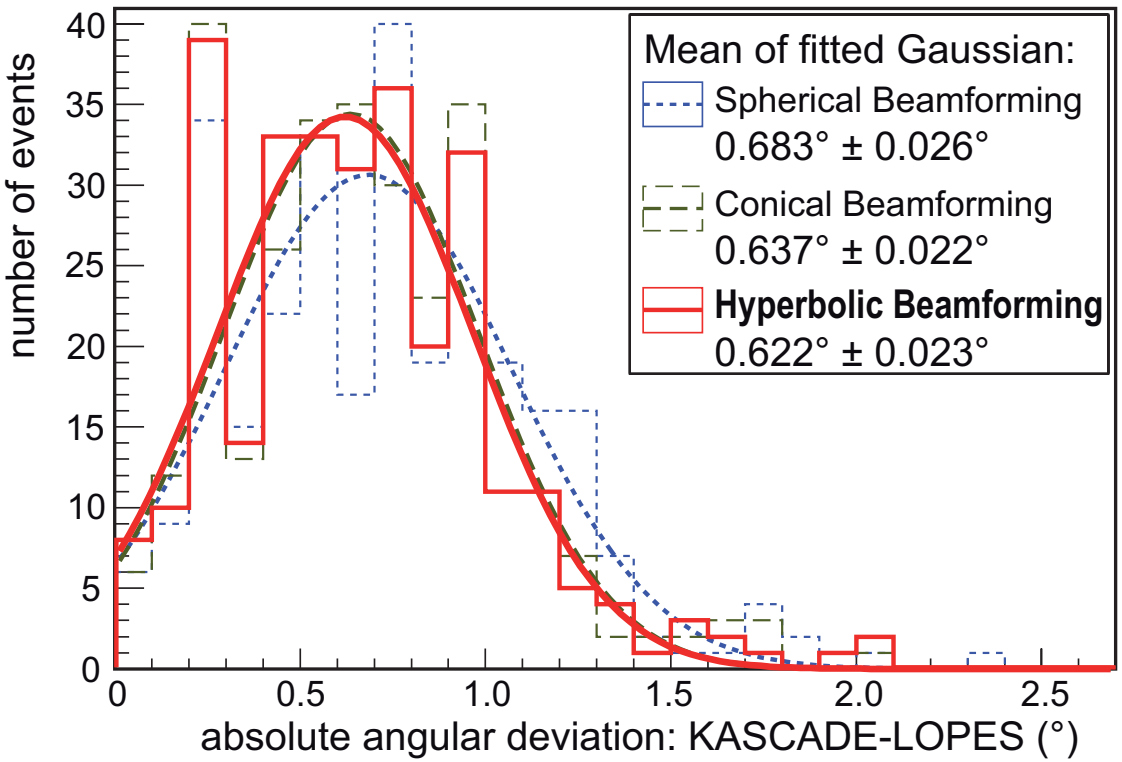

W.D. Apel et al., JCAP 1409 (2014) no.09, 025

A. Corstanje et al., Astropart. Phys. 61 (2015) 22

Accuracy of Shower Direction

angular difference between..

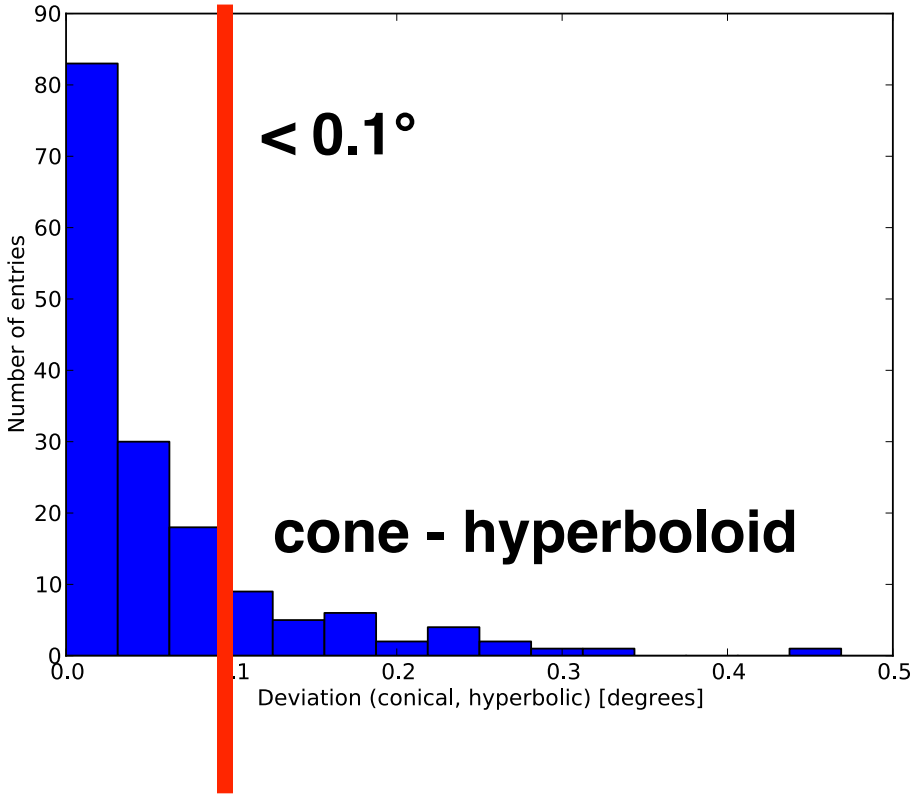

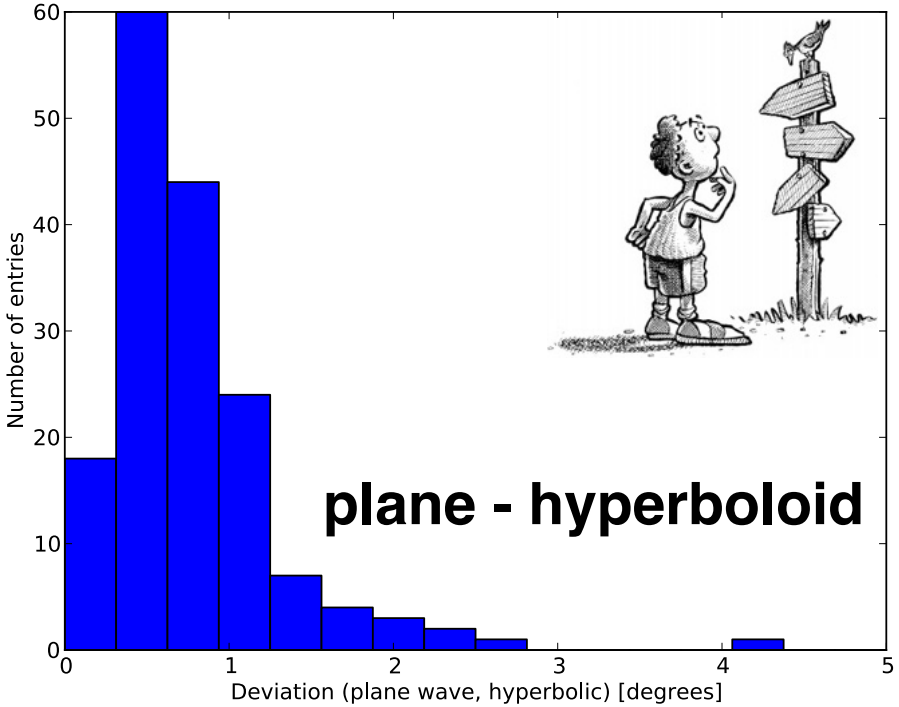

LOFAR

A. Corstanje et al., Astropart. Phys. 61 (2015) 22

Energy

Energy of primary particle

LOFAR

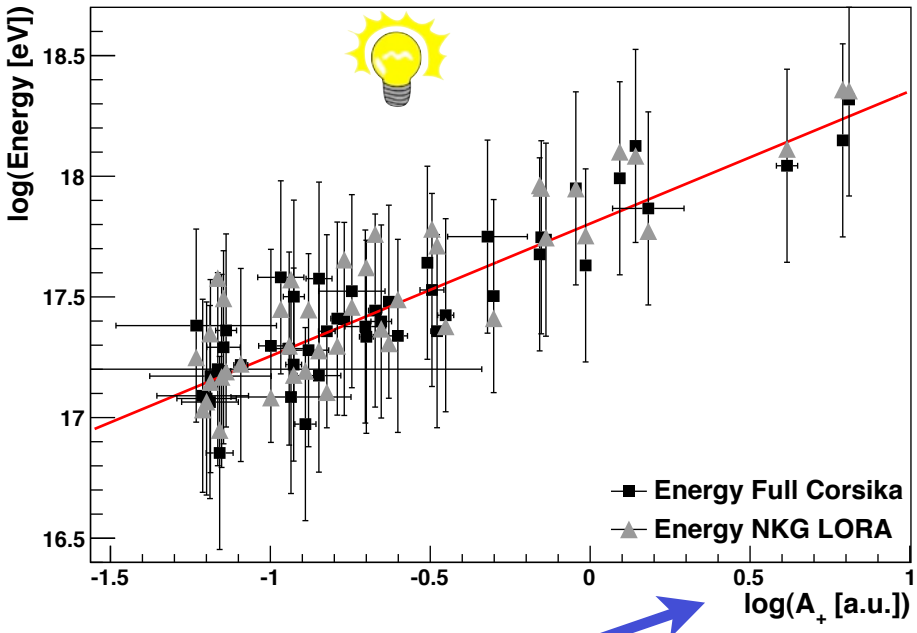

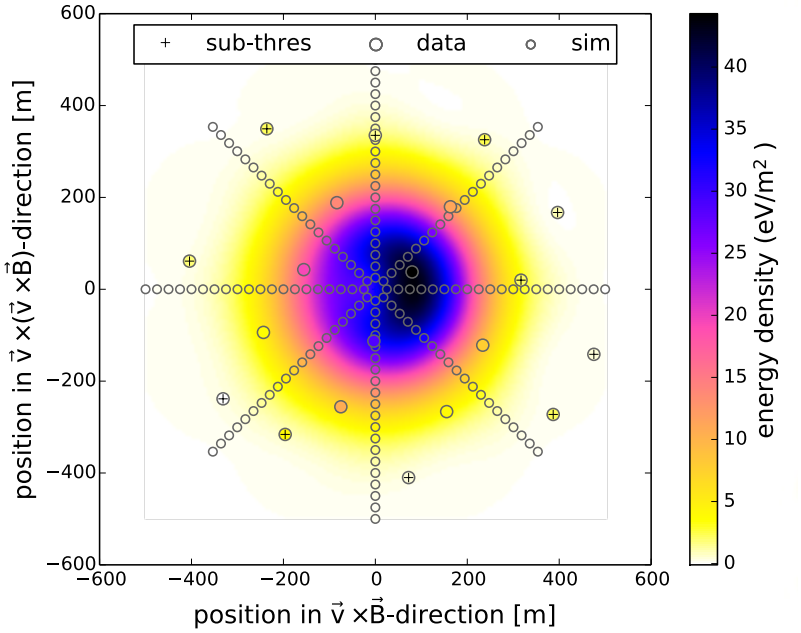

$$P(x', y') = A_+ \cdot \exp\left(\frac{-[(x' - X_+)^2 + (y' - Y_+)^2]}{\sigma_+^2}\right) - A_- \cdot \exp\left(\frac{-[(x' - X_-)^2 + (y' - Y_-)^2]}{\sigma_-^2}\right) + O$$

A. Nelles et al., JCAP 05 (2015) 018

Measurement of the Radiation Energy in the Radio Signal of Extensive Air Showers as a Universal Estimator of Cosmic-Ray Energy

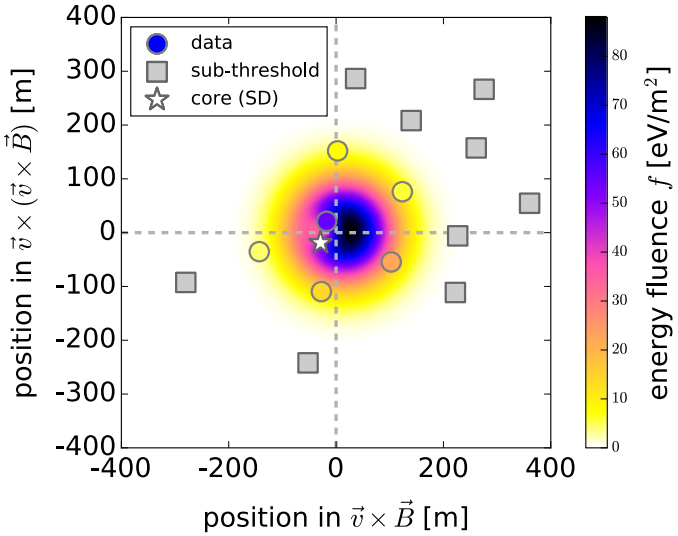

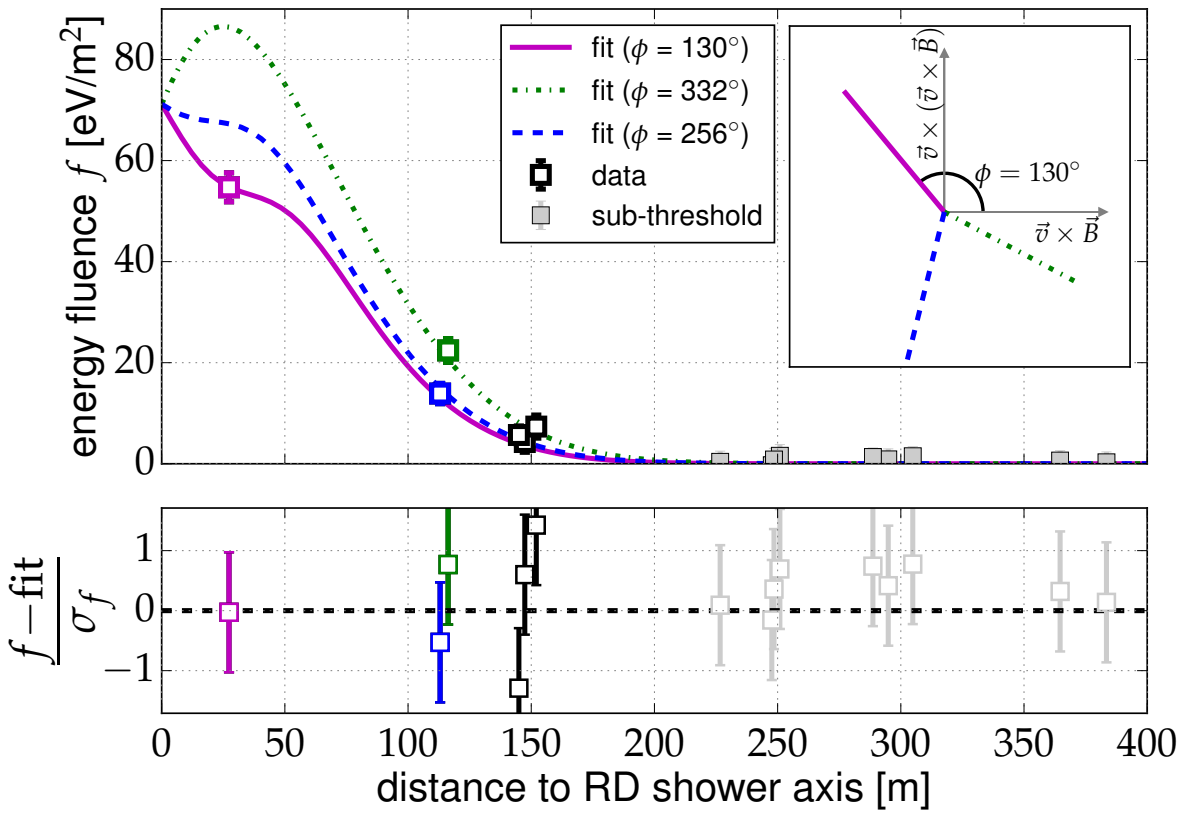

A. Aab et al., PRL 116 (2016) no.24, 241101

Measurement of the Radiation Energy in the Radio Signal of Extensive Air Showers as a Universal Estimator of Cosmic-Ray Energy

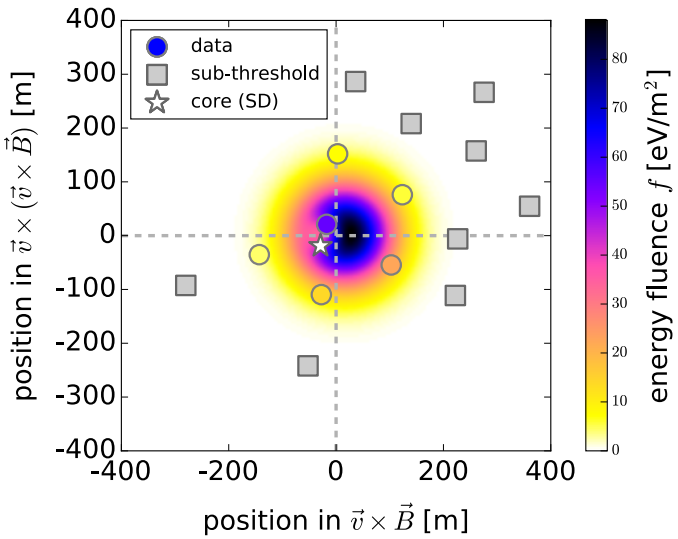

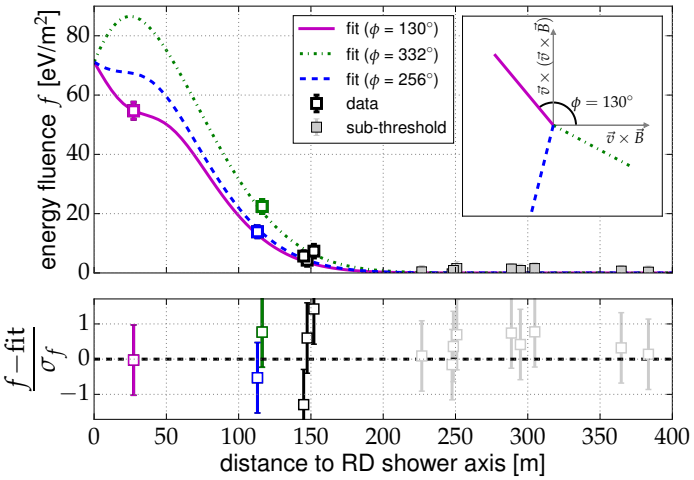

$E_{30\text{-}80\ \mathrm{MHz}}$ = 15.8 MeV @ 10^{18} eV

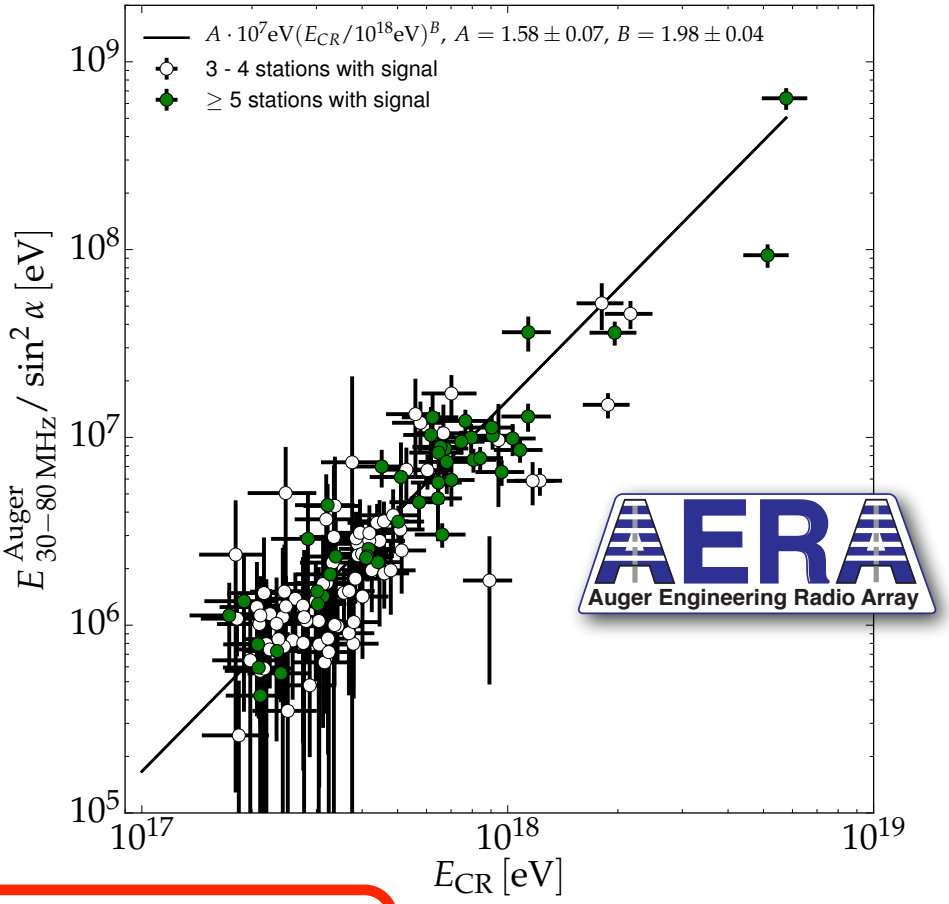

$$E_{30\text{-}80\ \mathrm{MHz}} = (15.8 \pm 0.7(\mathrm{stat}) \pm 6.7(\mathrm{syst})\ \mathrm{MeV}) \times \left(\sin\alpha \frac{E_{CR}}{10^{18}\ \mathrm{eV}} \frac{B_{Earth}}{0.24\ \mathrm{G}}\right)^2$$

A. Aab et al., PRL 116 (2016) no.24, 241101

Energy Estimation of Cosmic Rays with the Engineering Radio Array of the Pierre Auger Observatory

$E_{30\text{-}80\ \mathrm{MHz}} = 15.8\ \mathrm{MeV}\ @\ 10^{18}\ \mathrm{eV}$

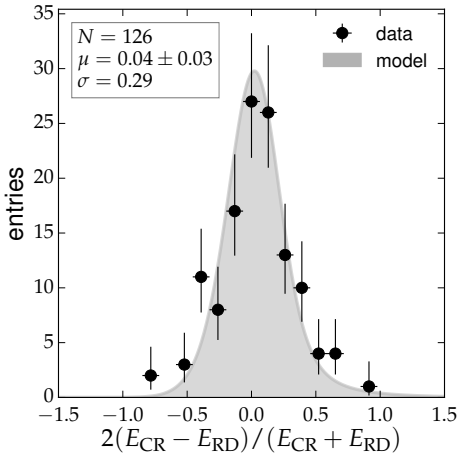

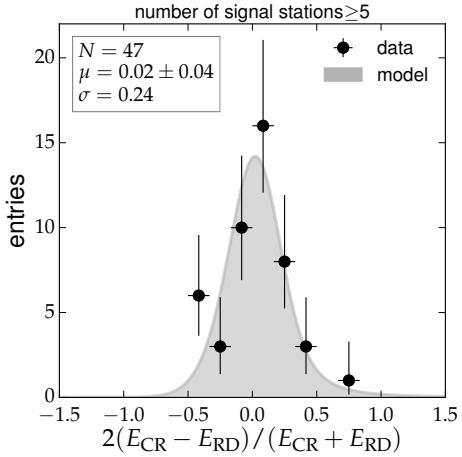

$$\sigma \approx 24\%$$

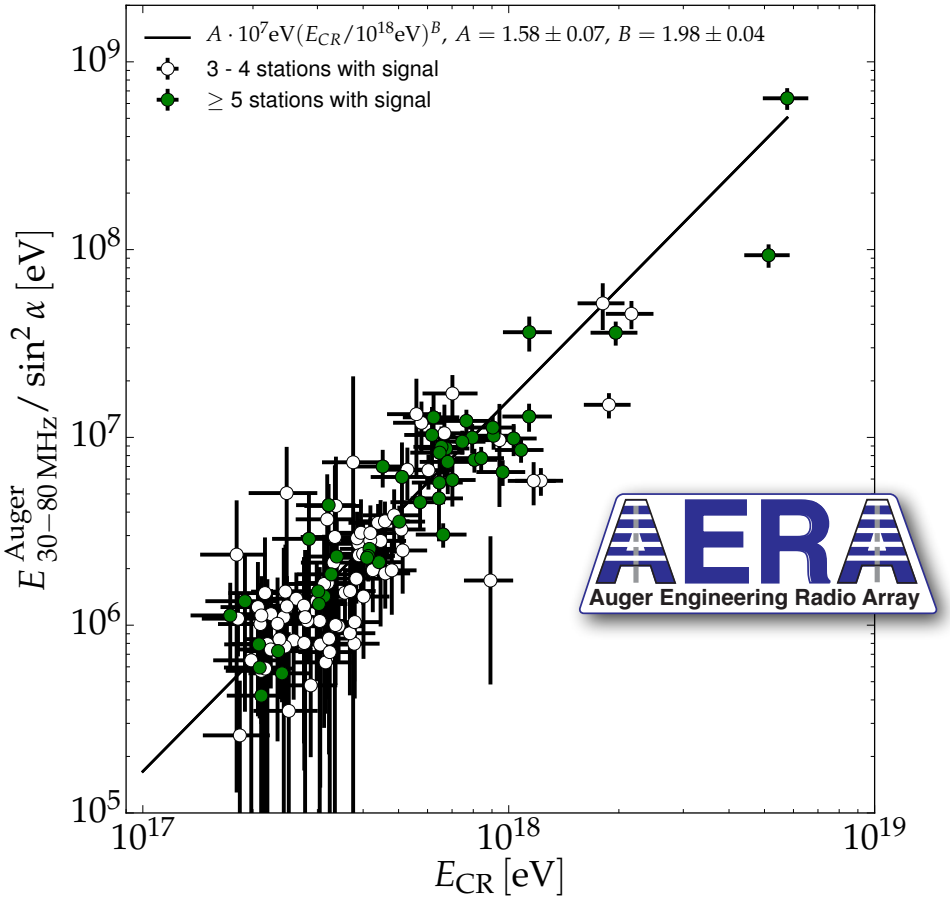

A. Aab et al., PRD 93 (2016) no.12, 122005

A. Aab et al., PRL 116 (2016) no.24, 241101

Mass

Properties of primary particle

energy

distance to Xmax

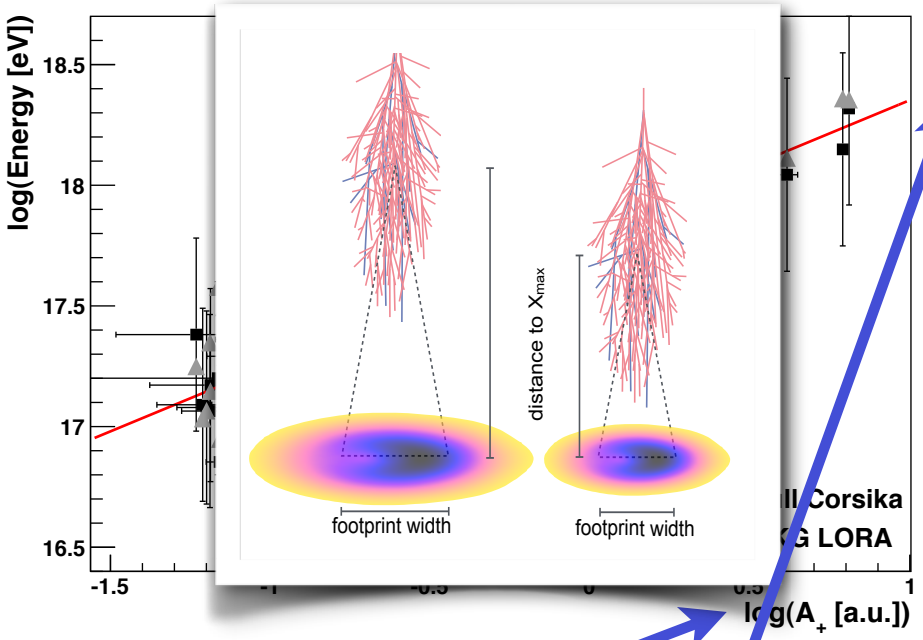

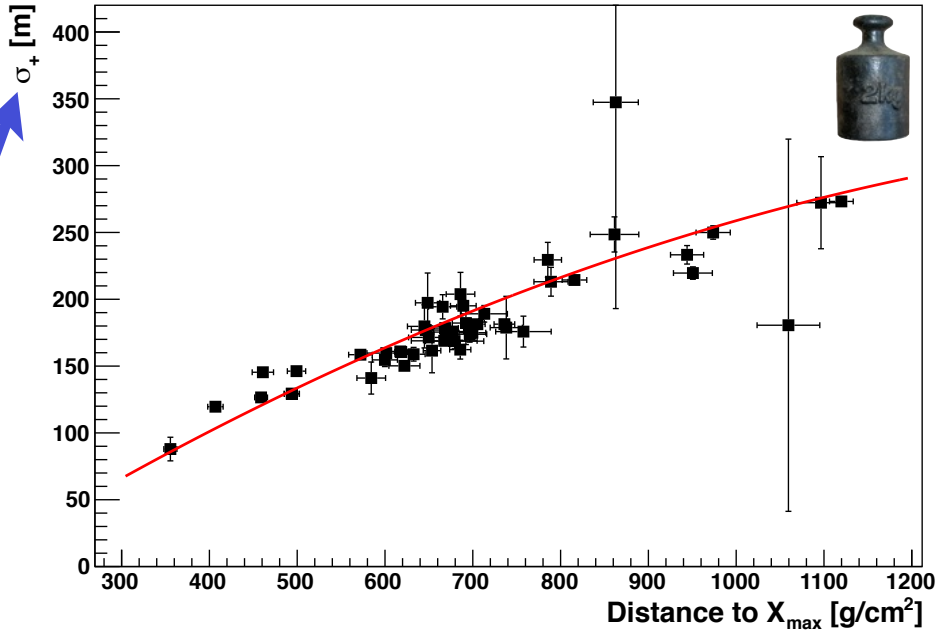

$$P(x',y') = A_+ \cdot \exp\left(\frac{-[(x'-X_+)^2+(y'-Y_+)^2]}{\sigma_+^2}\right) - A_- \cdot \exp\left(\frac{-[(x'-X_-)^2+(y'-Y_-)^2]}{\sigma_-^2}\right) + O$$

LOFAR

A. Nelles et al., JCAP 05 (2015) 018

Measurement of particle mass

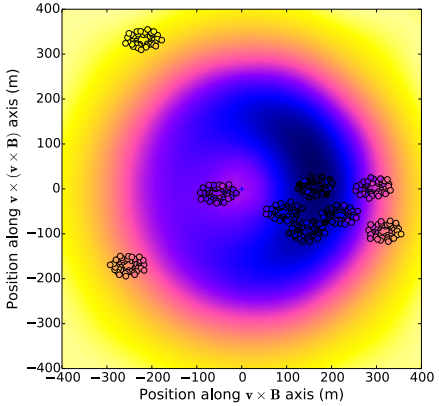

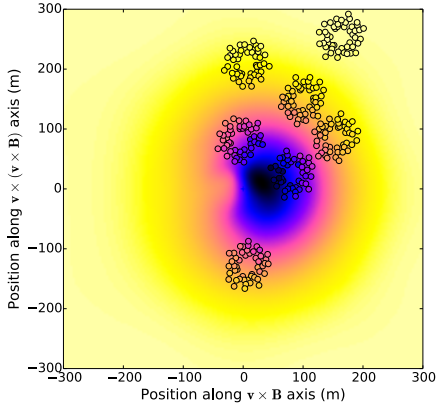

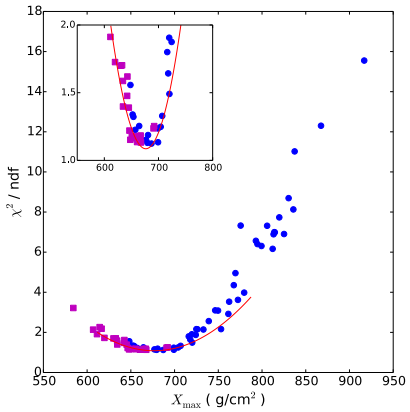

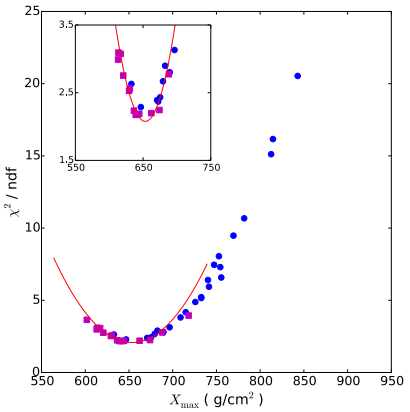

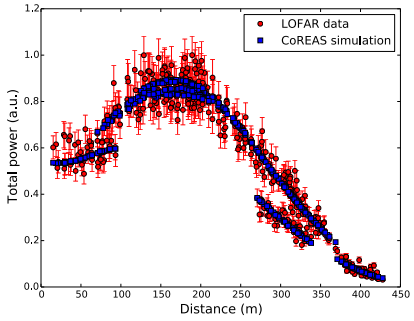

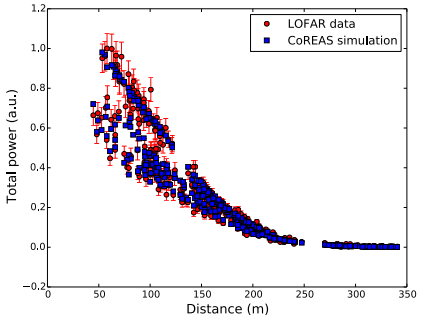

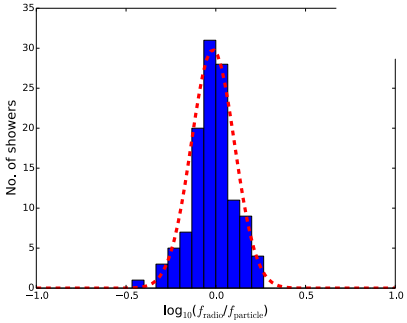

$\sigma_E \approx 32\%$

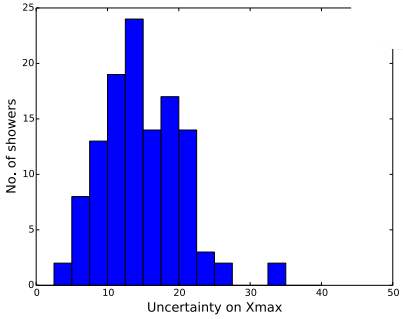

$\sigma_{X_{max}} \approx 17$ g/cm^2

S. Buitink et al., PRD 90 (2014) 082003

Depth of the shower maximum

LETTER nature
doi:10.1038/nature16976

A large light-mass component of cosmic rays at 10^{17}–$10^{17.5}$ electronvolts from radio observations

S. Buitink[1,2], A. Corstanje[2], H. Falcke[2,3,4,5], J. R. Hörandel[2,4], T. Huege[6], A. Nelles[2,7], J. P. Rachen[2], L. Rossetto[2], P. Schellart[2], O. Scholten[8,9], S. ter Veen[2], S. Thoudam[2], T. N. G. Trinh[8], J. Anderson[10], A. Asgekar[1,11], I. M. Avruch[12,13], M. E. Bell[14], M. J. Bentum[3,15], G. Bernardi[16,17], P. Best[18], A. Bonafede[19], F. Breitling[20], J. W. Broderick[21], W. N. Brouw[3,13], M. Brüggen[19], H. R. Butcher[22], D. Carbone[23], B. Ciardi[24], J. E. Conway[25], F. de Gasperin[19], E. de Geus[3,26], A. Deller[3], R.-J. Dettmar[27], G. van Diepen[2], S. Duscha[3], J. Eislöffel[28], D. Engels[29], J. E. Enriquez[2], R. A. Fallows[3], R. Fender[30], C. Ferrari[31], W. Frieswijk[3], M. A. Garrett[3,32], J. M. Grießmeier[33,34], A. W. Gunst[3], M. P. van Haarlem[3], T. E. Hassall[21], G. Heald[3,13], J. W. T. Hessels[3,23], M. Hoeft[28], A. Horneffer[2], M. Iacobelli[2], H. Intema[32,35], E. Juette[27], A. Karastergiou[30], V. I. Kondratiev[3,36], M. Kramer[2,37], M. Kuniyoshi[38], G. Kuper[2], J. van Leeuwen[3,23], G. M. Loose[2], P. Maat[3], G. Mann[29], S. Markoff[21], R. McFadden[3], D. McKay-Bukowski[39,40], J. P. McKean[3,13], M. Mevius[3,13], D. D. Mulcahy[21], H. Munk[3], M. J. Norden[3], E. Orrú[3], H. Paas[41], M. Pandey-Pommier[42], V. N. Pandey[3], M. Pietka[30], R. Pizzo[3], A. G. Polatidis[3], W. Reich[5], H. J. A. Röttgering[32], A. M. M. Scaife[21], D. J. Schwarz[43], M. Serylak[30], J. Sluman[3], O. Smirnov[17,44], B. W. Stappers[37], M. Steinmetz[29], A. Stewart[30], J. Swinbank[23,45], M. Tagger[33], Y. Tang[3], C. Tasse[44,46], M. C. Toribio[3,32], R. Vermeulen[3], C. Vocks[29], C. Vogt[3], R. J. van Weeren[16], R. A. M. J. Wijers[23], S. J. Wijnholds[3], M. W. Wise[3,23], O. Wucknitz[5], S. Yatawatta[3], P. Zarka[47] & J. A. Zensus[5]

Cosmic rays are the highest-energy particles found in nature. Measurements of the mass composition of cosmic rays with energies of 10^{17}–10^{18} electronvolts are essential to understanding whether they have galactic or extragalactic sources. It has also been proposed that the astrophysical neutrino signal[1] comes from accelerators capable of producing cosmic rays of these energies[2]. Cosmic rays initiate air showers—cascades of secondary particles in the atmosphere—and their masses can be inferred from measurements of the atmospheric depth of the shower maximum[3] (X_{max}; the depth of the air shower when it contains the most particles) or of the composition of shower particles reaching the ground[4]. Current measurements[5] have either high uncertainty, or a low duty cycle and a high energy threshold. Radio detection of cosmic rays[6–8] is a rapidly developing technique[9] for determining X_{max} (refs 10, 11) with a duty cycle of, in principle, nearly 100 per cent. The radiation is generated by the separation of relativistic electrons and positrons in the geomagnetic field and a negative charge excess in the shower front[9,12]. Here we report radio measurements of X_{max} with a mean uncertainty of 16 grams per square centimetre for air showers initiated by cosmic rays with energies of 10^{17}–$10^{17.5}$ electronvolts. This high resolution in X_{max} enables us to determine the mass spectrum of the cosmic rays: we find a mixed composition, with a light-mass fraction (protons and helium nuclei) of about 80 per cent. Unless, contrary to current expectations, the extragalactic component of cosmic rays contributes substantially to the total flux below $10^{17.5}$ electronvolts, our measurements indicate the existence of an additional galactic component, to account for the light composition that we measured in the 10^{17}–$10^{17.5}$ electronvolt range.

Observations were made with the Low Frequency Array (LOFAR[13]), a radio telescope consisting of thousands of crossed dipoles with built-in air-shower-detection capability[14]. LOFAR continuously records the radio signals from air showers, while simultaneously running astronomical observations. It comprises a scintillator array (LORA) that triggers the read-out of buffers, storing the full waveforms received by all antennas.

We selected air showers from the period June 2011 to January 2015 with radio pulses detected in at least 192 antennas. The total uptime was about 150 days, limited by construction and commissioning of the

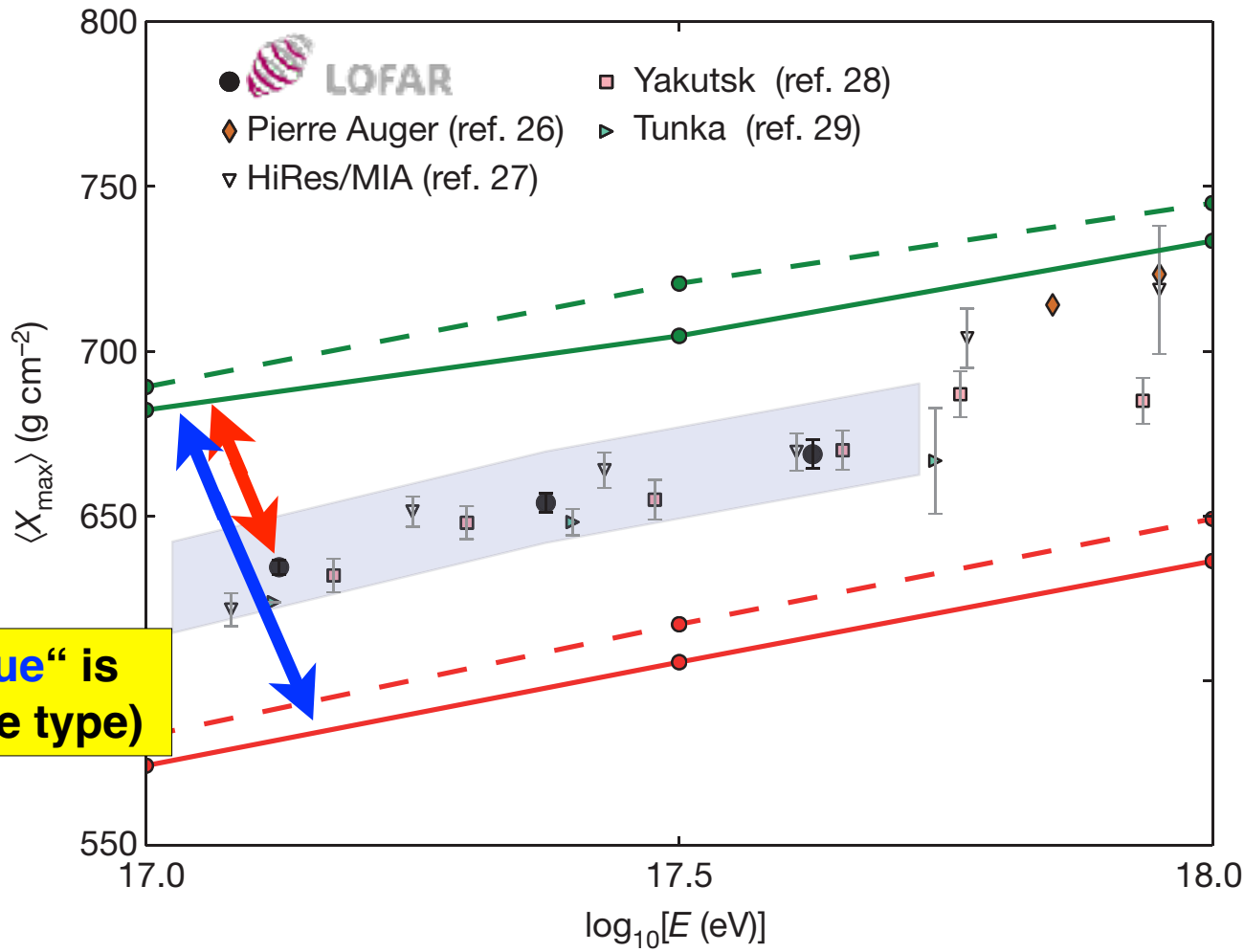

relative distance "red/blue" is measure for ln A (particle type)

S. Buitink et al., Nature 531 (2016) 70

Shower maximum: proof by Tunka-Rex

- One of several methods: slope of lateral distribution

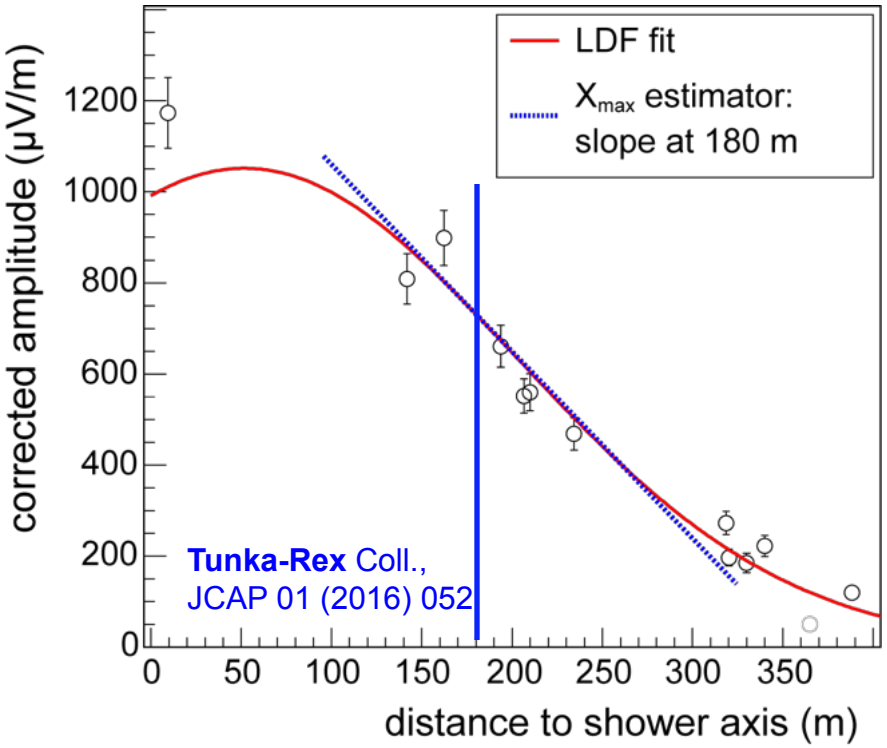

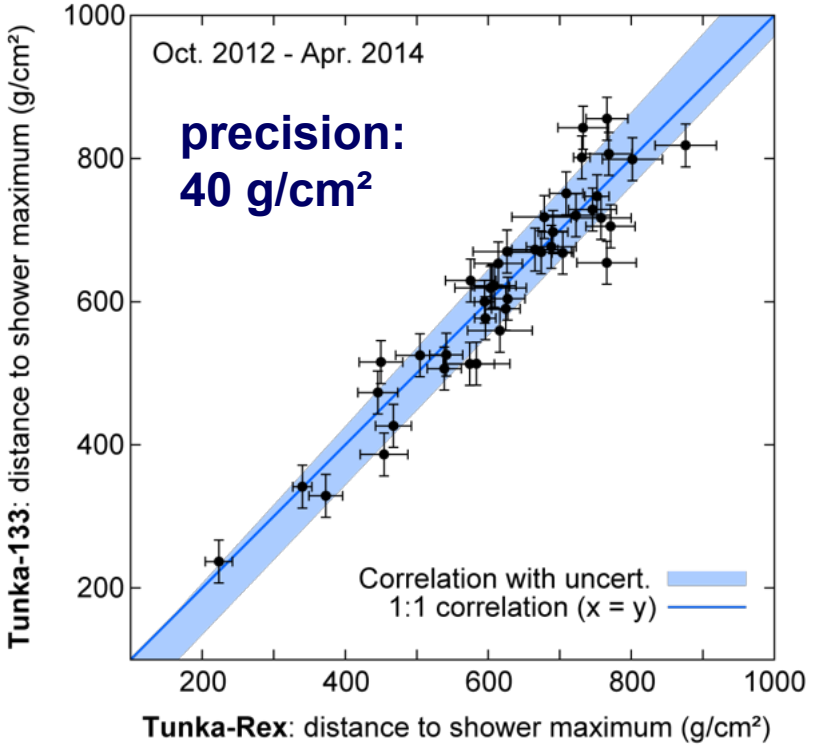

frank.schroeder@kit.edu
Institut für Kernphysik

Introduction: Radio footprint is sensitive to mass

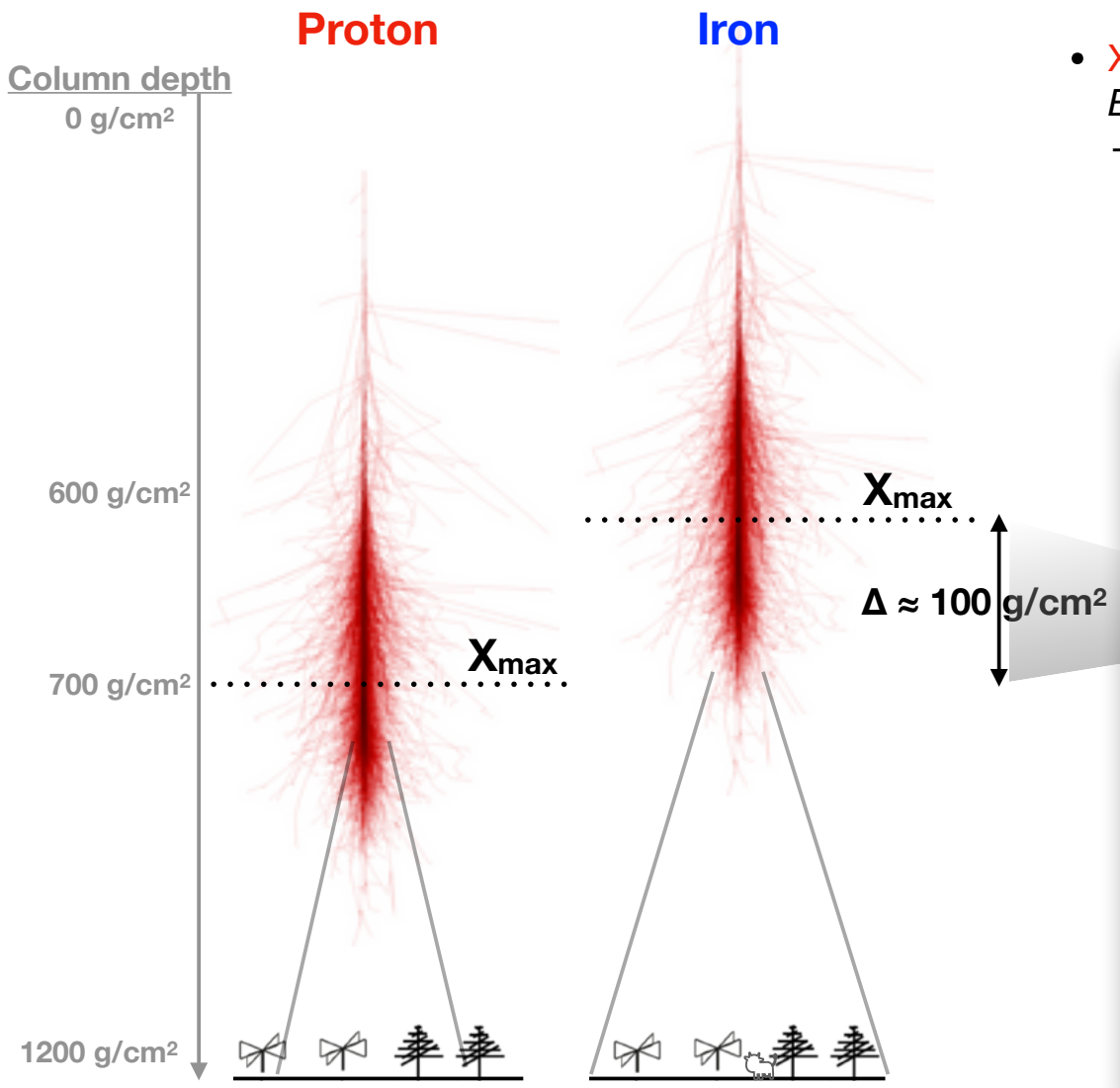

- X_{max} [g/cm²]: *column depth* where *Extensive Air Shower* is maximally developed.
  —> X_{max} depends on mass (particle type)

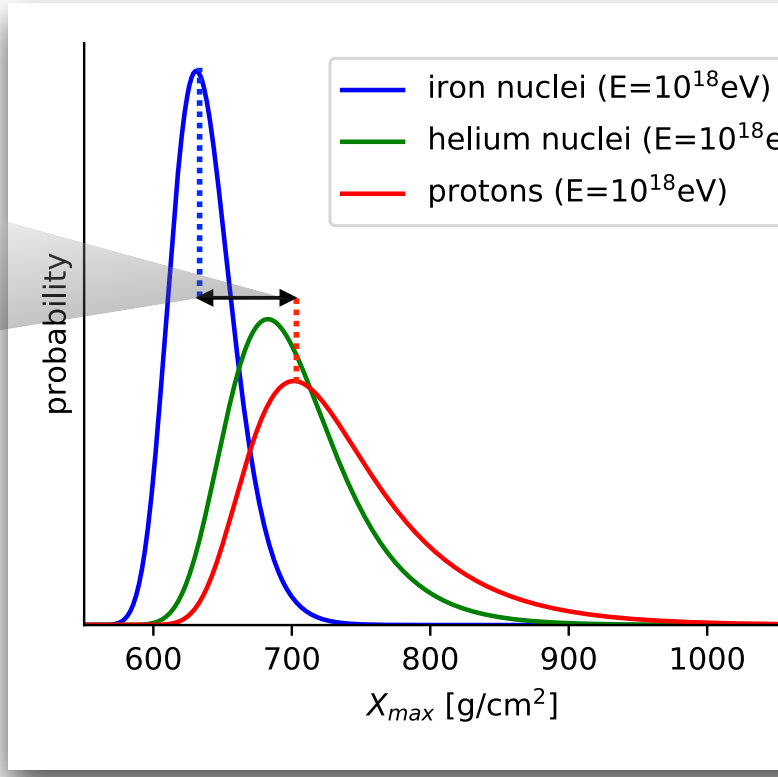

Introduction: Radio footprint is sensitive to mass

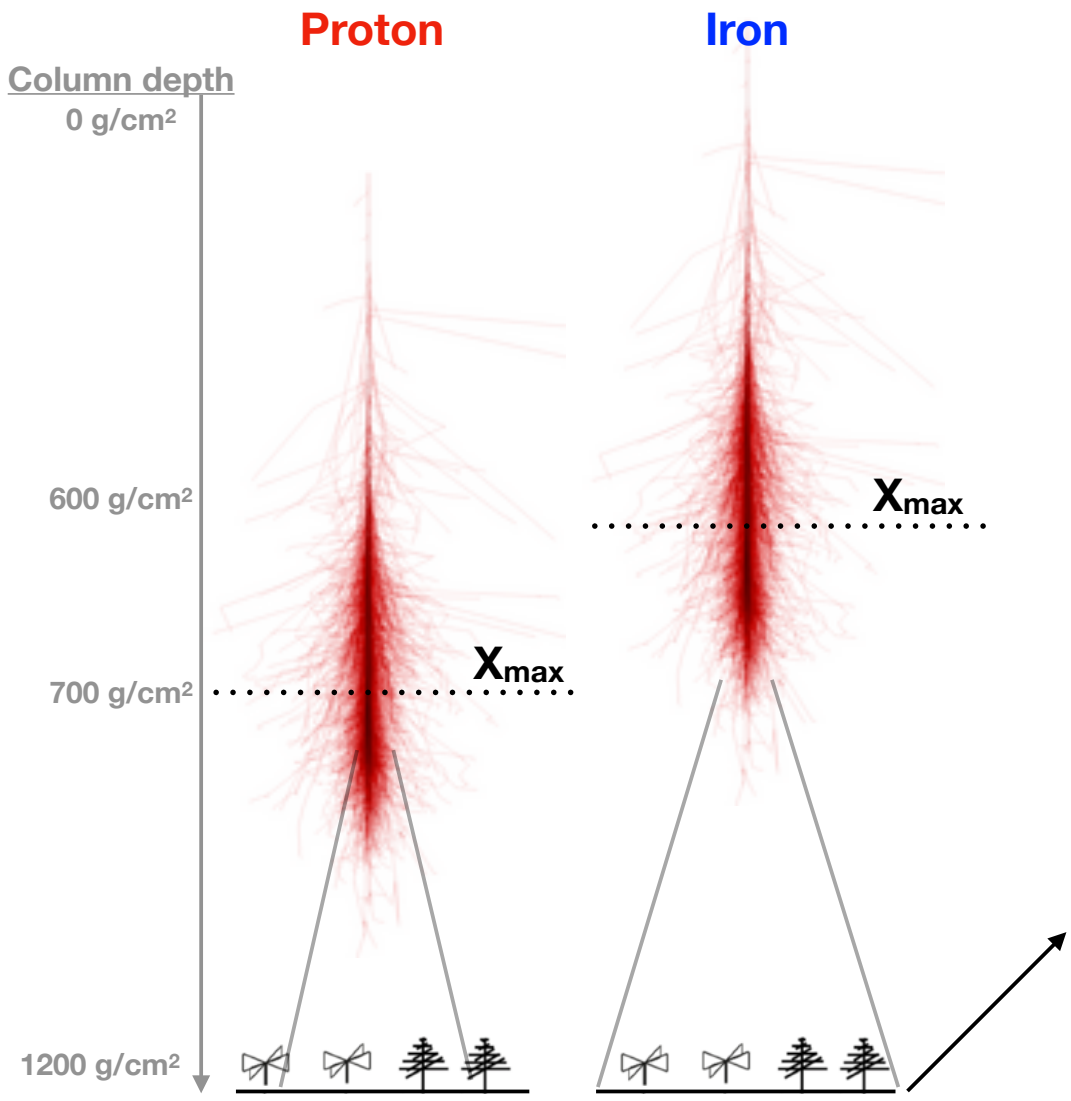

- X_{max} [g/cm²]: *column depth* where *Extensive Air Shower* is maximally developed.
  —> X_{max} depends on mass (particle type)
- Shape of radio footprint changes with X_{max}
  —> Radio footprint is probe for X_{max}.

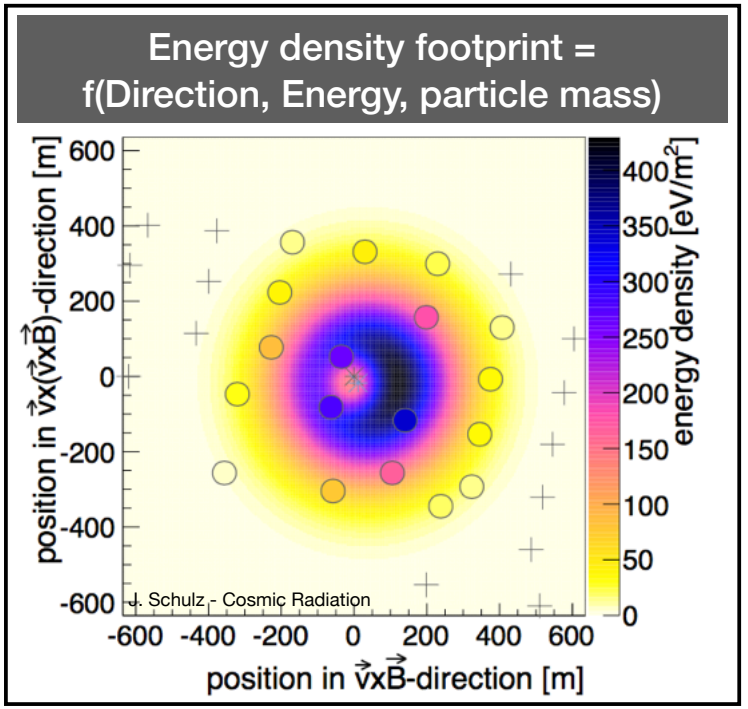

Method: Reconstructing X_{max} from the radio footprint

Reconstruction Air Shower → CORSIKA → Reconstruction Simulations

E, θ, ϕ, …

{X_{max}}

Using same reconstruction code
(includes detector and reconstruction effects)

Antennas

Measured

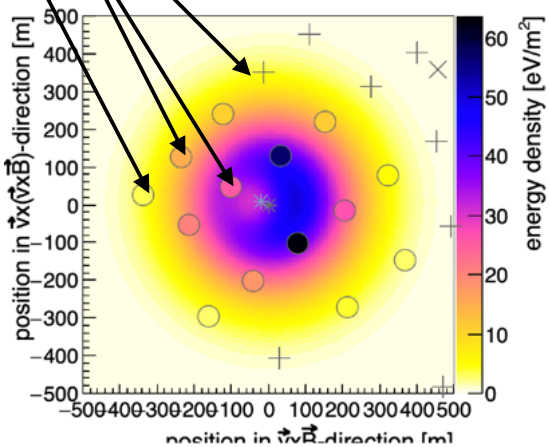

15x Proton **12x Iron**

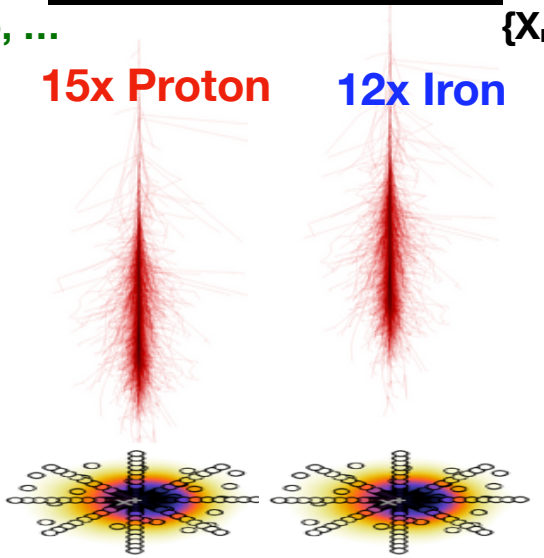

Proton **Iron**

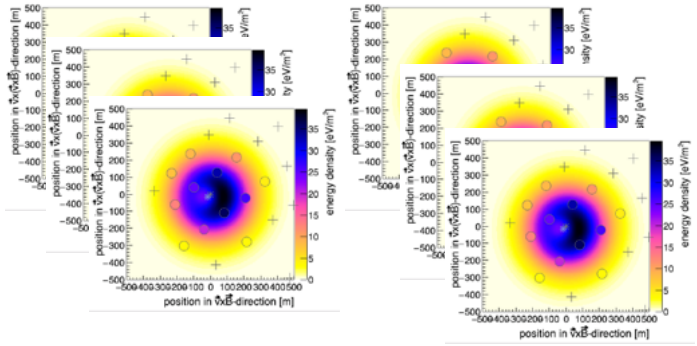

Minimise to find X_{max} of measured shower:

Based on Buitink+(2016)

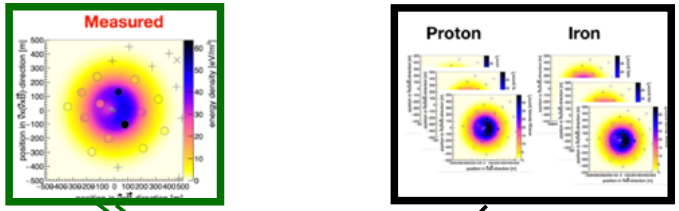

$$\chi^2 = \sum_{\text{AERA Stations}} \left(\frac{u_{\text{data}} - S \cdot u_{\text{sim}}(\Delta \vec{r}_{\text{core shift}})}{\sigma u_{data}} \right)$$

Minimize [S , r_{core}]

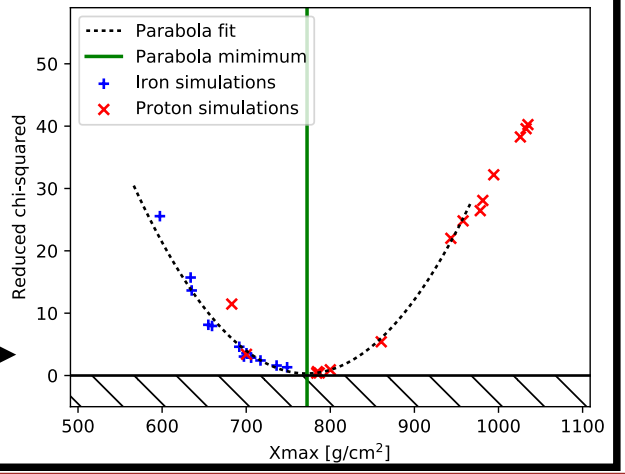

Results: Event-by-event FD vs AERA X_{max}

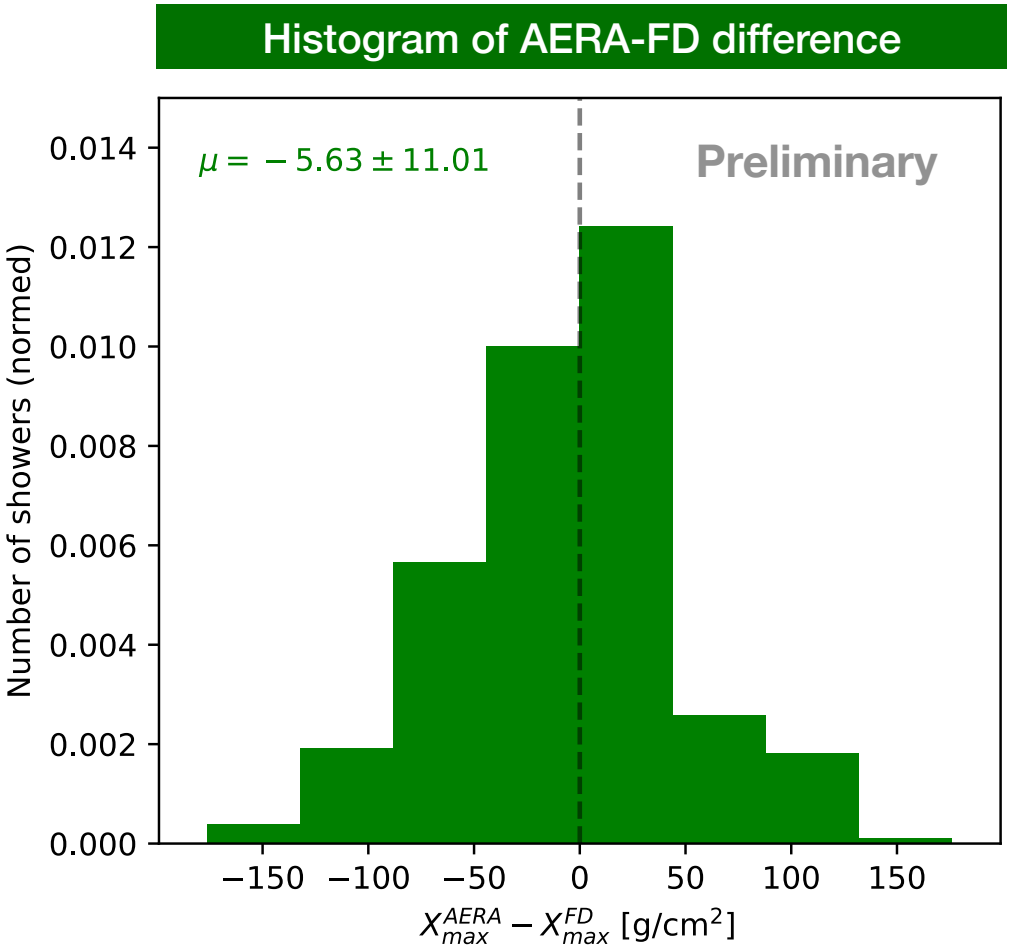

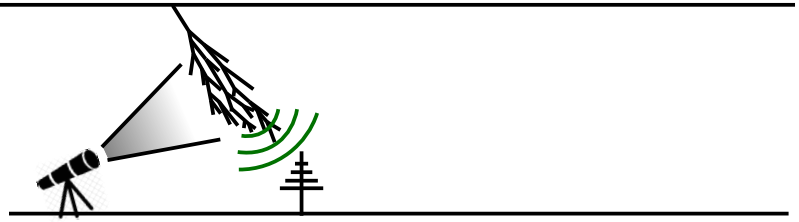

Auger has unique Radio-Fluorescence setup:

- X_{max} of **53** hybrid-showers with AERA and FD; (Are independent observations!)
- No significant bias radio X_{max} w.r.t. fluorescence X_{max}.
- Provides independent checks on:
  - X_{max} reconstruction methods
  - shower physics (probe different aspects)

Results: Resolution of AERA X_{max} method

Radio X_{max} resolution

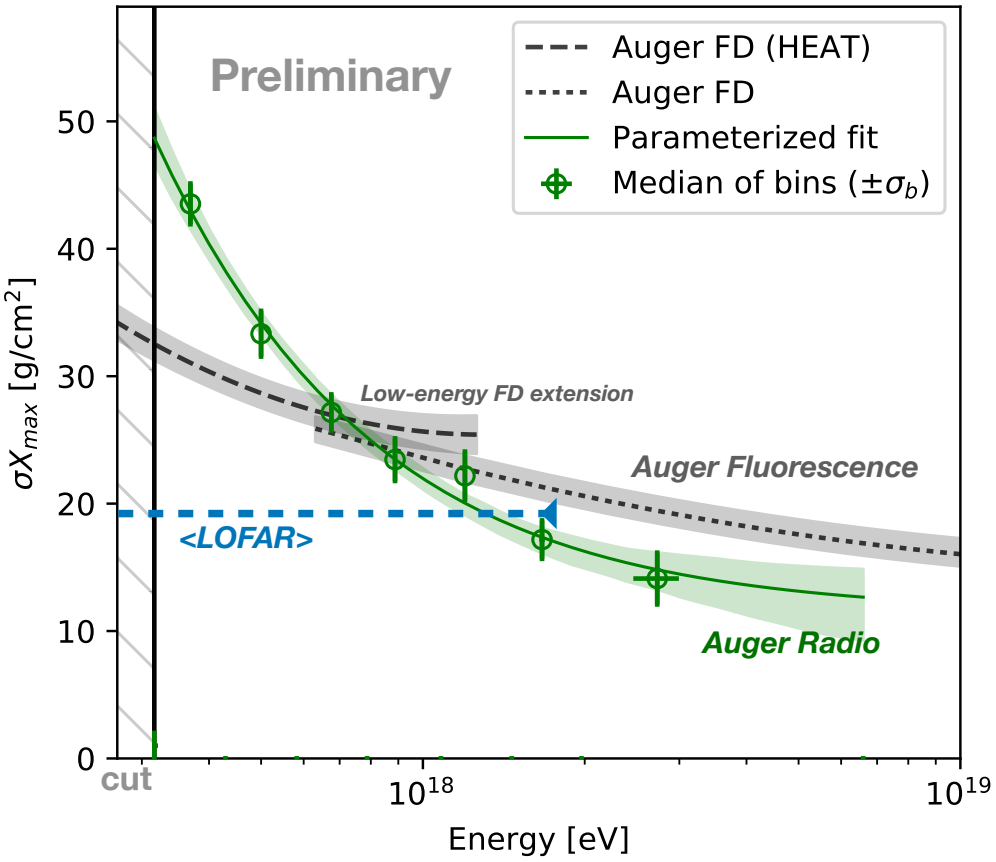

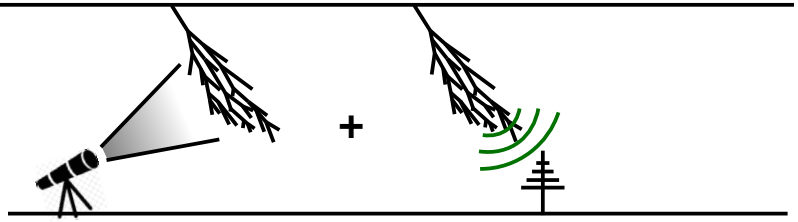

Resolution improves with energy.

- Up to 'better than 15 g/cm^2 '
- Trend driven by low SNR at low energy.

Resolution competitive with e.g.:

- Auger fluorescence
  [arXiv:1409.4809]
- LOFAR radio (E=$10^{16.8...18.3}$eV)
  [arXiv:2103.12549v2]

Side note:
High resolution is crucial for mass composition studies.

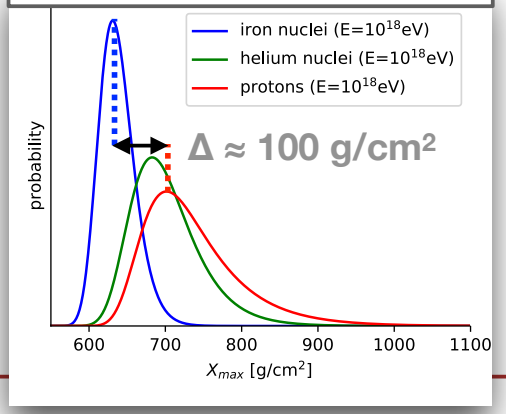

Results: Measured AERA X_{max} distribution

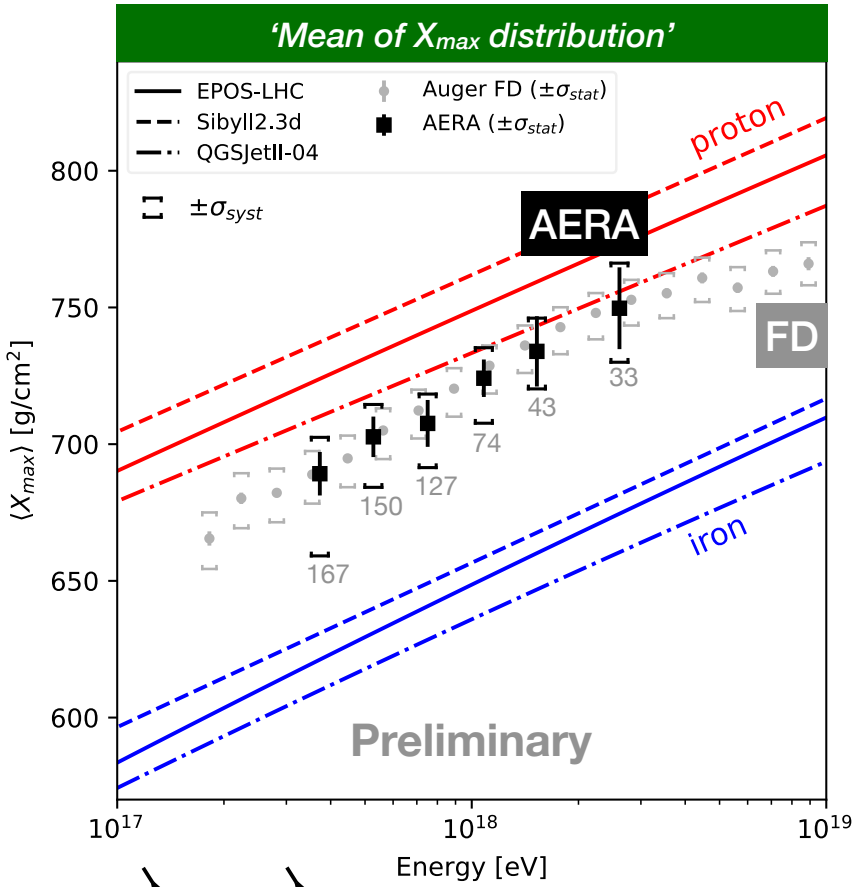

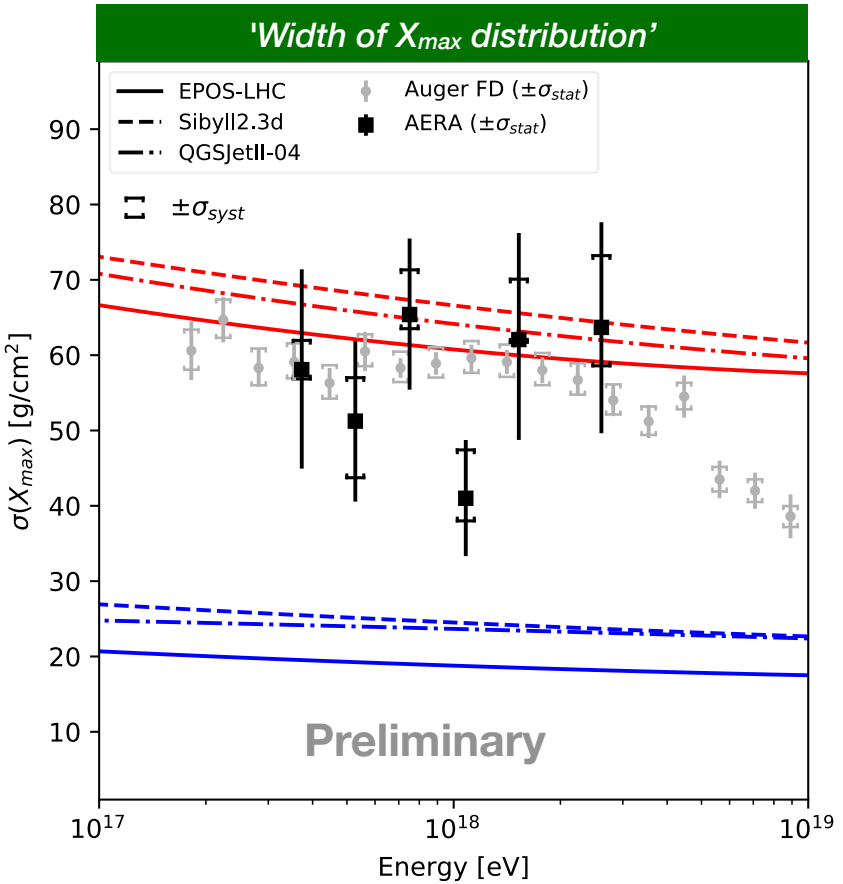

- ~600 showers after quality and anti-bias cuts.
- In agreement with Auger FD in mean, width, and (qualitatively) the X_{max} distribution.
- Light composition (p-He) at E=$10^{17.5}$ eV, seemingly becoming lighter towards E=$10^{18.5}$ eV.

Results: AERA vs other (radio) experiments

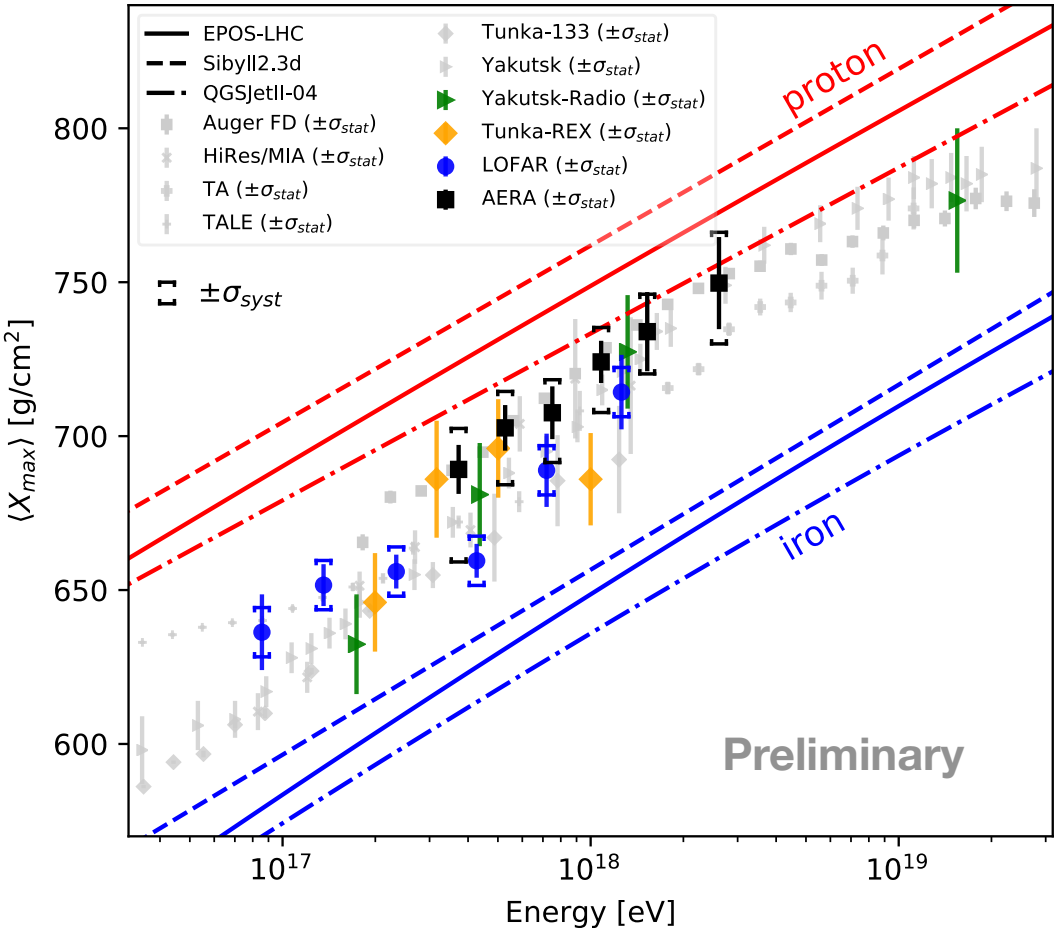

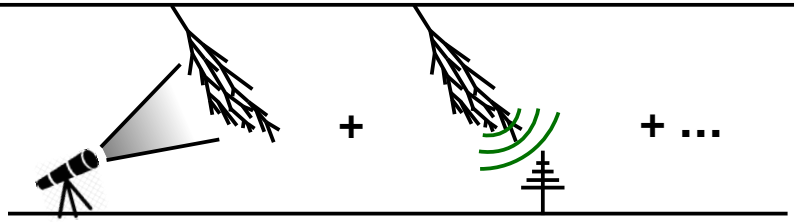

- No general radio-bias w.r.t other techniques (within uncertainties).
- Highlights that systematic uncertainties are key to interpret and compare.
- **LOFAR**-**AERA** differences are being investigated in a working group

—> come talk to us during coffee and lunch!

Determine the properties of the incoming particle with the radio technique

- direction ~ 0.1° - 0.5°
- energy ~ 20% - 30%
- type (X_{max}) ~ 15 - 40 g/cm^2

(depending on detector spacing)

—> radio technique is routinely used to measure properties of cosmic rays


The Future
NEXT EXIT

Upgrade of the Pierre Auger Observatory
(astro-)physics of the highest-energy particles in nature

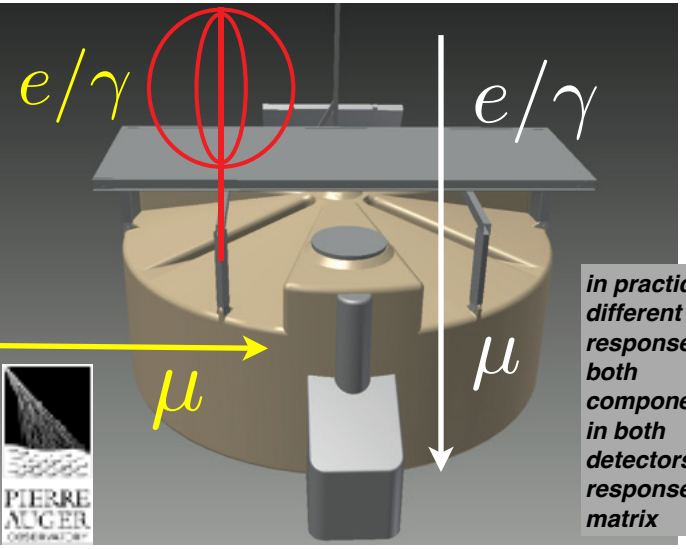

in practice: different response to both components in both detectors: response matrix

upgrade PAO

- electronics
- scintillator layer
- radio detector

Key science questions

- What are the sources and acceleration mechanisms of ultra-high-energy cosmic rays (UHECRs)?
- Do we understand particle acceleration and physics at energies well beyond the LHC (Large Hadron Collider) scale?
- What is the fraction of protons, photons, and neutrinos in cosmic rays at the highest energies?

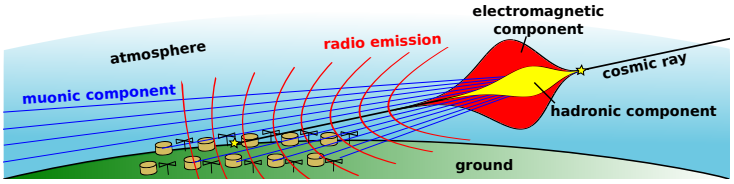

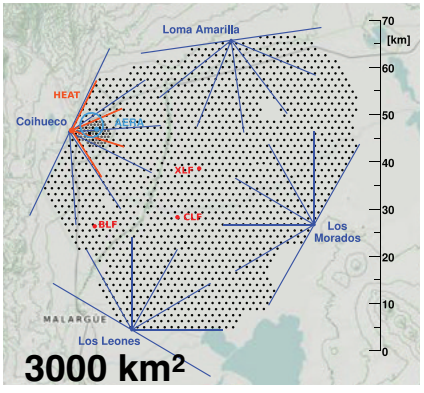

NWO

erc

Advanced Grant
Hörandel 2018

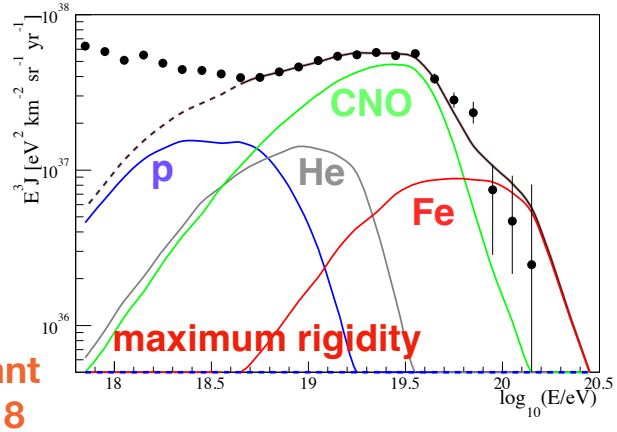

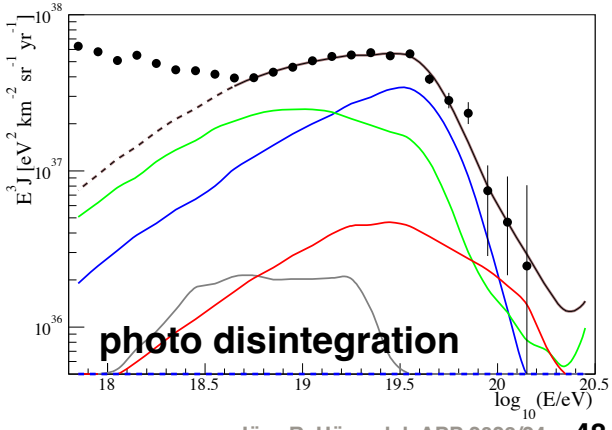

A large radio array at the Pierre Auger Observatory

preparatory work & feasibility

AERA 17 km²
--> 3000 km²

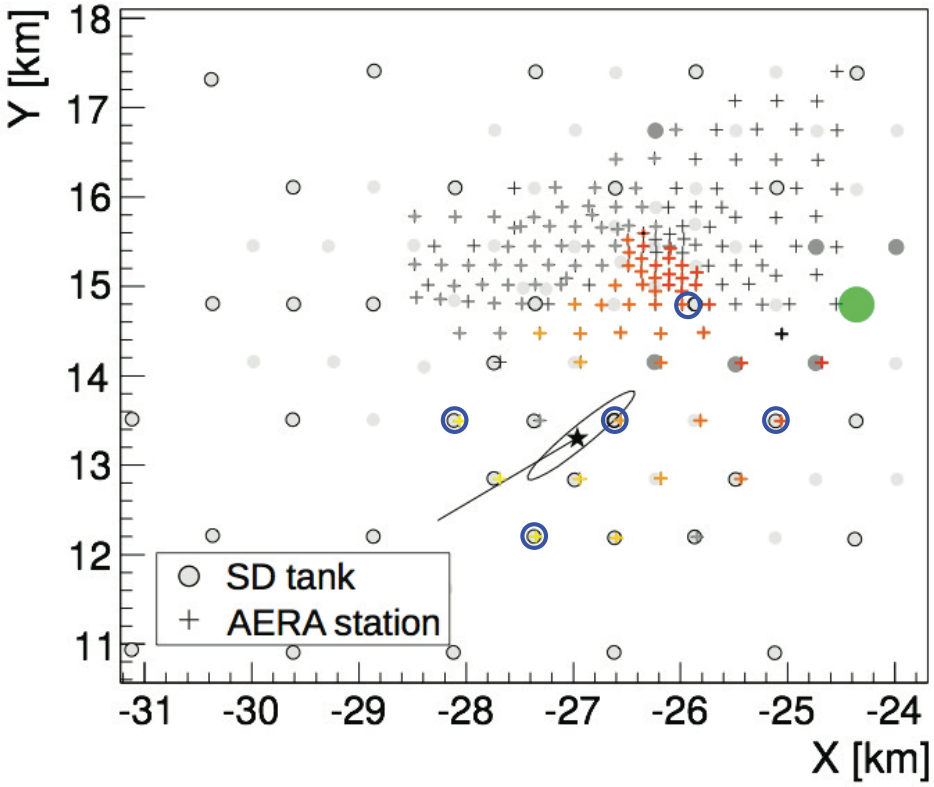

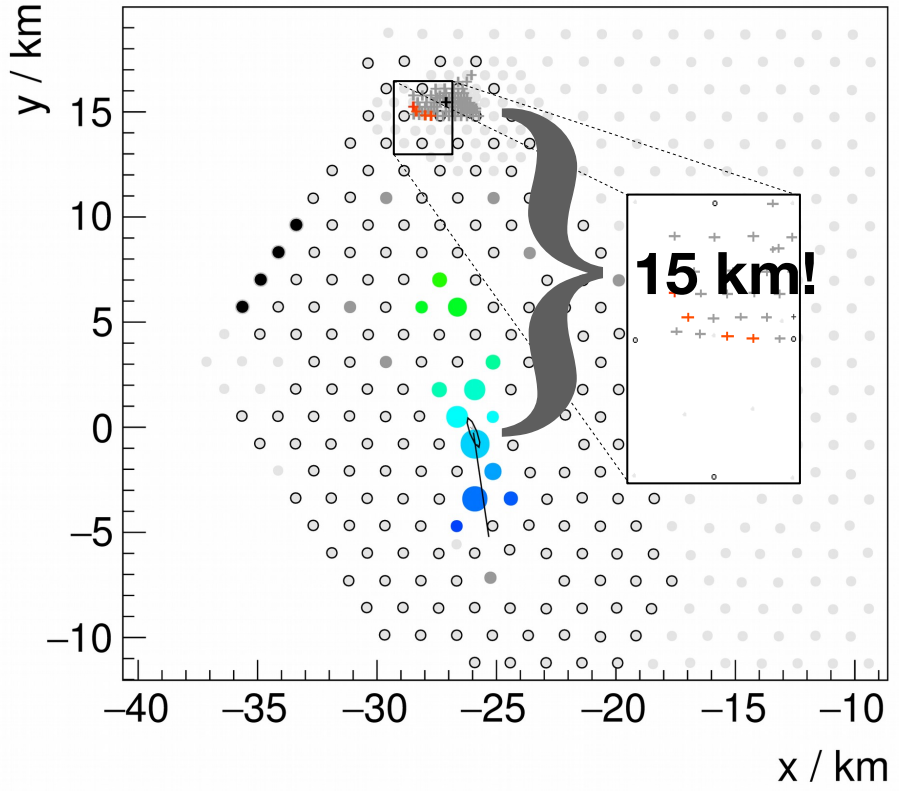

horizontal air showers registered and reconstructed with existing AERA

A. Aab et al., JCAP 10 (2018) 026

Horizontal air showers have large footprints in radio emission

M. Gottowik

AERA 17 km²
--> 3000 km²

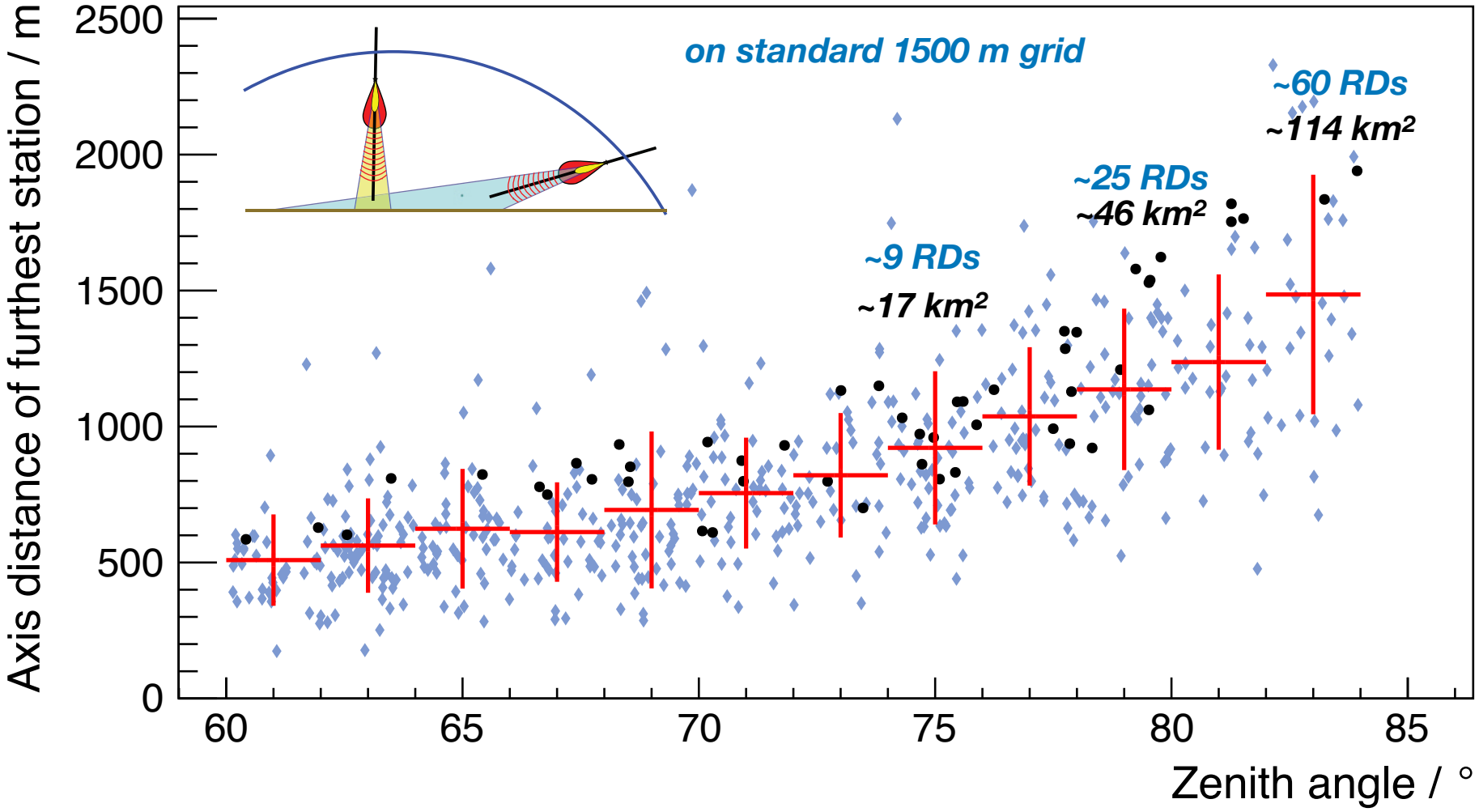

this is MEASURED with the *small* 17km² AERA

A. Aab et al., JCAP 10 (2018) 026

since May 2019 complete prototype at Auger observatory

- new SALLA antenna
- new LNA
- new digitizer/front end coupled to UUB

data are integrated in SD data stream and transported to CDAS

we have now *ONE* system comprising of WCD, SSD, RD

since November 2019
10 prototype stations installed

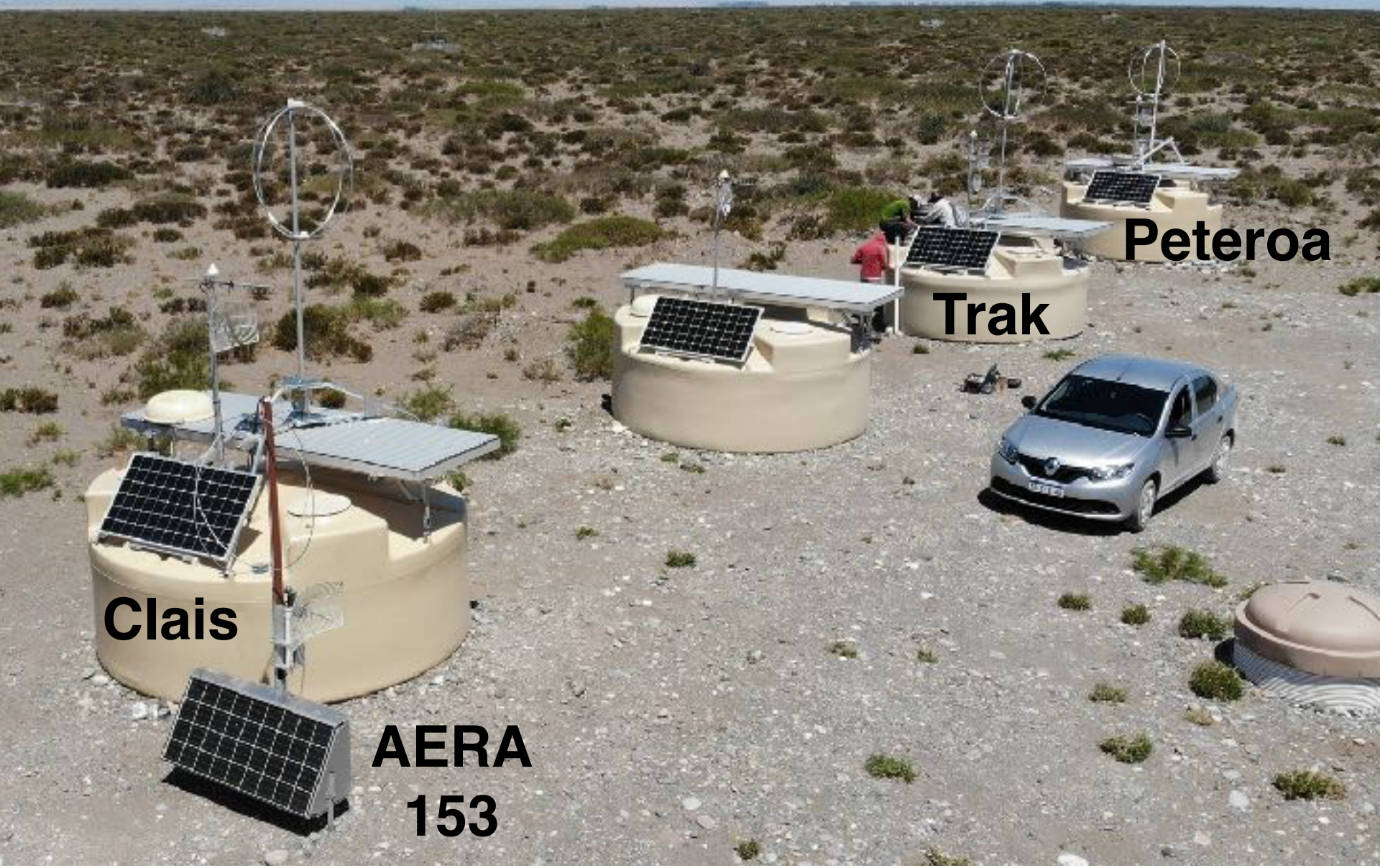

photo: Tim Huege

First Rd Signal

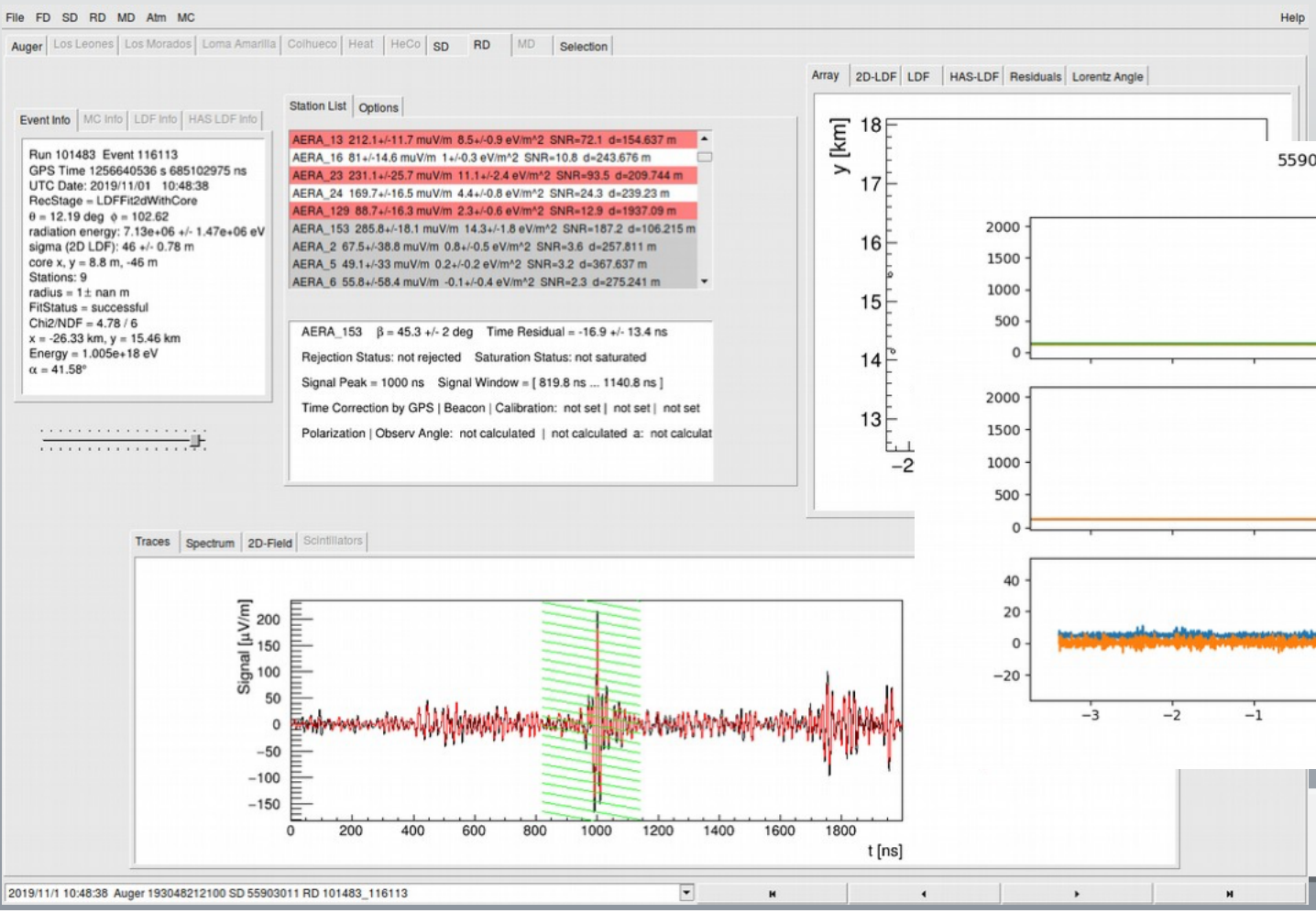

BERGISCHE UNIVERSITÄT WUPPERTAL

mechanical mounting of RD on wcd

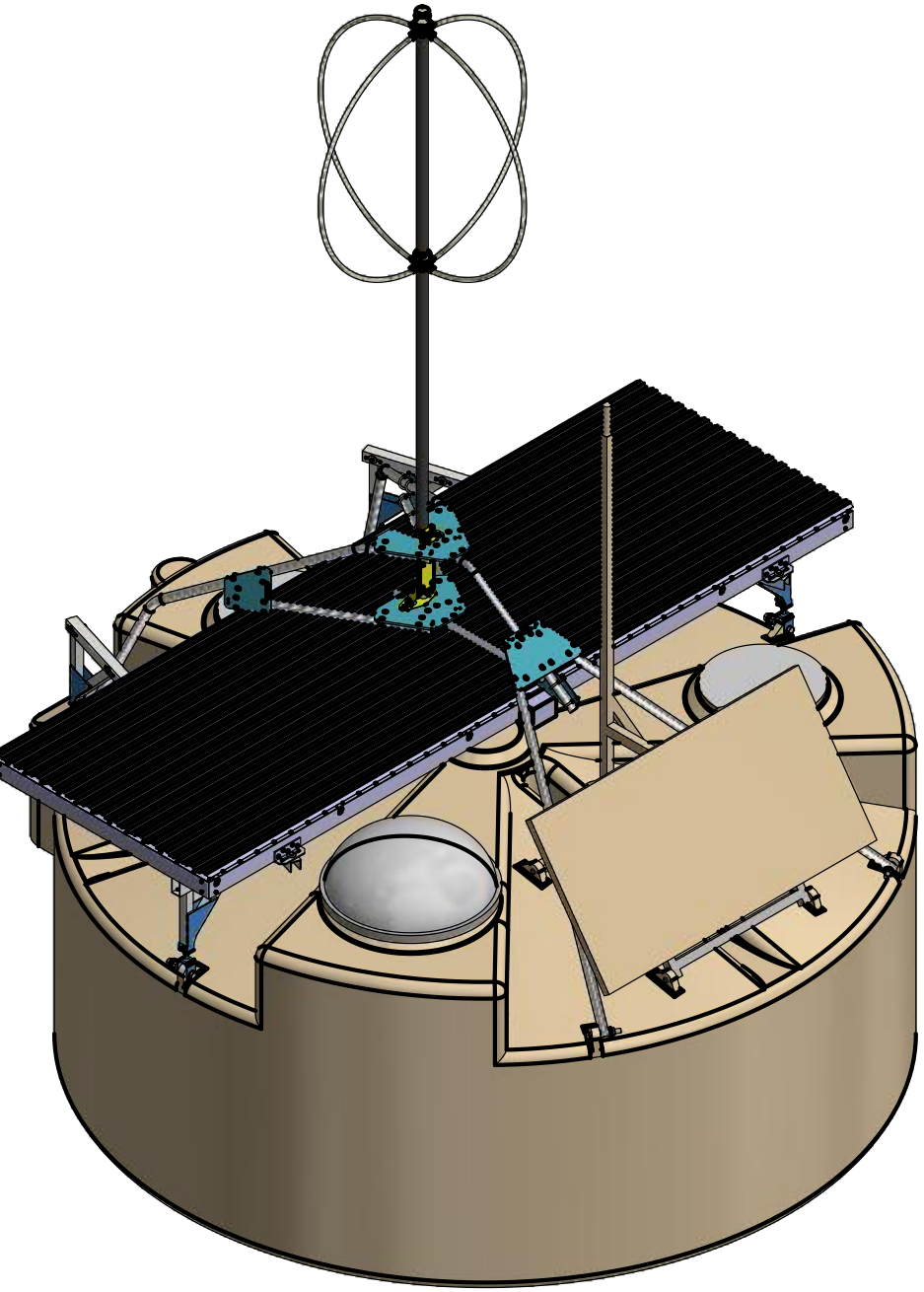

5 m above ground

designed to resist wind speeds of 120 km/h

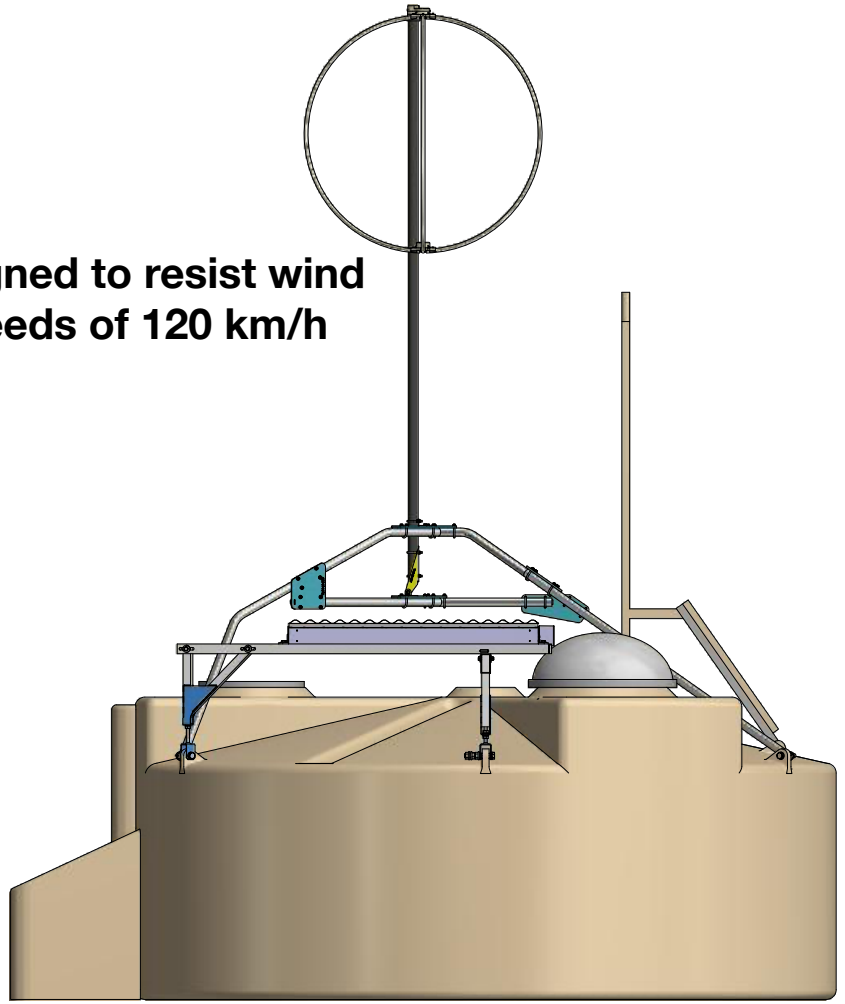

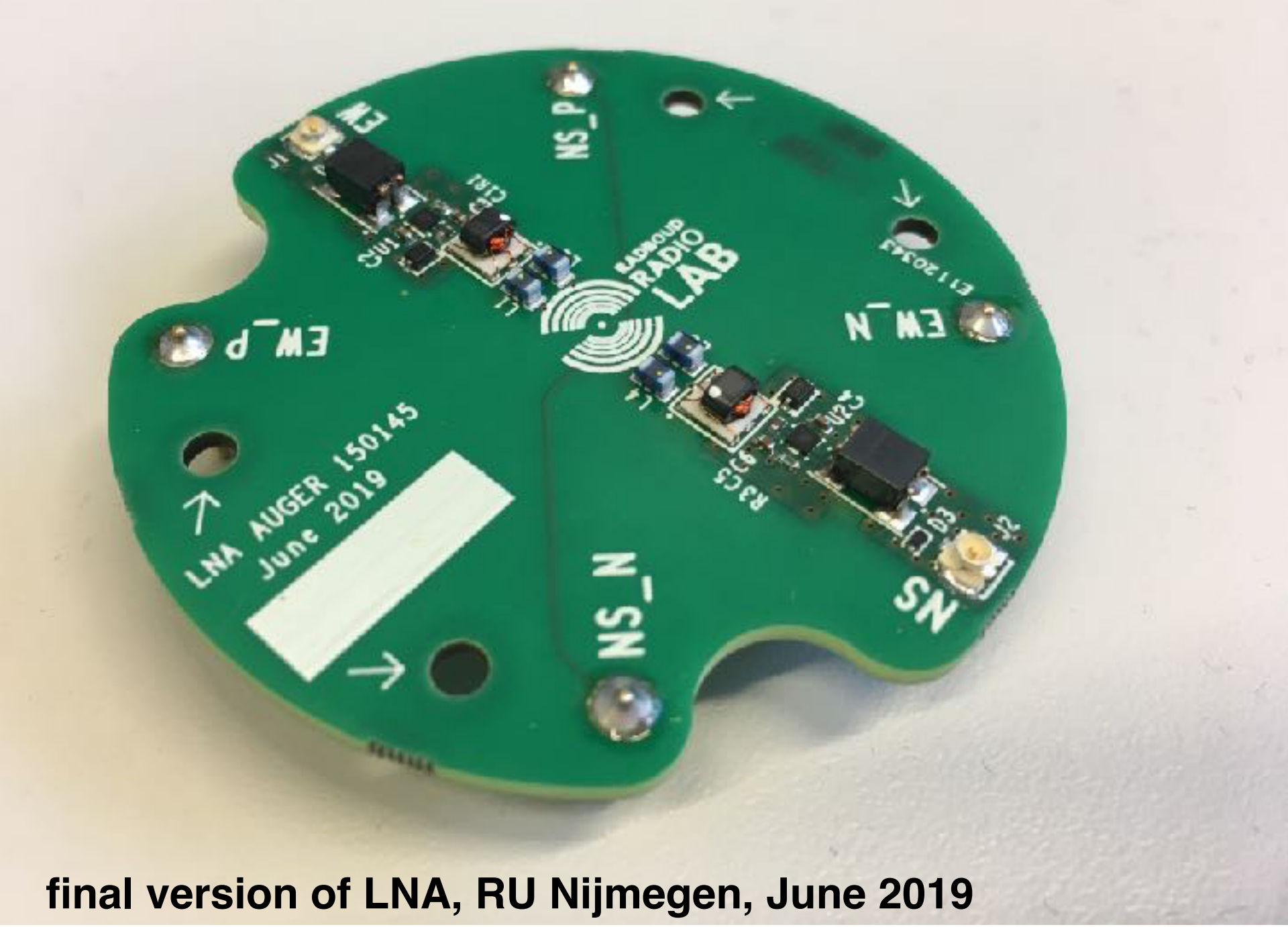

final version of LNA, RU Nijmegen, June 2019

radio digitizer

developed at RU Nijmegen

Detection aperture and event statistics

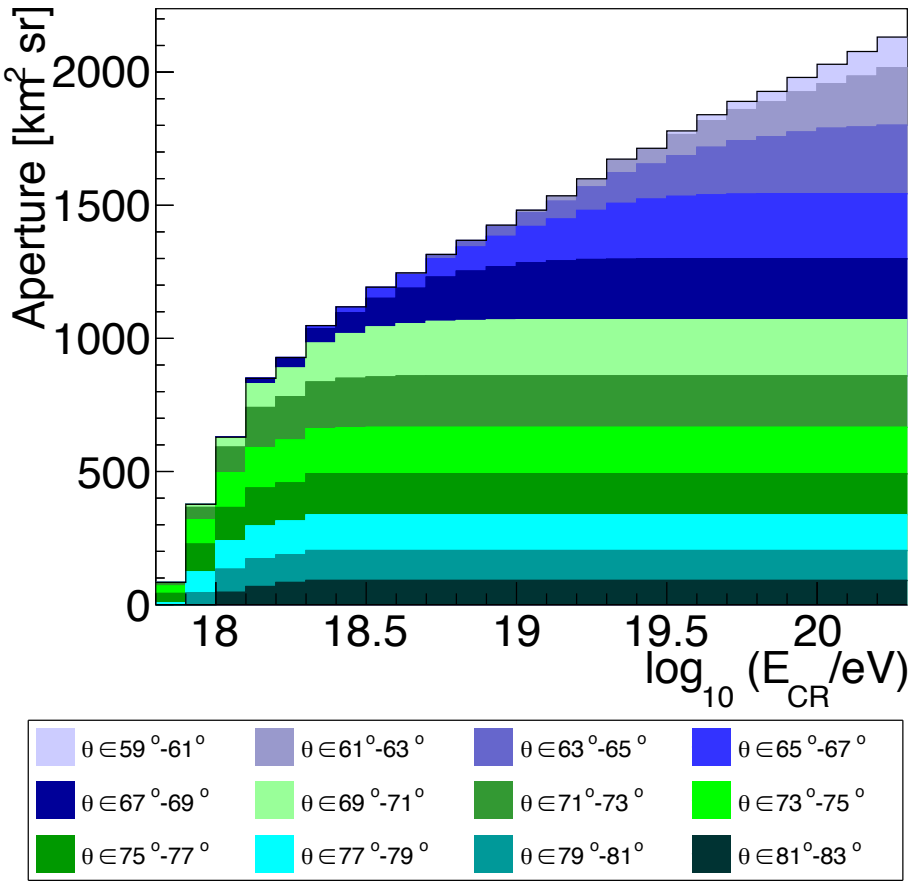

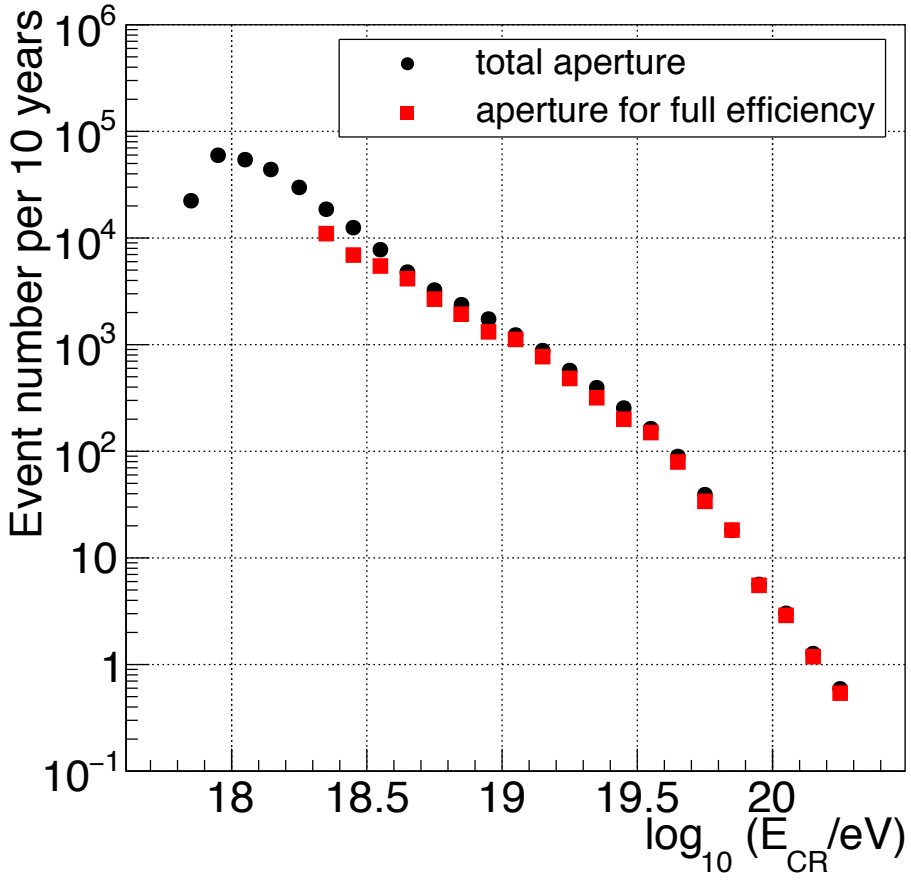

- **High zenith angles become efficient early, contribute smaller apertures**
- **Lower zenith angles contribute larger apertures, become efficient later**
- **3000 fully efficient events above 10^{19} eV in 10 years (300 above $10^{19.5}$ eV)**

Measurement of the fluctuations in the number of muons in inclined air showers with the Pierre Auger Observatory

Felix Riehn[*a] **for the Pierre Auger Collaboration**[†b]

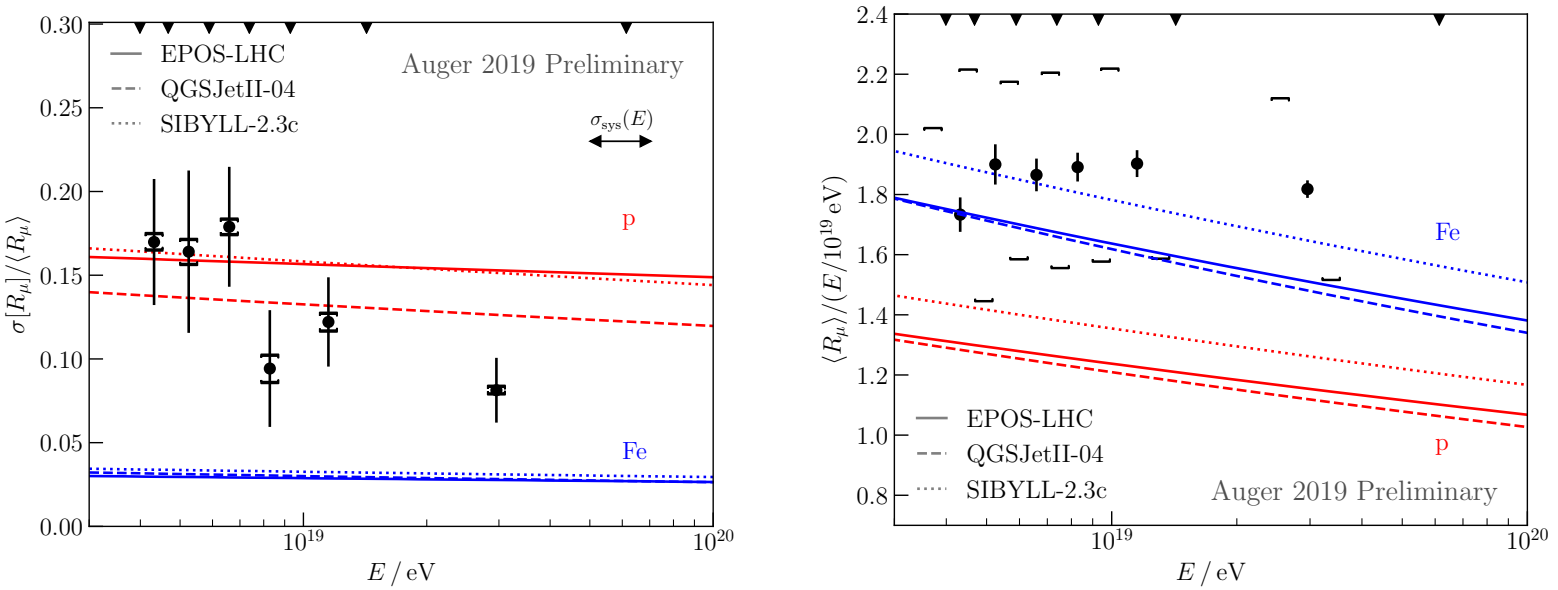

Figure 4: Shower-to-shower fluctuations (left) and the average number of muons (right) in inclined air showers as a function of the primary energy. For the fluctuations, the statistical uncertainty (error bars) is dominant, while for $\langle R_\mu \rangle$ the systematic uncertainty (square brackets) is dominant. The shift in the markers for the systematic uncertainty in the average number of muons represents the uncertainty in the energy scale.

PoS(ICRC2019)404

Muon content in horizontal air showers

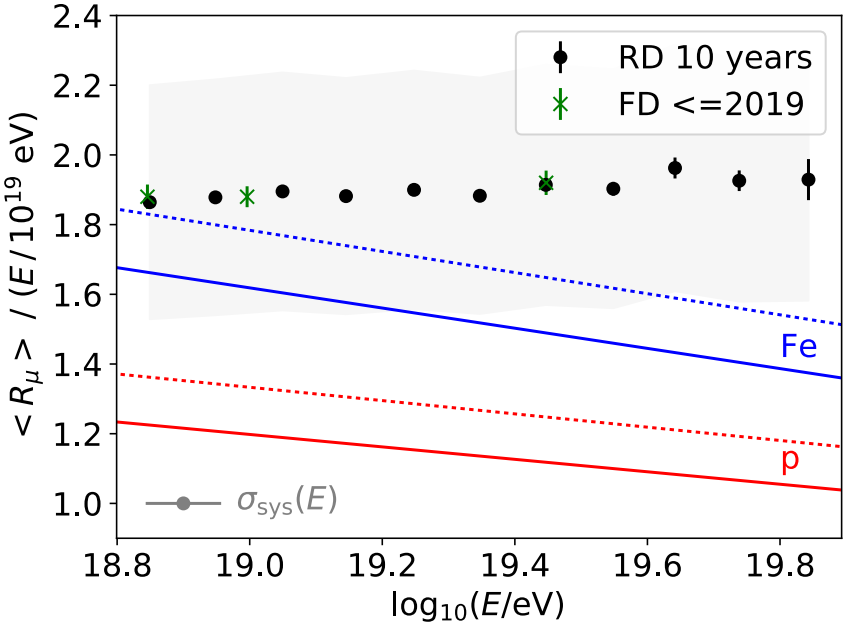

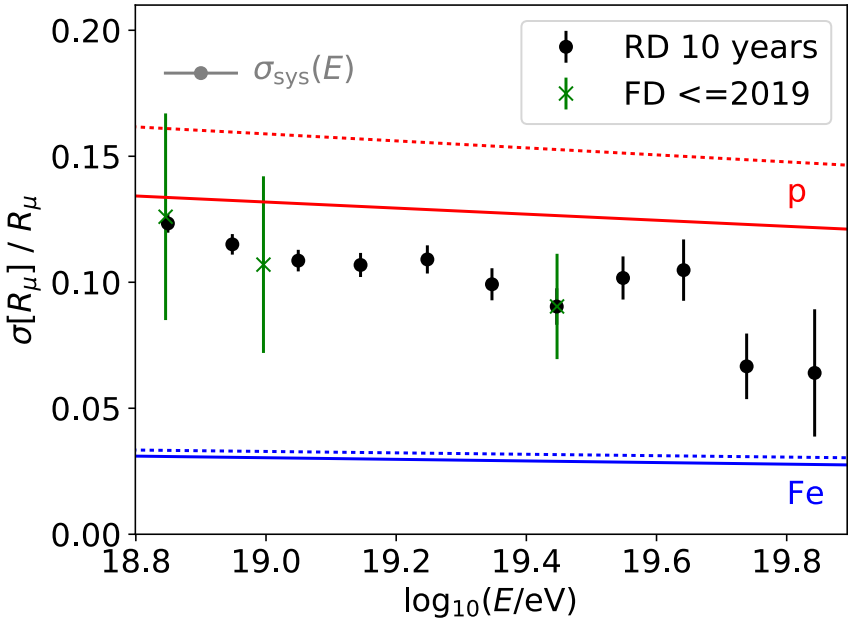

- **More than 6000 showers expected above $10^{18.8}$ eV in 10 years**
- **Energy resolution is not critical (assuming 20% here)**
- **Can also study zenith angle dependence**

Mass composition sensitivity

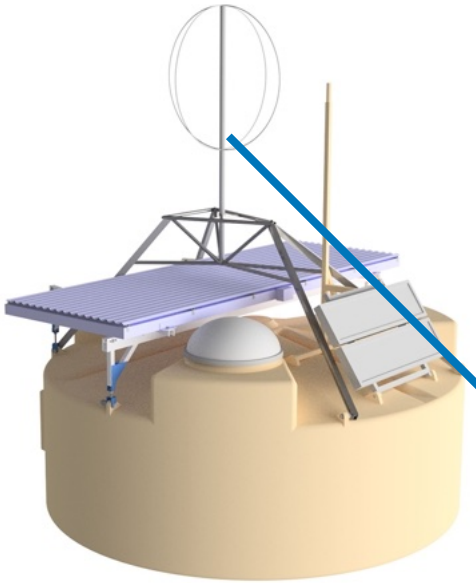

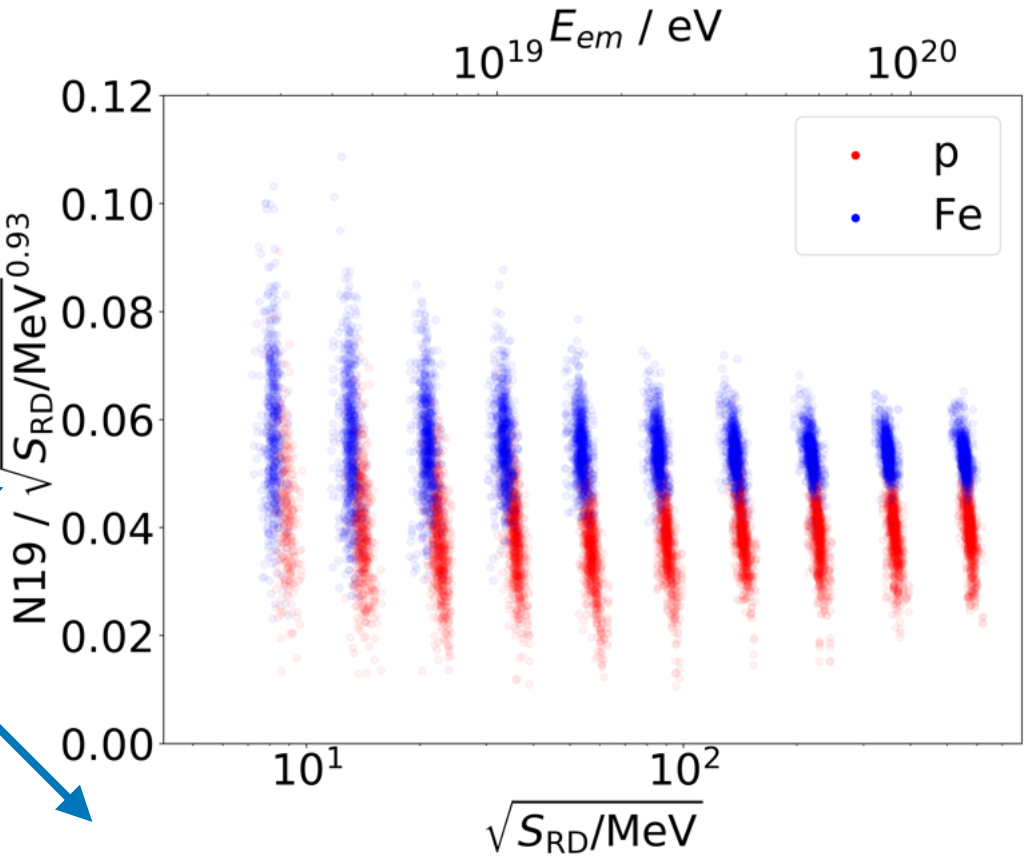

- **Energy from RD**
- **Muon number from WCD**
- **Correct for energy dependence of muon number to exploit its mass composition sensitivity**

Mass composition sensitivity

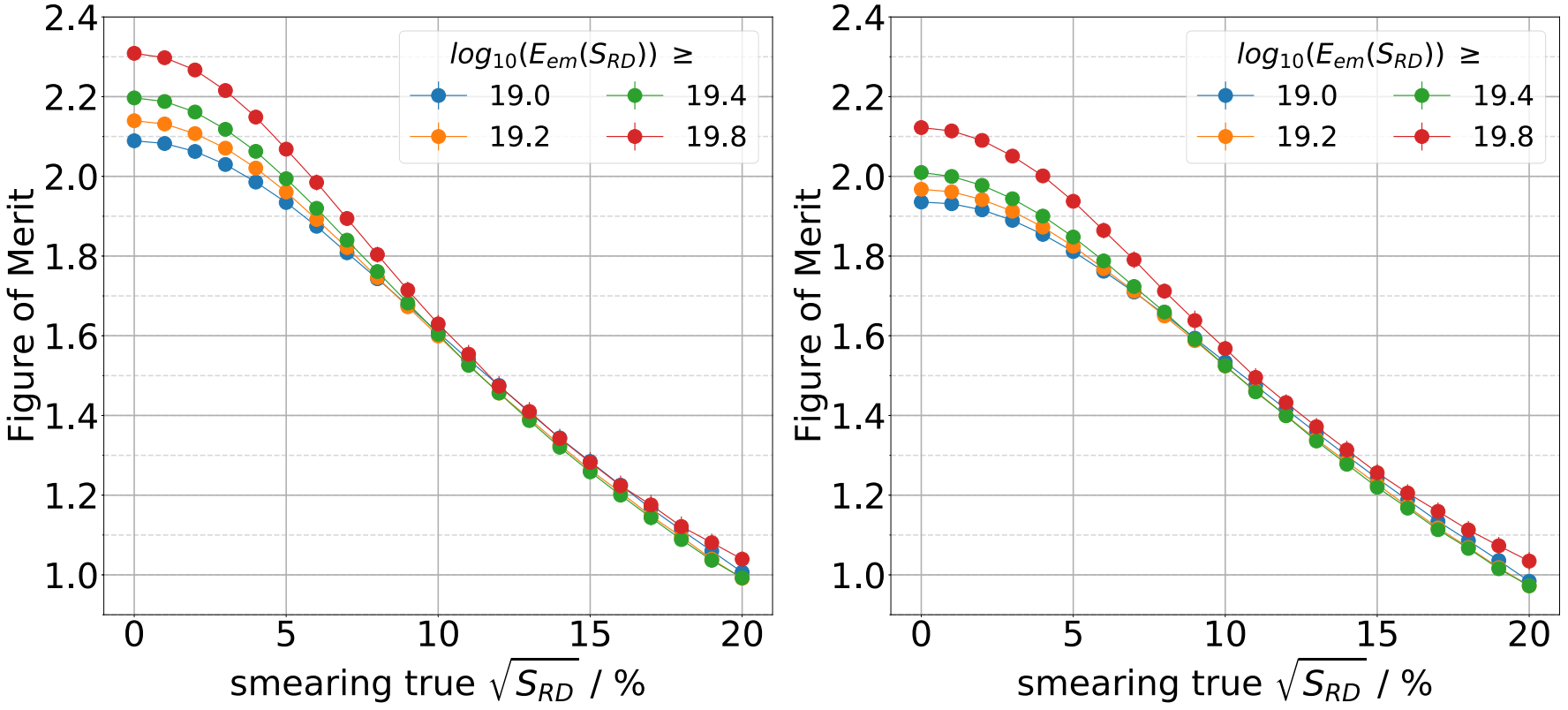

Figure 7: Figure of merit for the separation of proton-induced and iron-induced air showers using the ratio r defined in eqn. (1), various assumed resolutions for the determination of the electromagnetic energy with the Radio Detector, and different cut-offs for the lowest (smeared) electromagnetic energy. Left: using Monte-Carlo true arrival directions and knowledge of $X_{\max}$ for each individual air shower. Right: using arrival directions as reconstructed by the Surface Detector and $X_{\max}$ values known with a resolution of $100\,\mathrm{g/cm^2}$. [33]

Sky coverage with mass sensitivity

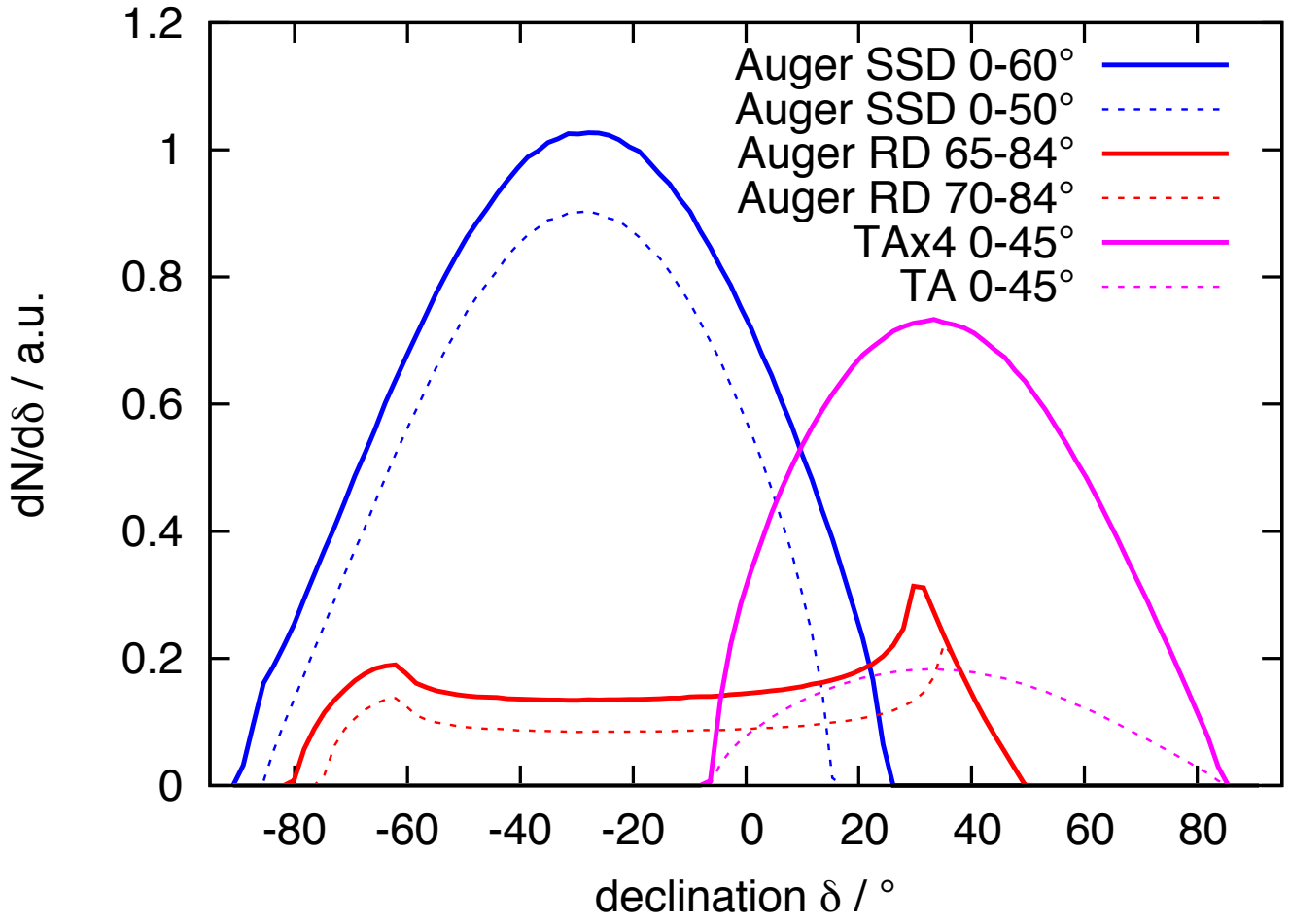

- **Add access at 20° - 45° northern declinations**
- **Shared energy scale**
- **Different systematics than SSD**

Antenna assembly

Transport to position

Replacing solar panels

Station assembly

Station assembly

More than 120 stations (7%) taking data!

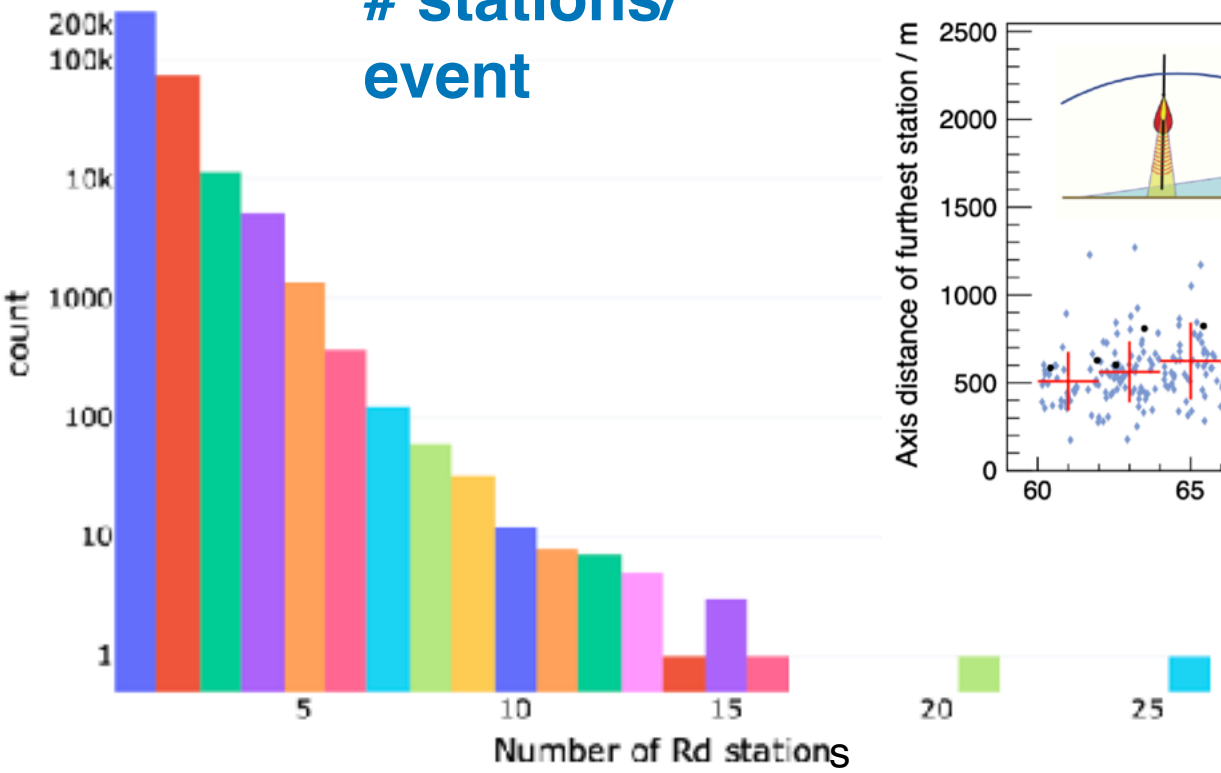

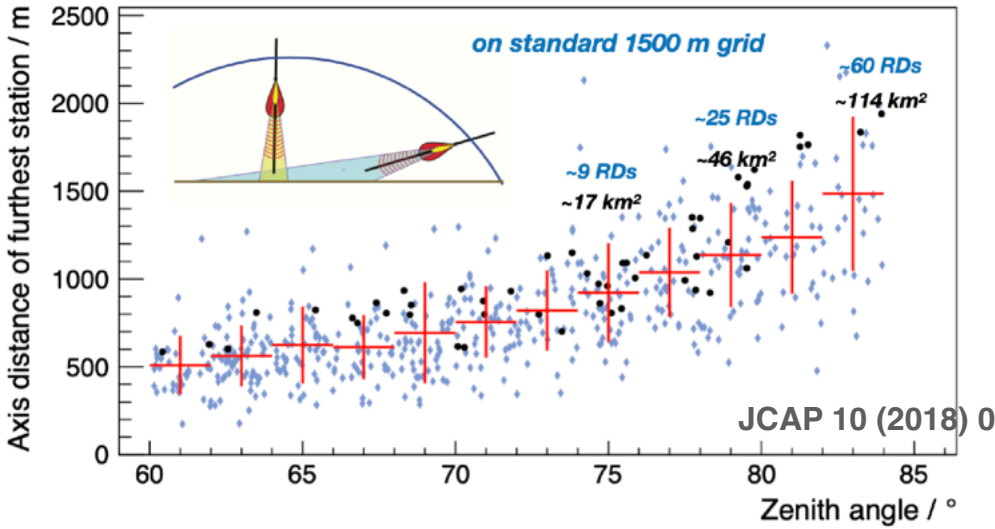

Look at 1st data

location of EAS axes

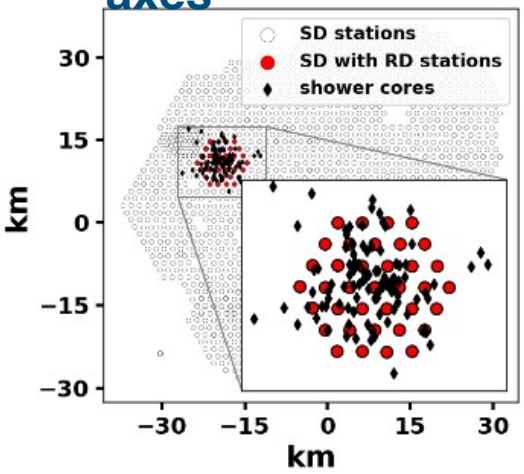

arrival direction

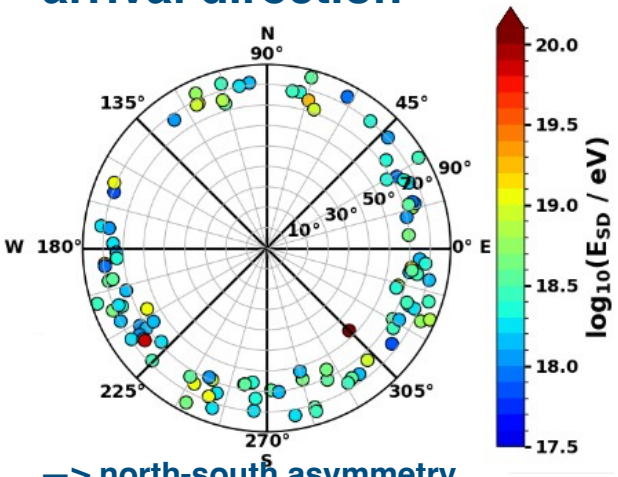

—> north-south asymmetry
—> emission mechanism vxB

of measured cosmic rays

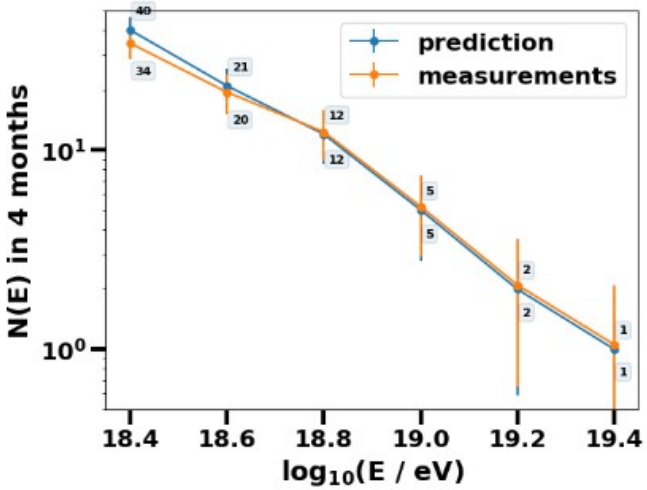

frequency spectra

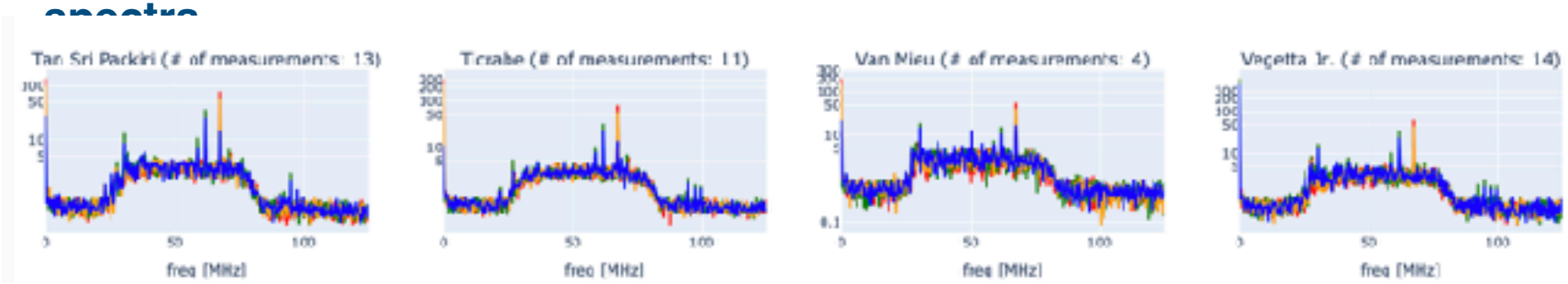

RD calibration concept

thermal cycling (aging) LNA & digitizer

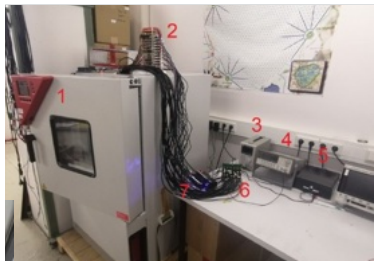

end-to-end calibration in lab LNA & digitizer

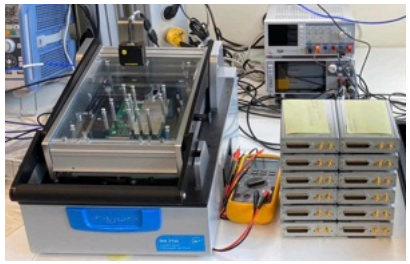

simulation of antenna pattern NEC

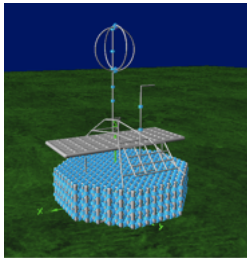

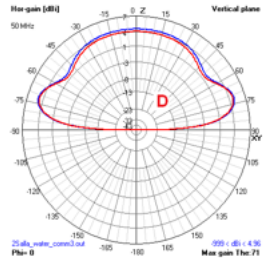

in-situ calibration with reference

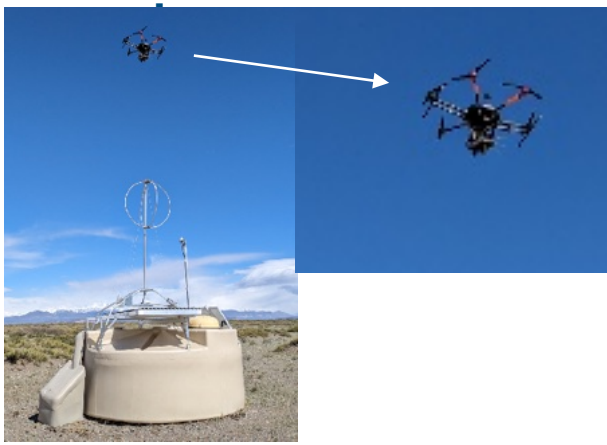

Galactic emission

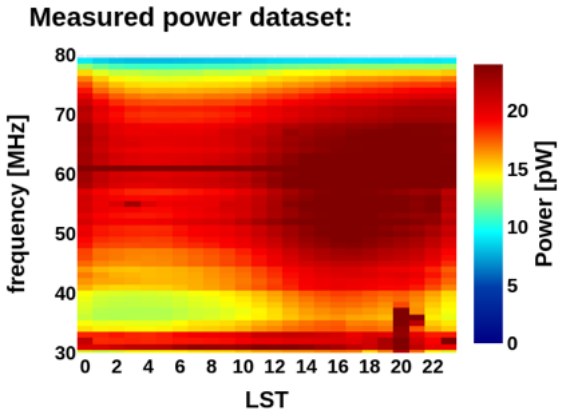

absolutely calibrated signals

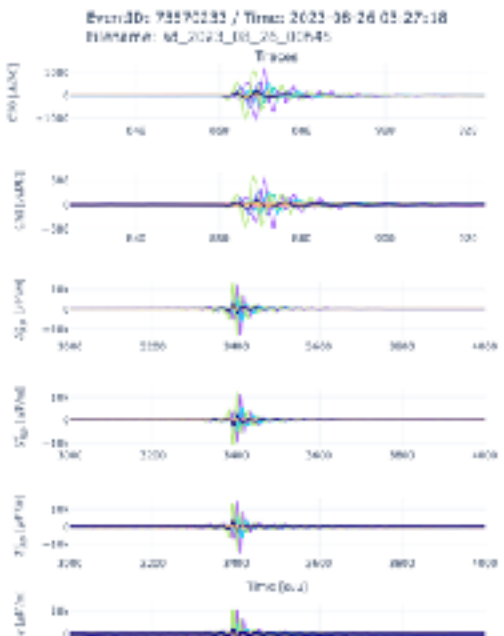

A measured air shower

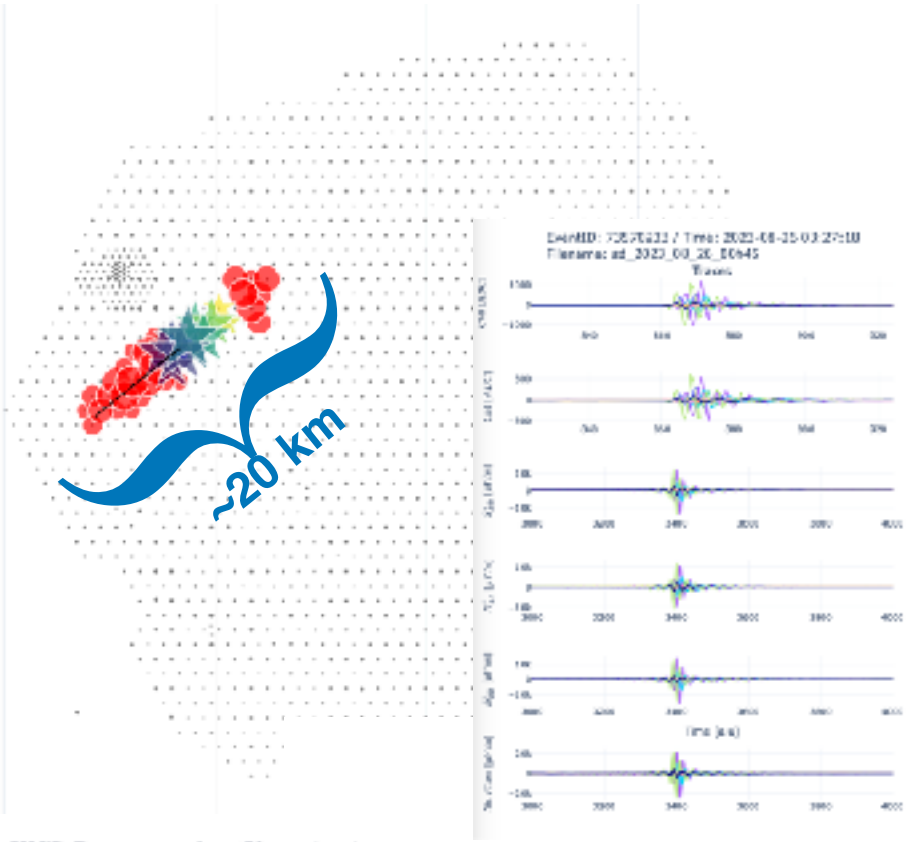

WCD Reconstruction (52 stations)

$E_{SD} = 74.30 \pm 3.4\ EeV$

$\theta_{SD} = 74.7 \pm 0.0\ deg$

$\phi_{SD} = 217.2 \pm 0.1\ deg$

$N_{19} = 12.1 \pm 0.5$

RD Reconstruction (11 stations)

$E_{RD} = 50.62 \pm 7.0\ EeV$

$\theta_{RD} = 74.6 \pm 0.1\ deg$

$\phi_{RD} = 217.1 \pm 0.0\ deg$

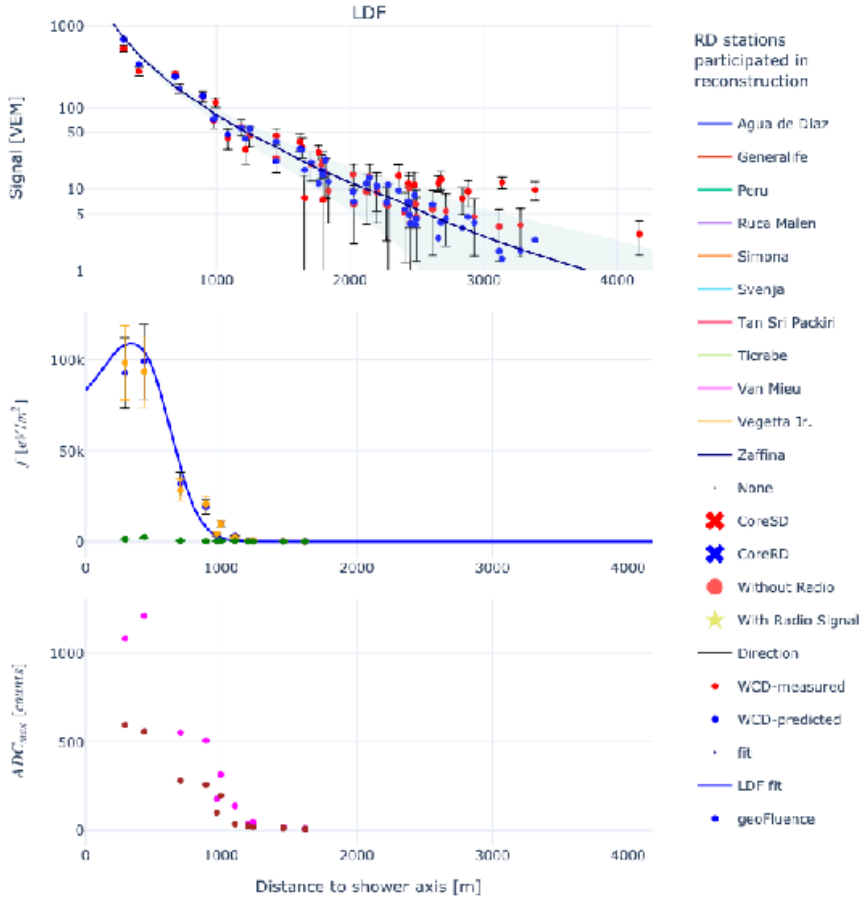

Hybrid measurements RD-WCD

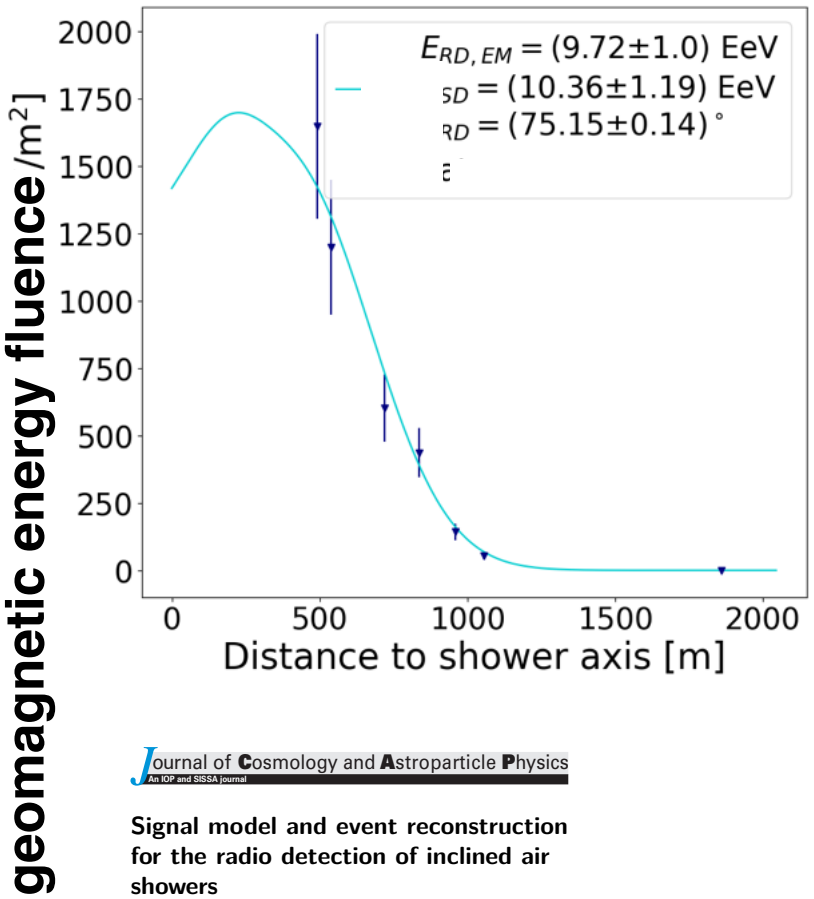

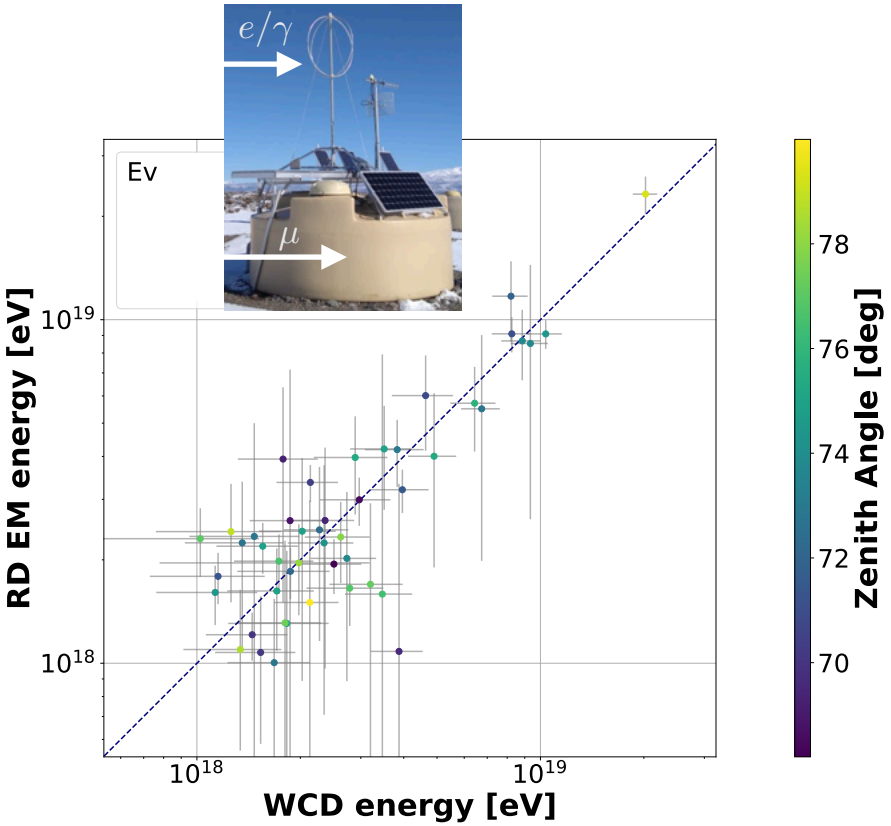

Journal of Cosmology and Astroparticle Physics
An IOP and SISSA journal

Signal model and event reconstruction for the radio detection of inclined air showers

F. Schlüter[a,b,*] and T. Huege[a,c] JCAP01(2023)008

measurement of e/m energy by RD

—> full end-to-end verification of complete chain

Auger Maps